EFFECTS OF INLET GUIDE VANE FLOW CONTROL ON FORCED RESPONSE OF A TRANSONIC FAN

By

Samuel Todd Bailie

DISSERTATION SUBMITTED TO THE FACULTY OF
VIRGINIA POLYTECHNIC INSTITUTE & STATE UNIVERSITY
IN PARTIAL FULFILLMENT OF THE REQUIREMENTS FOR THE DEGREE OF

DOCTOR OF PHILOSOPHY
IN
MECHANICAL ENGINEERING

Dr. Wing F. Ng, Chair
Dr. William W. Copenhaver, Co-Chair
Dr. Ricardo A. Burdisso
Dr. Clinton L. Dancey
Dr. Walter F. O'Brien
Dr. Alfred L. Wicks

OCTOBER 21, 2003
BLACKSBURG, VIRGINIA

Keywords: blade vibration, forced response, compressor, transonic, flow control, trailing edge blowing

Effects of Inlet Guide Vane Flow Control on Forced Response of a Transonic Fan

Samuel Todd Bailie

(ABSTRACT)

The main contributor to the high-cycle fatigue of compressor blades is the response to aerodynamic forcing functions generated by an upstream row of stators or inlet guide vanes. Resonant response to engine order excitation at certain rotor speeds is especially damaging. Studies have shown that flow control by trailing edge blowing (TEB) can reduce stator wake strength and the amplitude of the downstream rotor blade vibrations generated by the unsteady stator-rotor interaction. In the present study, the effectiveness of TEB to reduce forced blade vibrations was evaluated in a modern single-stage transonic compressor rig. A row of wake generator (WG) vanes with TEB capability was installed upstream of the fan blisk, the blades of which were instrumented with strain gages. Data was collected for varied TEB conditions over a range of rotor speed which included one fundamental and multiple harmonic resonance crossings. Sensitivity of resonant response amplitude to full-span TEB flowrate, as well as optimal TEB flowrates, are documented for multiple modes. Resonant response sensitivity was generally characterized by a robust region of substantial attenuation, such that less-than-optimal TEB flowrates could prove to be an appropriate design tradeoff. The fundamental crossing amplitude of the first torsion mode was reduced by as much as 85% with full-span TEB at 1.1% of the total rig inlet flow. Similar reductions were achieved for the various harmonic crossings, including as much as 94% reduction of the second leading edge bending mode resonant response using 0.74% of the rig flow for full-span TEB. At least 32% reduction was achieved for all modal crossings over the broad flow range of 0.5 to 0.9% of the rig flow. Thus the results demonstrate the modal- and flowrate-robustness of full-span TEB for reducing forced response in a modern, closely-spaced transonic compressor. Reduced spanwise TEB coverage was generally found to provide less peak reduction. Widely varying sensitivities of the vibration modes to the spanwise TEB distribution were also noted. While the second chordwise mode experienced roughly the same maximum response reduction of 80% for all of the spanwise TEB configurations, some other modes were amplified from the baseline case under part-span TEB conditions. Part-span TEB was thus found to be less modally-robust than full-span TEB.

Acknowledgements

I would like to preface my acknowledgements with some general comments. Not only as a stepping stone, but also as "my life" of the past five years, my graduate studies have been quite rewarding. I am thankful for the many opportunities that have been presented to me, for the experiences I have had and for the many friends I have made here.

This work was supported in large part by NASA Glenn Research Center, under grant NAG3-2098, monitored by Mr. Oral Mehmed. The financial support afforded the author by an NSF Graduate Research Fellowship is also gratefully acknowledged. The project also involved considerable collaboration with the staff of the Compressor Aero Research Lab (CARL) at the Air Force Research Lab (AFRL), including use of the world-class facilities there. I am thankful for the opportunity I had to work with such distinguished researchers, not to mention how welcoming and encouraging they all were. For the same reasons, special thanks are due to Oral Mehmed and Tony Kurkov from NASA for their collaboration in the experiments. In addition, the signal processing expertise and practical advice provided by Prof. Al Wicks have contributed greatly to the success of this work. I am also indebted to those who provided shelter during my experiments at AFRL: Dr. & Mrs. Doug Rabe, and Mr. & Mrs. Allan Cage.

I am especially grateful to both of my advisors, Prof. Wing Ng and Dr. Bill Copenhaver. Both have consistently provided a wealth of research expertise, balanced with a practical, real-world perspective. Along the way, they have also generously provided encouragement, opportunity and advocacy in the interest of my personal and professional development.

I would also like to acknowledge those who contributed a great deal behind the scenes. Lt. Chris Blackwell, Terry Norris, Bob Wirrig and Bob Allen provided much of the practical support needed for the experiments, and made that stressful time much more enjoyable as well. My fellow graduate students have contributed in many ways, including friendship, encouragement, and experimental advice and assistance. But perhaps their biggest contribution has been in helping me retain some measure of sanity. An exhaustive list would require more than this page, but those to whom I am especially indebted include Nikhil Rao, Oliver Popp and Bo Song.

The benefits of the love and support from my family and close friends are immeasurable. I am quite certain that I could not have persevered through the various challenges encountered along the way without their support and encouragement. And now, after some reflection on my life and graduate studies, and with an eye to the future, I arrive at the most important acknowledgement I must offer. I do so with sincere joy and thanksgiving, and, on the following page, with words much better than my own.

Soli Deo Gloria,

S. Todd Bailie

Blacksburg, Virginia

October 2003

When all thy mercies, O my God,
my rising soul surveys,
transported with the view, I'm lost
in wonder, love, and praise.

Unnumbered comforts to my soul
thy tender care bestowed,
before my infant heart conceived
from whom those blessings flowed.

When worn with sickness, oft hast thou
with health renewed my face;
and when in sins and sorrows sunk,
revived my soul with grace.

Ten thousand thousand precious gifts
my daily thanks employ;
nor is the least a cheerful heart
that tastes those gifts with joy.

Through ev'ry period of my life
thy goodness I'll pursue;
and after death, in distant worlds,
the glorious theme renew.

Through all eternity to thee
a joyful song I'll raise;
for oh, eternity's too short
to utter all thy praise.

– Joseph Addison, 1712

Contents

List of Tables

List of Figures

Chapter 1

Introduction

1.1 Problem Statement

The occurrence of high cycle fatigue (HCF) failures in military turbine engines has increased dramatically in the past 25 years. HCF has been cited as the cause of 56% of USAF engine-related "Class A" failures[1] in fighter aircraft between 1982 and 1996. Additionally, HCF-related maintenance costs are estimated at more than 400 million dollars per year [1]. In response to this alarming trend, many recent research efforts have focused on understanding and mitigating HCF problems in turbine engines.

Fleeter [2] cited that the primary mode of surprise failure in current field engines is the loss of blades or disks by HCF. Compressor and turbine blades have always been at risk for HCF damage, as they experience continuous forced excitation from neighboring blade rows. However, for many years the incidence of HCF blade failure was rather low, indicating that mechanical design and manufacturing practices were sufficiently keeping pace with increases in engine operating loads. Fleeter clearly explained the reason for the unfortunate and marked increase of HCF-induced blade failures in recent times as follows:

[1]Failures resulting in loss of pilot life and/or more than $1 million in equipment damage.

> "For axial flow machines, this is a direct result of the introduction of high thrust-to-weight ratio engines which required [new] materials, manufacturing techniques and engine configurations. Namely, higher pressure ratios per stage and therefore higher efficiencies for a given engine weight required closely spaced rows of low aspect ratio blades. Cost, weight and durability issues led to the introduction of material and manufacturing techniques that resulted in very low levels of mechanical damping. As a result, these high thrust-to-weight ratio engine configurations are highly susceptible to HCF caused by flow induced vibrations, either forced response or flutter, with rotor blades particularly susceptible because of the large mean stresses from centrifugal forces." (Fleeter [2])

The excitation of rotor blades is primarily the result of unsteady aerodynamic interactions with neighboring blade rows [3, 4, 5]. As rotor blades pass through the viscous wakes shed by upstream stator vanes, they experience highly unsteady periodic loading, inducing forced blade vibrations. Because potential flow interactions present an additional forcing function, downstream vanes can also excite rotor blade vibration. Both of these aerodynamic excitations occur at the fundamental vane passing frequency (VPF) and its harmonics, which scale linearly with the rotor speed and thus correspond to fixed engine orders.

As long as such excitation sources are present, some degree of rotor blade vibratory response is expected. For much of the operating range, these vibrations are well within design limits. However, operation at a resonance "crossing", where the rotor speed is such that an engine order excitation coincides with a blade natural frequency, can result in large amplitude vibrations that are especially damaging.

Such crossings are graphically represented in a speed-frequency plot, as provided in Figure 1.1 for the present investigation. This widely-used tool is more commonly referred to as the Campbell diagram, being so named in honor of Wilfred Campbell, whose diagnostic investigations of steam turbine failures [6] in the 1910's and 20's did much to establish turbomachinery forced response analysis. The figure is generated for the system in question by

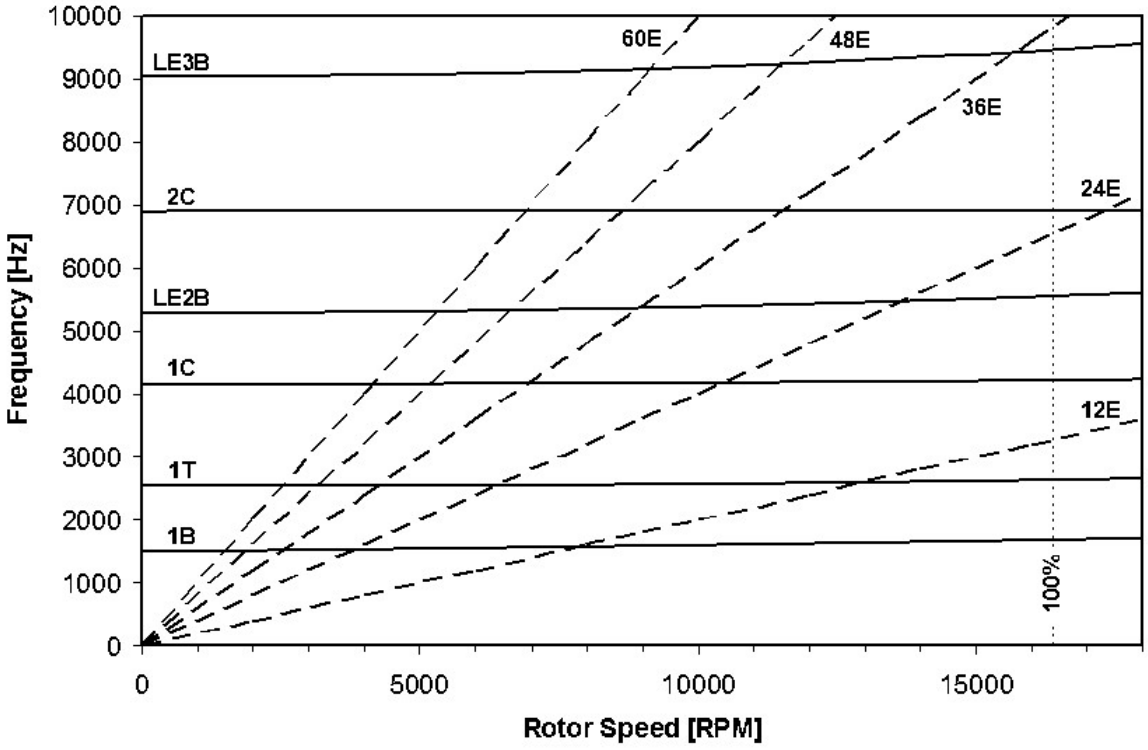

Figure 1.1: Campbell diagram used in forced response analysis.

overlaying the rotor blade vibration mode characteristics (in this case, the solid lines) with the expected synchronous forcing functions (the dashed lines), which usually correspond to harmonic orders of the neighboring stator row vane counts. Wherever the lines intersect, a resonance occurs. The magnitude of the resonance (and the damage potentially caused by it) depend primarily on the strength of the excitation and the structural and aerodynamic damping available at that particular operating condition.

Because load cycles are rapidly accumulated at the high rotational speeds typical in turbomachinery, high-amplitude resonant vibrations can quickly lead to fatigue failure. Thus it is a standard, and often iterative, design practice to try to locate blade modes such that resonance crossings do not occur near the intended steady operating speed(s) of the rotor. However, as evident from Figure 1.1, rotor blades will experience multiple resonance crossings during engine run-up and run-down [3]. Also, rotor blades are now typically designed with

very low aspect ratios. These blades look and act more like plates than traditional blades. As a result the modal responses are grouped very closely, making it all the more difficult to avoid numerous crossings. To make matters worse, modern rotor designs typically have very low structural damping. Thus accumulation of damage is largely unavoidable and, in the event that the residual strength falls below the applied load, a failure will occur, often with catastrophic results.

1.2 Approaches to the Problem

Considering the documented and ongoing cost of HCF to critical machinery and human life, it is a principal objective to minimize the forced response, particularly at resonance, of HCF-prone components. This section is an attempt to summarize the major strategies for reducing forced response in rotors of axial turbomachinery.

Forced response strategies can generally be divided into two basic categories. To alter the response of a particular component, either or both of the following elements can be modified:

- the responding component itself
- the force input, or stimulus, to that component

It is usually not feasible to altogether remove the stimulus source, as this is often another essential component of the same system. Moreover, mechanical constraints and the interdependence of components (such as multi-stage aerodynamics) typically limit the degree to which any particular component can be modified. The impact of any modifications on system-level objectives (e.g. engine weight and performance) must of course also be considered.

1.2.1 Modification of the Responding Component

Kielb [7] noted that forced response can be managed in part by "frequency control". By adjusting the frequency of the blade modes, resonance crossings can be relocated to preferable rotor speeds. As means of such frequency control, he suggested modifying geometric design variables, including aspect ratio, taper, solidity, and radius ratio. This approach, in conjunction with the Campbell diagram, is part of typical aeromechanical design practices (or *re*-design, as is sometimes the case).

A primary problem in the forced response of most modern rotor designs, particularly the integrally machined compressor "blisks", is that they inherently have very low mechanical damping [2]. Thus many research efforts have attempted to reduce response by adding damping, in various forms, to the rotor blades. These efforts have included such novel approaches as: the addition of viscoelastic layers; the use of shunted piezoelectric elements for energy dissipation by Cross and Fleeter [8]; and the incorporation of self-tuning vibration dampers by Duffy et al. [9]. While these and other approaches have produced promising results, implementation of substantial damping enhancement without reducing the structural integrity of the rotor remains a challenge [10].

Alternately, instead of directly addressing the forced response issue, a designer can try to improve damage tolerance. While simply thickening the rotor blades can increase damage tolerance, the associated weight and dynamic load penalties are often unacceptable. There appears to be promise, and some progress, in the development of materials with reduced susceptibility to crack propagation.

1.2.2 Modification of the Stimulus

The stimulus, or forcing function, can be modified in several ways. The excitation frequency, and the corresponding slope of the excitation line(s) in the Campbell diagram, can be altered by using a different number of vanes in the neighboring blade rows. This primarily relocates

the resonance crossings, without directly changing the amplitude of the excitation.

Increasing the axial spacing between blade rows provides reduction of potential field strength, which drops exponentially with distance. Increasing spacing also allows some dissipation of the viscous wakes. However, the axial distances needed for complete wake mixing are quite impractical for aircraft engine design; in fact, the design trend is to place the rows ever closer together.

Other passive techniques try to spread out, or "dilute", excitation energy over a wider frequency or phase range. Fagan and Fleeter [11] numerically investigated the use of circumferentially nonuniform spacing of upstream vanes on noise generation and forced response of a compressor rotor. This alters the harmonic content of the forcing function, effectively broadening the (usually distinct) excitation lines in the Campbell diagram, and thereby reducing the peak amplitude of the excitation. Alternately, vane lean can be used to slightly change the relative time-of-arrival (phase) of the forcing function along the blade span. Hsu and Wo [12] also noted that, for some cases, multi-row clocking can be used to adjust the relative phase of different forcing functions to achieve a combined forced response benefit.

A different approach, employed by von Flotow et al. [10], is referred to as "active wake management". This approach can take various forms, including the manipulation of the frequency, phase, or magnitude of a vortical forcing function. Von Flotow's approach was to selectively extend round bars into the flow field between the inlet guide vanes (IGVs) and rotor of the same compressor facility presently used. This novel idea allowed an additional wake forcing function of variable magnitude to be imposed, out of phase with respect to the original wake excitation, thereby producing a canceling effect. This technique was demonstrated to be highly effective for reducing selected forced modal responses. However, the rod count, position and insertion depth must be calibrated for each specific crossing (specific mode and excitation order), and as such would generally be implemented only *after* a fatigue problem has been diagnosed. Also, to produce the additional forcing function, engine system complexity and performance losses may be substantially increased. There is also, of course,

the risk that a new HCF problem may be introduced.

1.3 Present Approach & Contribution

The present approach is based on another form of active wake management for stimulus modification. Since the dominant stimulus (i.e. the set of wakes shed by the upstream vane row) is aerodynamic in nature, it is intuitive to seek an aerodynamic means of mitigating the effect of the stimulus.

The most direct approach for reducing the forced response is to attempt to *reduce the amplitude* of the stimulus. Thus, in contrast to the approach of von Flotow [10], the goal of the present study was to promote as much flowfield *uniformity* as possible, primarily in the circumferential direction (i.e. to "smooth out" the path traveled by each rotor blade). The objective of uniformity can be defined, at least ideally, in basic aerodynamic terms; there is therefore the potential that a uniformity-promoting scheme could be developed using standard aerodynamic design tools and be implemented without *a priori* knowledge of the modal characteristics of the downstream rotor or its most problematic resonance crossings.

Waitz et al. [13] discussed the feasibility of two flow control concepts for active wake management, with the goal of reducing turbomachinery fan noise. The two concepts evaluated, known as boundary layer suction (BLS) and trailing edge blowing (TEB), are illustrated in Figure 1.2 (from [13]).

In the early 1990's, trailing edge blowing was tested by Naumann [14], Corcoran [15], and Park and Cimbala [16] for wake reduction behind flat plates as simulated blades. These studies demonstrated large reductions in the time-mean wake velocity deficit and wake velocity fluctuations by TEB. However, these studies all involved low speed (incompressible) flows, and the geometries and axial spacings considered were not suitable for turbomachinery applications. Waitz et al. [13] provided the first documented evaluation of the wake management concepts on curved airfoil shapes at conditions of relevance to modern turbomachinery.

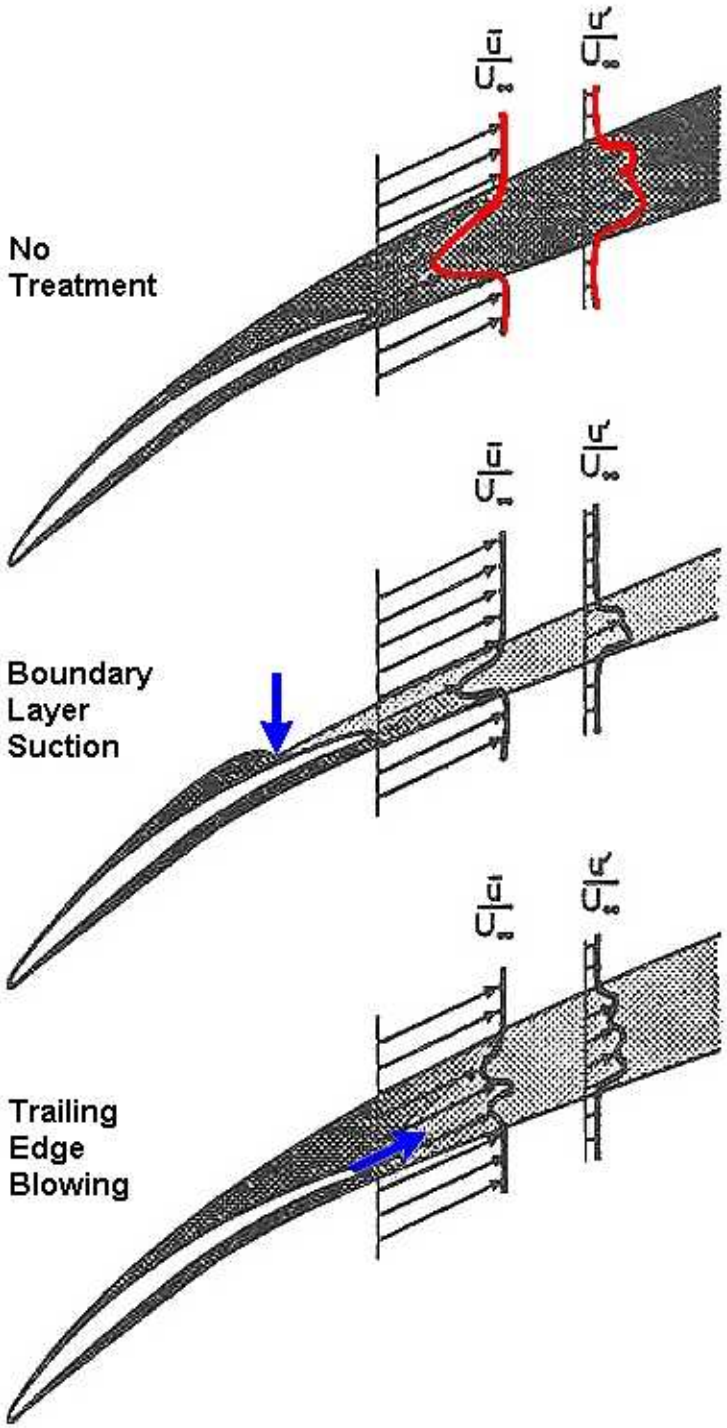

Figure 1.2: Flow control concepts for wake management (courtesy of I.A. Waitz).

Their study suggested that the trailing edge blowing technique should be more effective than boundary layer suction for reduction of viscous wakes.

In the TEB technique, fluid (typically air) is ejected from the trailing edge of the wake source to reduce the original momentum deficit of the viscous wake region. Blade row spacing of modern turbomachinery is typically insufficient for complete mixing of the blowing jet with the wake flow, as would be desirable for best circumferential uniformity. Thus for close spacings it is typical that TEB will yield a "W"-shaped wake velocity profile as illustrated in the figure. However, most of the maximum velocity deficit is seen to be greatly reduced, and the small-scale non-uniformity (e.g. the "W") can be reduced by using blowing configurations that promote more mixing (such as discrete holes instead of spanwise slots) [14, 16].

The present study applies the TEB technique to a set of IGVs in a modern compressor rig. The compressor is a highly loaded transonic design with close stage row spacings. As such it is representative of engine technology currently in service, while also being of design and construction that is particularly prone to HCF failure. The effects of various TEB conditions and configurations on rotor blade forced response are evaluated.

There are several key contributions of this work. This work represents the first demonstration of a multiple-vane TEB system in a modern transonic compressor. While the effects of TEB on forced response have been previously documented for subsonic conditions, this is the first documented investigation of TEB effects on forced response of a transonic compressor. In addition to a wide range of TEB flowrates, forced response data is collected for different degrees of TEB coverage along the IGV span. To the author's knowledge, no previous turbomachinery-related studies have documented the effects of varying the extent of spanwise TEB coverage.

1.4 Previous Research

Quite a few studies involving trailing edge blowing have been conducted in recent years, and for a variety of turbomachinery applications. Much of the previous work is briefly summarized in the following section to provide the reader with an overview and some historical context. Only a few studies, however, were found to be of direct relevance to the present forced response study.

TEB has found application in aeroacoustics research, particularly with the goal of reducing noise generated by unsteady blade row interaction. As previously discussed, Waitz et al. [13] conducted some of the early evaluations in this area. A series of experiments followed shortly at Virginia Tech, with TEB being used from the inlet struts of a small-scale turbofan simulator. Leitch [17] conducted experiments in an anechoic facility to assess the effectiveness for reducing levels of radiated fan noise. He measured noise reductions as high as 7 dB. Saunders [18] performed a similar investigation for an axisymmetric supersonic inlet, with reduction of 6 dB being achieved. Rao [19] and Feng [20] extended the turbofan simulator work with the application of active control of the TEB flow using MEMS-based microvalves. Sutliff et al. [21] also recently configured a low-speed fan rotor with TEB and assessed the effects of a range of blowing conditions on in-duct and far-field acoustics. Analytical predictions as well as selected hot-wire and unsteady surface pressure data were documented.

A number of TEB studies have focused on aerodynamic performance enhancement for turbomachinery blades and vanes. In cascade tests, Vandeputte [22] applied both TEB and boundary layer suction to the variable-angle downstream flap of a tandem IGV design. Despite substantial separation of the baseline flow around the IGV, due to the large 40° flap angle, the application of both TEB and BLS reduced the total pressure loss coefficient by 48%. Better reductions were expected for a redesign of the TEB configuration to better coincide with the wake centerline. Carter et al. [23] used a novel approach to combine

both BLS and TEB as part of a single control element. This design was applied to a high-turning compressor stator and evaluated in cascade tests at Mach 0.79. As much as 65% reduction in the pressure loss coeffient was achieved using motive massflow of 1.6% of the passage throughflow. In addition, up to 4.5° of increased flow-turning were measured with application of the flow control scheme.

Kozak [24] investigated TEB wake-filling downstream of a single symmetric IGV installed in the inlet of an F109 turbofan engine. Data was acquired with the IGV installed far upstream as well as close to the fan, which was operated at both subsonic and transonic (rotor-relative) conditions. This study provided the first TEB data under the influence of passing rotor shocks. Kozak noted that TEB provided effective wake-filling at both subsonic and transonic rotor conditions, but he found that complete wake-filling was not achieved for transonic conditions. Perhaps more significant than the TEB data were the measurements of the ensemble-averaged unsteady baseline wake profiles, with and without rotor shock effects. The shock interaction was found to substantially deepen the wakes as compared to the subsonic rotor case. Some turning of the wake flow, in the direction of rotor rotation, was also inferred from the measurements.

Only a pair of previous studies were found in which the effects of TEB on the forcing of downstream airfoils have been investigated. Morris et al. [25] studied TEB effects in a linear cascade of stator vanes and subsequently in a 17-inch (43.2 cm) scaled fan rig, which had a rotor instrumented with strain gages. Very little detail was provided about the operating conditions, TEB design or the blowing conditions. However, maximum rotor blade stress reductions of 43% for the third LE bending mode and 90% for the first chordwise bending mode were reported with TEB massflow for twenty vanes at 1.4% of the total rig flow.

The work of Morris et al. provided the first demonstration of forced response reduction by TEB, and indeed the study bears similarity to the present one. However, more resonance crossings and a much broader range of TEB conditions are presently documented. More significantly, shock interaction was not present in Morris' experiment, as the fan was operated

at high-subsonic conditions [26].

Shock-wake interaction, present for most of the data presently collected, has been previously observed to substantially increase wake depth [24]. Shock interaction has also been noted in the current test facility to have a strong effect on the global dynamics of the wake, including some turning of the wake (in the direction of rotor rotation) [24, 27]. Additionally, it was unknown if and how the strong trailing edge forcing imposed by the passing shocks [24, 28] would affect the TEB flow. There was some concern that the shocks impacting the IGV might interrupt or retard the TEB jets, or that the jets might not, as desired, follow the wake centerline (as a consequence of shock-induced wake-turning).

Wo et al. [29] conducted a TEB investigation in a low-speed, large-scale axial compressor. TEB was applied to the rotor of the single rotor/stator stage, with much effort being applied to generate a uniform blowing distribution. Hot-wire measurements were used to map the three-dimensional ensemble-averaged rotor wake profile. Unsteady pressure transducers, embedded in the suction and pressure surfaces of a downstream stator passage, were used to quantify the effects of TEB on the unsteady wake-induced forcing of the stators. Data was collected for both near-design and high-loading conditions at three different TEB injection conditions.

All of the blowing cases were found to reduce the unsteady stator loading, even though near-wake measurements (0.15 chordlengths downstream) indicated that the blowing flow was not coincident with the wake centerline. For the intermediate TEB case, which corresponded to a 72% reduction of the baseline wake momentum defect, reductions in stator unsteady force amplitude of 25 and 35% were achieved for the near-design and high loading cases, respectively. Decomposition of the hot-wire data showed that the magnitude of the transverse gust, the most offensive component of the vortical forcing function, decreased linearly with the increase in wake momentum by TEB.

Chapter 2

Description of Experiment

2.1 Experimental Approach

Though the ultimate objective of the present work was to test a flow control design for IGV wake management in a modern transonic compressor rig, such rig tests, and the associated hardware, are complex and expensive. As such it was essential to first establish a high degree of confidence regarding the feasibility of the flow control technique prior to its implementation in the compressor rig.

As discussed in the preceding sections, many previous studies have used flow control for wake management. However, the trailing edge blowing (TEB) research documented in the open literature has generally only involved low-speed, far-wake studies, which are of limited relevance to modern turbomachinery applications, including the present transonic compressor rig application. The rig's axial Mach number can exceed 0.6 at the flow control location, and the axial gap between the wake source (row of IGVs) and the downstream rotor is rather small at 0.26 IGV chordlengths, which inhibits much of the normal wake mixing evident in the far-wake. Moreover, due to the transonic rotor operating condition, strong shock waves impinge on the IGV trailing edge at the high rotor blade passing frequency (BPF), influencing the IGV wake development and hence leading to a strongly coupled

aerodynamic interaction between the blade rows.

Since the available literature lent no particular confidence that a TEB design would be effective in the closely-spaced transonic compressor environment, the first phase of the overall research program was a parametric investigation of the TEB technique on isolated airfoils similar to those to be used in the rig tests. This initial phase was conducted at Virginia Tech in a small-scale wind tunnel. While the transonic rotor shock and potential field effects were not included, the tunnel flow conditions were otherwise comparable to those expected in the subsequent rig application. Several TEB design parameters (discrete blowing hole diameter, shape and spacing) were evaluated for wake-filling effectiveness at the same relative axial station as the rotor leading edge (LE) in the rig experiments.

After the TEB concept was validated and its design refined through experimental iterations in the wind tunnel, the final TEB configuration was incorporated into a flow control system for a set of inlet guide vanes (IGVs). This system was then implemented in the SMI transonic compressor rig at the Air Force Research Laboratory (AFRL). In this rig, which is representative of modern military compressor designs, experiments were undertaken to measure the effects of TEB flow control on rotor blade forced response.

For historical context it is worth mentioning that two phases of rig experiments were conducted, with the first set being completed in April 2000 and the latter being completed in August 2002. Due to a combination of factors, including a small test window and specific limitations of the data acquisition and compressed air supply systems, the test plan for the first set of experiments had to be substantially truncated. The limited forced response data set that was acquired included only a few steady rotor speeds and one flow control condition. While many important questions were left unanswered, the results from the first phase qualitatively confirmed the feasibility and merits of the TEB technique in the previously untested transonic compressor environment.

Building on lessons learned in the first rig experiments, and in conjunction with improvements to the data system and the compressed air delivery, a second set of rig experiments

was designed and executed. Additionally, the inclusion of a powerful signal processing technique, called "order tracking analysis" (see Section 2.3.1.1), provided a safer and much more efficient means of forced response data collection. Thus in the second and final phase of rig experiments, a much broader and more useful data set was collected, effectively superseding results from the first rig experiments. Accordingly, the description provided in the following sections is primarily limited to the experimental facilities and techniques as employed in the final set of compressor rig tests. For information regarding the first rig experiments, and the results thereof, the reader is referred to Bailie et al. [30].

2.2 Experimental Facility

2.2.1 SMI Transonic Compressor Rig

The Stage Matching Investigation (SMI) rig is a single stage transonic compressor in the Compressor Aero Research Lab (CARL), part of the U.S. Air Force Research Laboratory (AFRL) at Wright-Patterson AFB, Ohio. The rig can be built up with one of two different highly-loaded stages, both consisting of a transonic rotor followed by stator row. The two compressor configurations, geometrically similar but having different aerodynamic design parameters, represent a core stage and a fan stage. A cross-section of the rig is provided in Figure 2.1. As illustrated in the figure and described in the next section, a row of wake generator (WG) vanes can be installed in various configurations upstream of either compressor stage.

The two stages were designed by Law and Wennerstrom [31] as robust examples of the state-of-the-art in modern high-speed low-aspect-ratio compressor design, with the intent of studying blade-row interactions and their effect on stage matching. Table 2.1 summarizes the aerodynamic design details of the fan stage, which was used for the present investigation.

The compressor rotor is driven by a 2000 horsepower electric motor. The motor operates

Table 2.1: Aerodynamic design parameters of the SMI fan stage (from [32]).

PARAMETER	FAN STAGE	
	Rotor	Stator
Number of Airfoils	28	49
Aspect Ratio - Average	0.916	0.824
Inlet Hub/Tip Ratio	0.750	0.833
Flow/Annulus Area, lbm/s/ft^2	40.000	--
Flow/Frontal Area, lbm/s/ft^2	17.502	--
Flow rate, lbm/sec	34.460	--
Tip Speed, Corrected, ft/sec	1360	--
Relative Mach, LE Hub	1.100	0.830
Relative Mach, LE Tip	1.389	0.700
Pressure Ratio, Rotor	2.183	--
η_{iso} Rotor, %	90.9	--
Pressure Ratio, Stage	--	2.130
η_{iso} Stage, %	--	87.7
Diffusion factor, Hub	0.545	0.506
Diffusion factor, Tip	0.541	0.556
LE Tip Diameter, in.	19.000	19.000
LE Hub Dia., in.	14.250	15.824
TE Tip Dia., in.	19.000	19.000
TE Hub Dia., in.	15.508	16.248

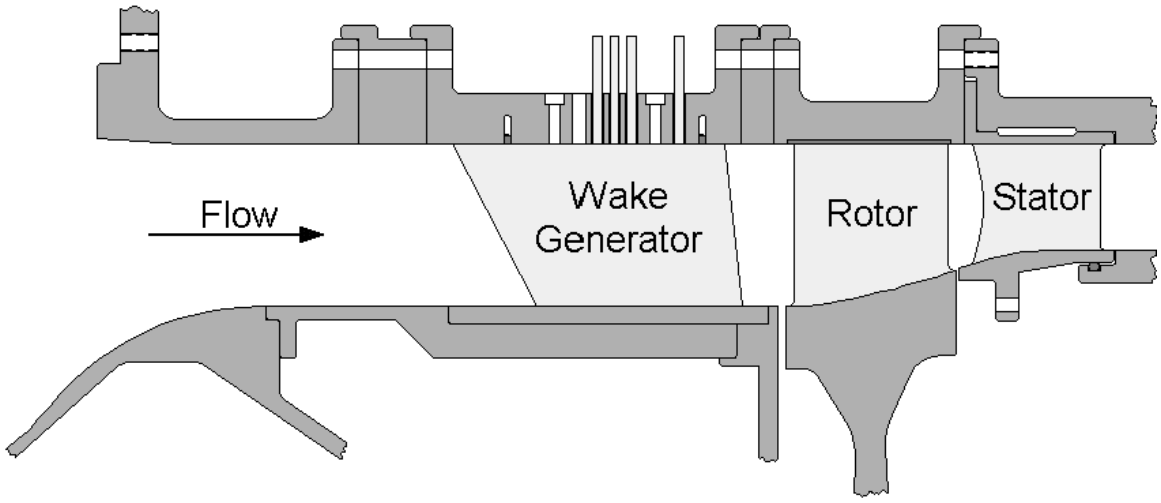

Figure 2.1: Flowpath of the SMI rig, with WG at "mid" spacing.

at constant speed, while an adjustable eddy-current coupling attached to the motor is used to reduce and control the drive speed. A gearbox is installed between the eddy-current coupling and the compressor to increase the rotor speed to a maximum of 21,500 rpm [33]. A variable-area exit flow throttle is used to adjust the stage aerodynamic loading.

2.2.2 Wake Generators

The WG vanes are symmetric (uncambered) three-dimensional airfoils with a sharp leading edge and blunt trailing edge to simulate the deep, broad wakes typically generated by highly-loaded front compressor stages, or by IGVs with substantial camber [33]. A drawing showing the basic WG geometry and the relative hub, midspan and tip cross-sections is provided in Figure 2.2.

Using interchangeable spacers, three WG vane-to-rotor axial positions were available, as denoted and quantified in Table 2.2. The "mid" spacing, illustrated in Figure 2.1, was chosen for the present investigation as being consistent with axial gaps found in typical Pratt & Whitney fans [32]. While the "close" spacing follows the current design trend of reducing

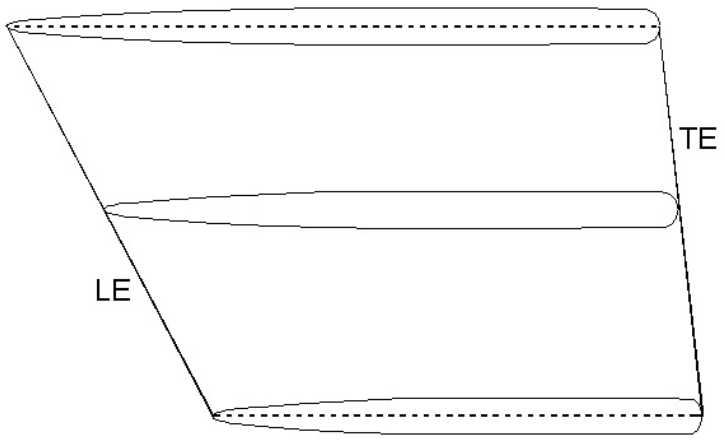

Figure 2.2: Wake generator vane profile with hub, midspan and tip cross-sections shown.

Table 2.2: Variable SMI wake generator vane-to-rotor axial spacing (from [32]).

Spacing	ax/c (mean)	ax/c (hub)	ax/c (tip)
Close	0.13	0.10	0.14
Mid	0.26	0.26	0.26
Far	0.55	0.60	0.52

ax = axial spacing
c = wake generator chord

blade-row spacing (to minimize engine length), this was deemed to be overly aggressive for the first evaluation of TEB in a transonic compressor.

The WG vane count is also variable and can be set at 12, 24 or 40. Alternately, the rig can be run in a baseline "clean inlet" configuration with no wake generators. While the higher vane counts are more representative of typical compressor design, the 12-vane configuration was selected for reduced cost and complexity of the required flow control system. Despite the reduced vane count, strong forced blade vibrations were still induced by the WGs such that the effects of the flow control technique could be readily measured.

Detailed WG wake measurements were obtained by Gorrell [33] for the 24- and 40-vane configurations. Measurements were acquired with the SMI core stage operating at design

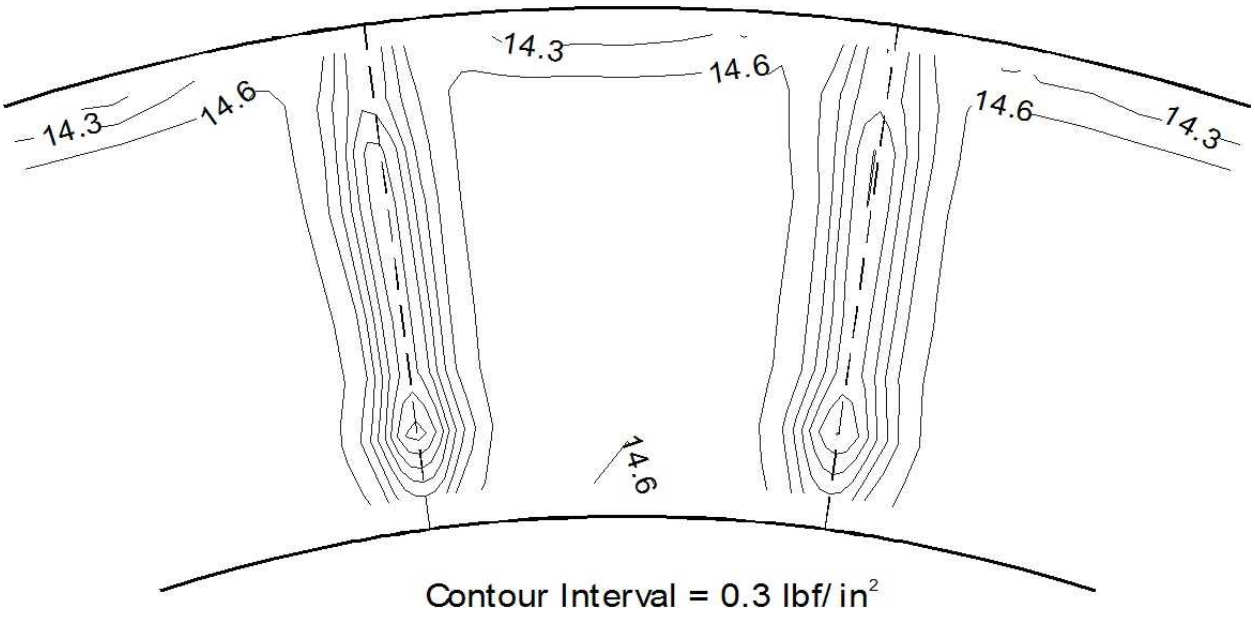

Figure 2.3: Steady wake total pressure contours for the 24WG configuration at mid-spacing (from [33]).

speed (with the same design flowrate as the fan stage presently used). The WGs and rotor were spaced much farther apart than the three normal spacings to allow for insertion of instrumentation. The data thus do not include the rotor shocks or other unsteady effects on the upstream wakes. Rakes were placed between the WGs and rotor at positions corresponding to the relative fan-face stations of the three normal axial bladerow spacings. The rakes were traversed circumferentially to characterize the time-mean wake flowfield. Figures 2.3 and 2.4 provide total pressure contours and velocity profiles at the "mid" spacing for the 24-WG configuration. These data illustrate that the wakes are deep and predominantly two-dimensional through the mid-span. However, substantial variation in the wakes and inter-vane flowfield is noted near the hub and tip due to endwall interaction.

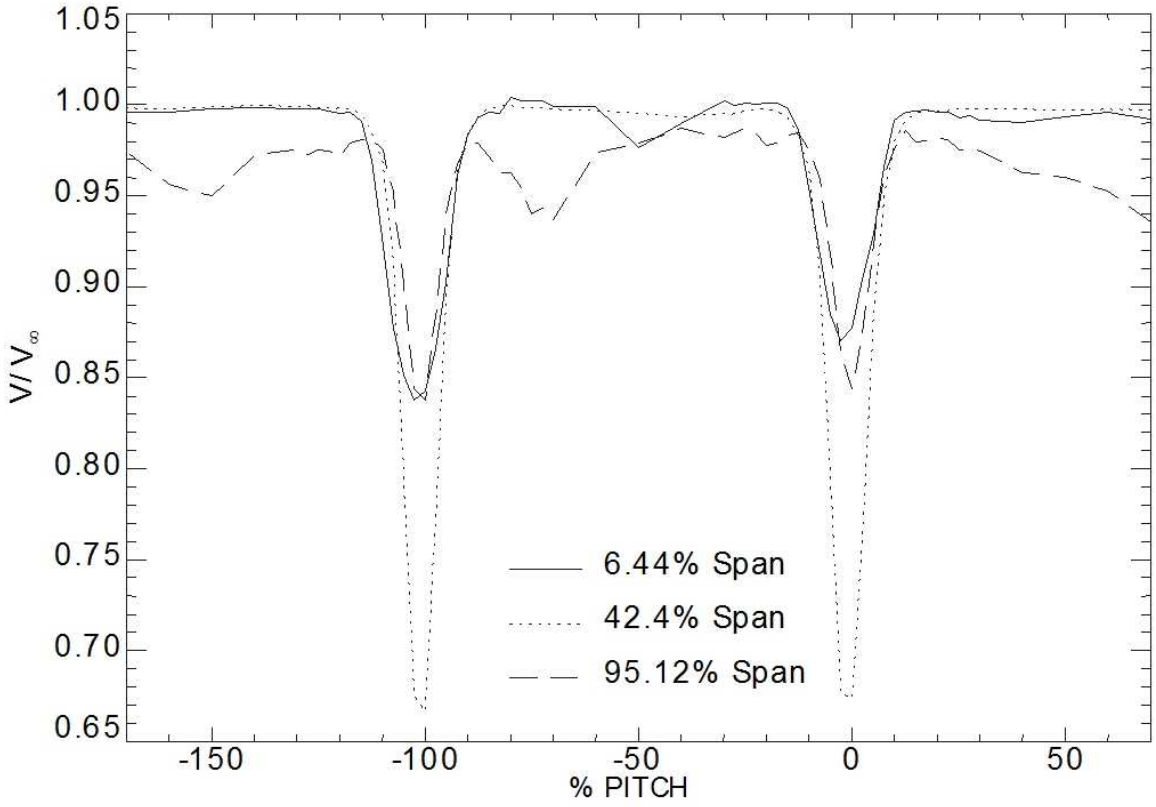

Figure 2.4: Steady wake velocity profiles at hub, midspan and tip locations for the 24WG configuration at mid-spacing (from [33]).

2.2.3 TEB Flow Control System

A description of the TEB flow control system is provided with respect to the major components of the system: the TEB design implemented in the WGs of the SMI rig; the compressed air supply; and the intermediate system used to distribute and control the compressed air delivery to the wake generator vanes.

2.2.3.1 Wake Generator TEB Design

The wake generator TEB design was developed from a series of experiments in a small high-speed blowdown wind tunnel at Virginia Tech. Steady velocity field measurements were taken downstream of the WG to assess the influence of discrete TEB hole size, shape, and pitchwise spacing on the wake-filling effectiveness. The tests were conducted at an inlet Mach number of 0.6. These experiments confirmed the feasibility of TEB at high subsonic speeds and close axial distances, and led to selection of a final TEB configuration for the subsequent SMI compressor rig experiments. This configuration is illustrated in Figures 2.5 and 2.6.

In order to minimize unsteady rotor blade loading, it is desirable to promote as much circumferential flowfield uniformity as possible. As such it was deemed unnecessary, even undesirable, to place TEB holes within the endwall boundary layers, which are present for the entire circumference. The selected TEB design consisted of seven axially-oriented blowing holes per WG. The holes were spaced uniformly, filling most of the span between the endwall boundary layers. The constant hole diameter of 0.082 inches (2.08 mm) was approximately 40% of the trailing edge thickness. A pitch-to-diameter ratio of 2.5 was used, which was demonstrated in the wind tunnel testing to provide effective coverage for almost the entire span between the endwall boundary layers.

While complete wake-filling would maximize circumferential flowfield uniformity, the

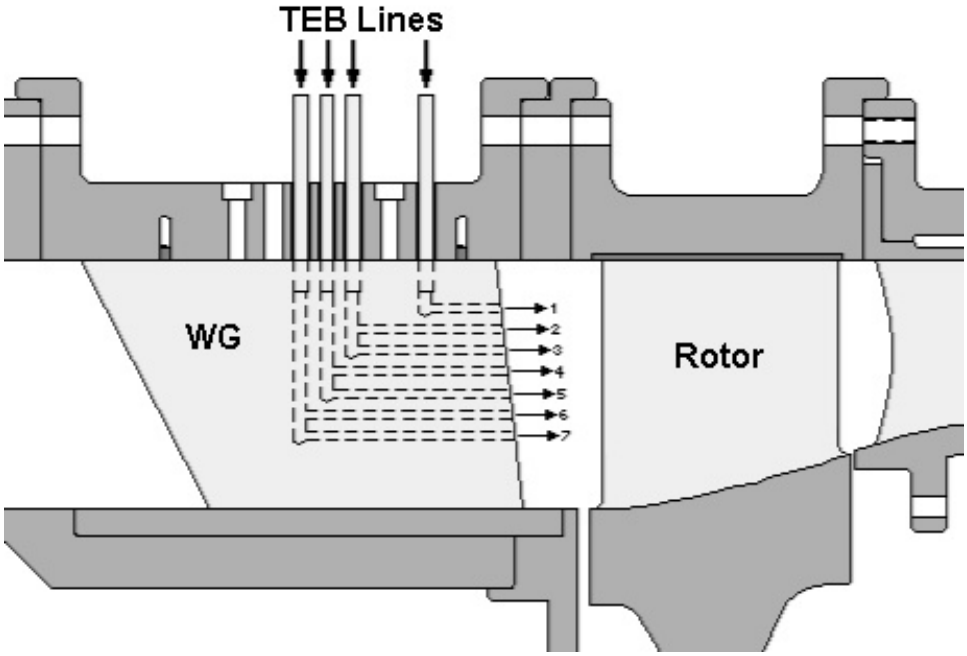

Figure 2.5: Implementation of wake generator TEB design into SMI compressor rig.

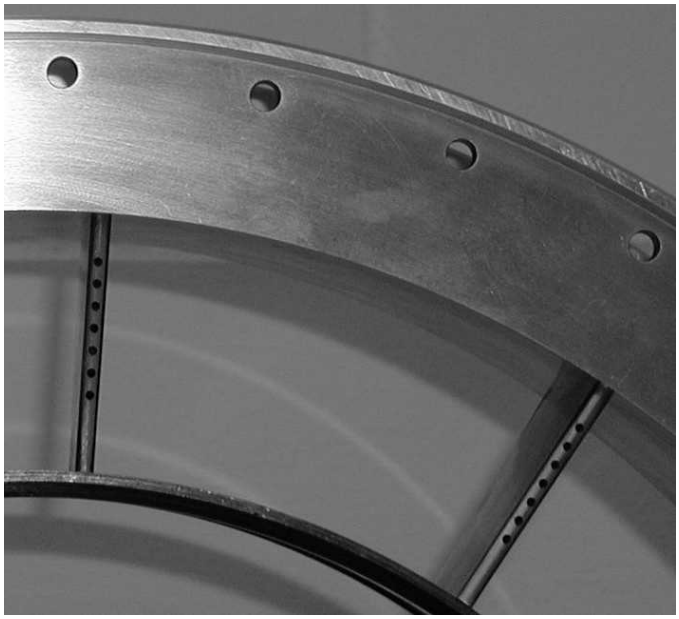

Figure 2.6: Trailing edge view of wake generator TEB design.

compressor bleed air requirement to achieve this may be prohibitively costly to overall engine performance. It was desired to characterize the sensitivity of the forced response to the flowrate of TEB air and its spanwise distribution. Thus the TEB plumbing was designed to permit independent adjustment of flow to different spanwise sectors of holes. As shown in Figure 2.6, four independent lines supplied the seven holes. One supply line fed a single tip hole, while the remaining three lines each supplied a pair of TEB holes. Maximum flow variation between paired holes was estimated to be 5%. The specific spanwise TEB cases used will be discussed in Section 2.4.2.

2.2.3.2 Compressed Air Supply

Because the single-stage compressor rig did not have sufficient pressure ratio to feed the flow control system by bleed recirculation, high-pressure air was supplied for TEB from an external supply. Since no air compression system with sufficient flowrate and pressure output for continuous operation was installed at the facility, compressed air was received from storage tanks.

Compressed dry air was supplied in the form of a "tuber", which is a large flat-bed trailer with multiple high-pressure cylindrical vessels. The tuber, shown in Figure 2.7, was supplied at an initial pressure of 3000 psig (20.7 MPa). Flow from the tuber had to be throttled to a much lower pressure for distribution to the rig. This proved to be no trivial matter; in fact, the inability of the original two-stage pressure regulation system, installed for the first phase of rig experiments, to operate at off-design flowrates was the primary reason for the drastic reduction of the first rig test matrix. Details of the final flow throttling, distribution, and control system are provided in the following section.

2.2.3.3 Flow Distribution & Control

A schematic of the overall flow distribution and control system is provided in Figure 2.8. Flow was received from the tuber at pressures ranging from 3000 psig (20.7 MPa) at full

Figure 2.7: Tuber truck supplying high-pressure air for the TEB flow control system.

charge to about 500 psig (3.45 MPa). It was then throttled to a typical settling tank pressure of 100 psig (690 kPa) by a single-stage Jordan Mk 708QC pneumatically-actuated control valve.

The valve featured a quick change bonnet to enable in-line replacement of the internal needle and seat. This feature was used frequently during the experiments to change between valve flow coefficients (Cv) of 0.2 and 1 to maintain the desired flow range as the supply pressure of the tuber dropped. One bank of tubes was reserved at high pressure while the other bank was dropped to lower pressure as it was consumed. This practice, in conjunction with the variable valve flow coefficient, provided enough throttling control to accommodate the wide range of tuber supply pressure encountered during the experiments.

TEB flow was distributed from the settling tank, in an instrumentation room below the rig test bay, to four rig-mounted manifolds by rubber hoses, one-half inch (1.3 cm) in internal diameter by 50 feet (15 m) long. Each of the four manifolds (see Figure 2.9), with pressures

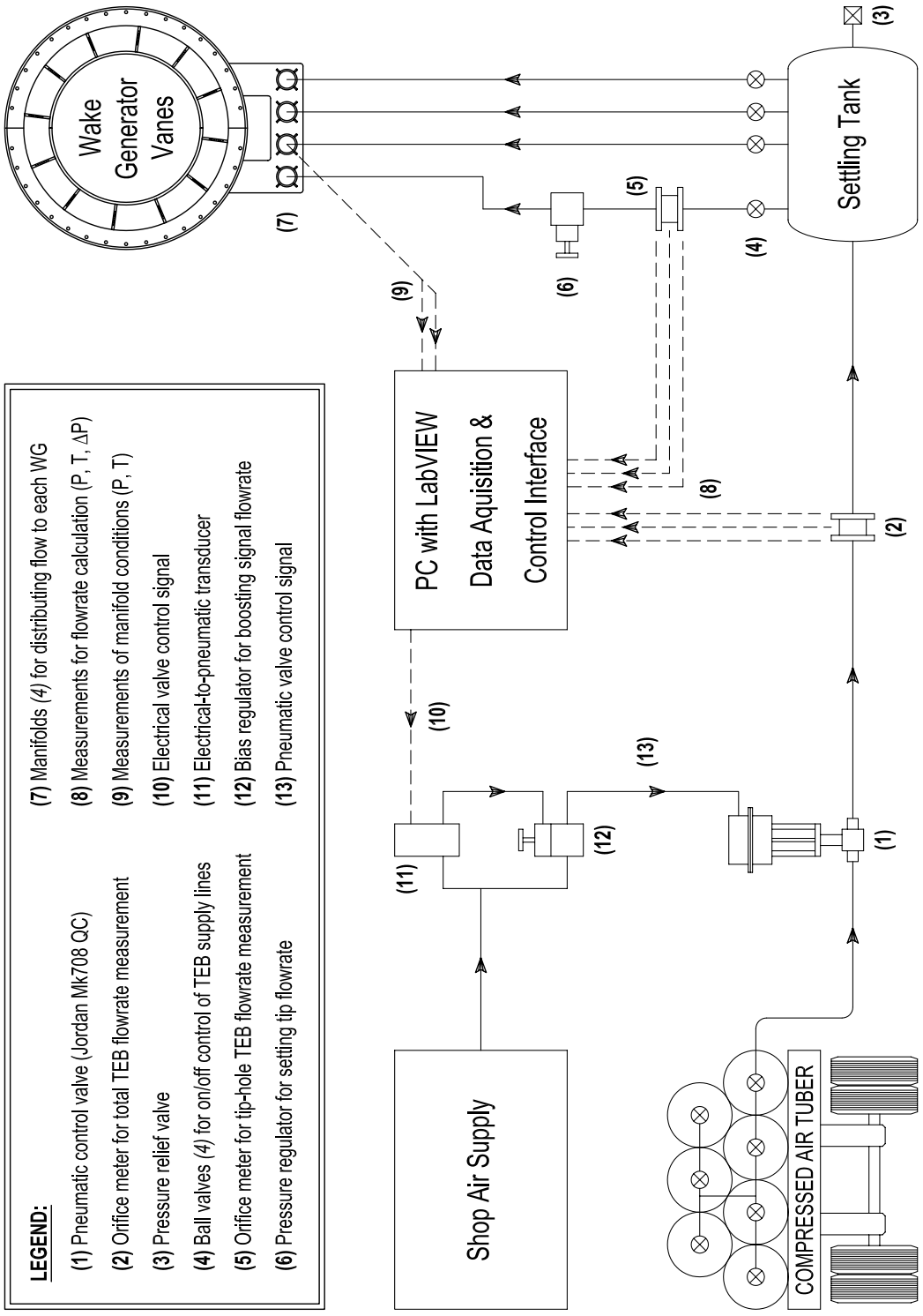

Figure 2.8: Schematic of the TEB flow distribution and control system.

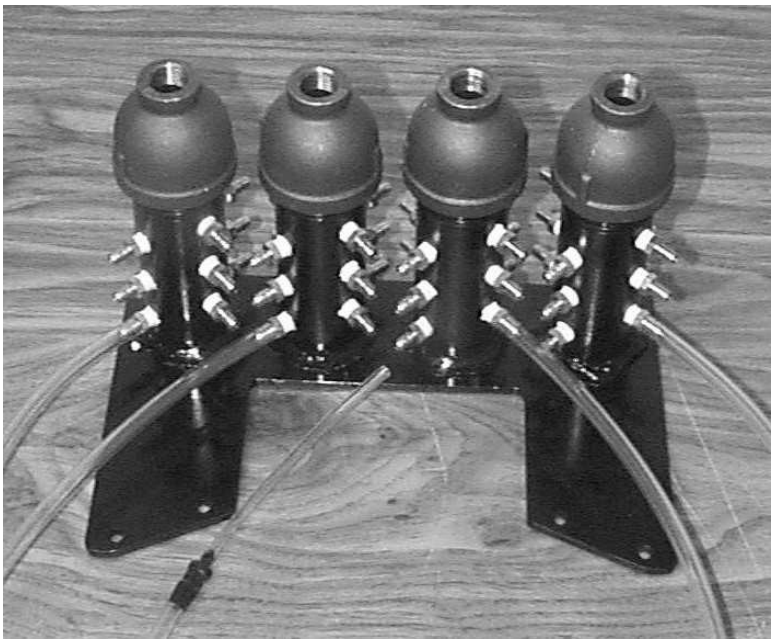

Figure 2.9: Array of four manifolds for distributing TEB flow evenly to the WG vanes.

ranging as high as 85 psig (586 kPa), distributed flow evenly by small diameter polyurethane tubing to the same radial sector of TEB holes of all 12 WGs (see Figure 2.10). The same length of tubing was used to connect between the manifolds and each respective blowing hole to ensure that the tubing pressure drops were consistent. Figure 2.11 illustrates the SMI rig assembly with manifolds and tubing installed for TEB.

The small-diameter tubing and the L-shaped TEB passages in the WGs (Figure 2.6) were rather restrictive for the typical TEB flow and hence produced a large pressure drop. This was the case because the plumbing was designed for installation ease and experimental flexibility rather than for minimizing pressure losses. Consequently, substantially higher blowing pressure ratios (that is, from the manifolds to the fan inlet) were required in the experiments than should be necessary for implementation of an efficient TEB plumbing design.

TEB flow characteristics for each of the four supply lines (including the rig-mounted plumbing and WGs) were measured by varying the supply pressure. The supply line for the

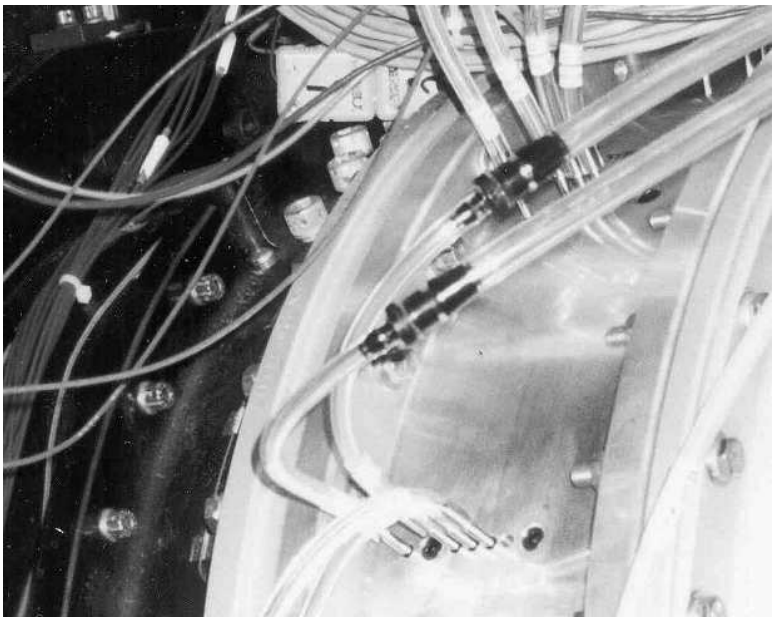

Figure 2.10: Detail of TEB tubing connection to the wake generators.

single blowing hole at the tip location had a distinct characteristic from the other lines, and hence required a separately regulated (and much lower) supply pressure. The other three lines, however, had similar enough flow characteristics that they could be fed from a common supply.

Hence, as shown in Figure 2.8, all four supply lines proceeded from a single settling tank, with a pressure regulator being used to adjust the tip flow supply line independently from the other three lines. Though flow through these three lines could not be independently regulated, it could be independently shut off by ball valves installed on each line. This feature allowed a basic means of controlling the spanwise TEB distribution, as will be elaborated for the specific TEB cases in Section 2.4.2.

The standard mode of operation for the TEB system involved the same mass flowrate being distributed to all of the blowing holes that were in use. This objective required that the supply line feeding the set of individual tip holes had to receive half of the flow to each of the other three lines, which each supplied a pair of holes on each WG. While the

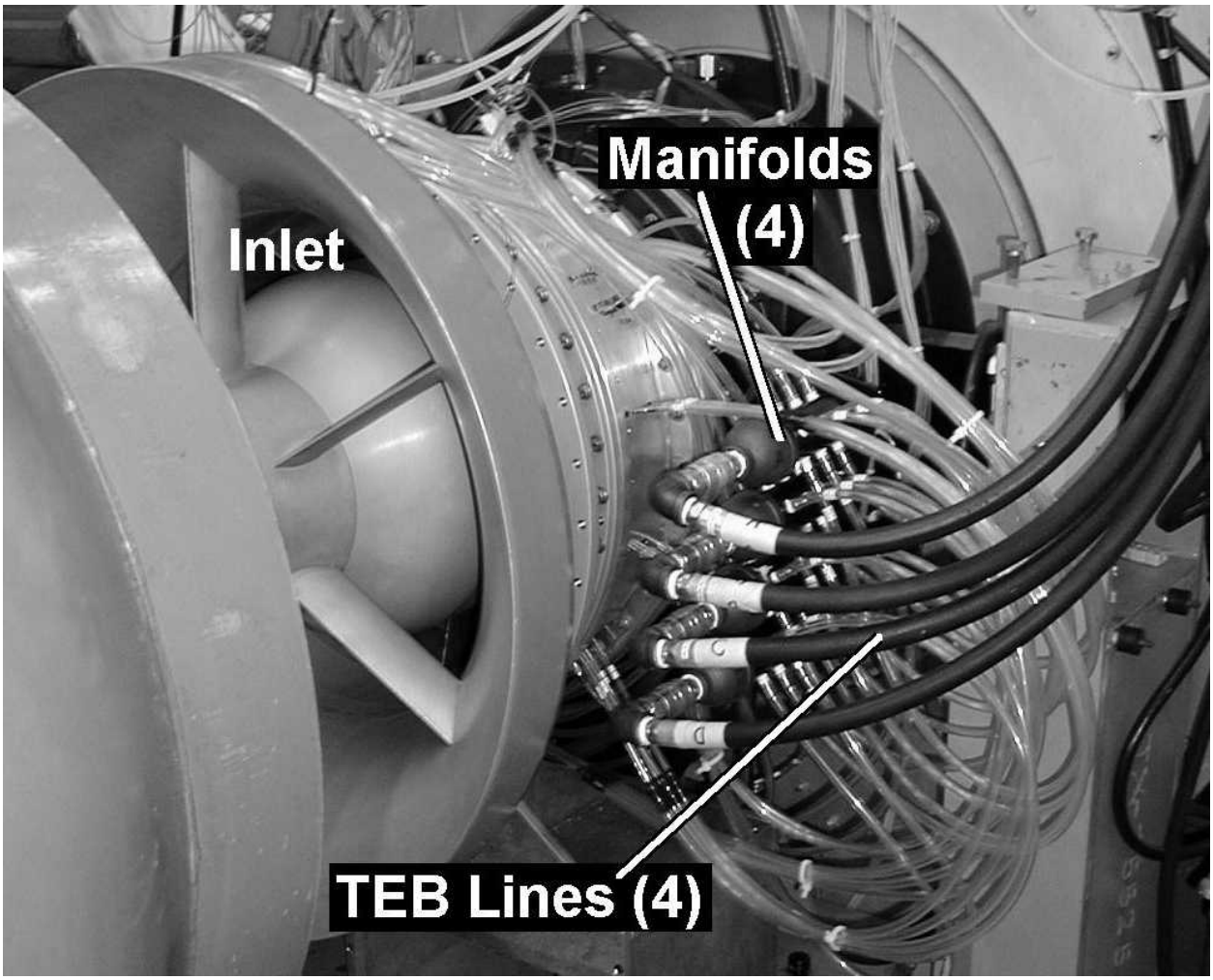

Figure 2.11: SMI rig assembly with TEB manifolds and tubing installed.

above-mentioned regulator provided the means of adjusting the tip flow proportion, it did not inherently ensure the correct proportioning.

To simplify the proper spanwise proportioning of the TEB flow and provide overall condition monitoring, a LabVIEW^{TM} PC-based data acquisition and control system was developed. The system acquired relevant data (see Section 2.3.2) and computed both the overall TEB mass flowrate (measured before the settling tank) and the TEB flowrate in the tip-hole supply line. Using the number of holes in use (per WG; e.g. 1, 3, 5, or 7) as a multiplier for the measured tip flow, the error in the overall flow proportioning was computed and monitored:

$$Error\,[\%] = \frac{\#\,of\;Holes\,Used \times Tip\,Flowrate - Total\,Flowrate}{Total\,Flowrate} \times 100\% \qquad (2.1)$$

The same flow proportioning comparison was used as the basis for a PID (Proportional-Integral-Derivative) feedback control algorithm. The basic control logic was as follows:

1. The tip flowrate set point was adjusted manually with the pressure regulator.

2. The tip flowrate measurement was scaled by the number of holes in use (per WG) to compute the target (i.e. properly proportioned) total flowrate.

3. The measured total TEB flowrate (feedback) was compared to the target total flowrate to define an error function.

4. The PID algorithm then attempted to minimize the error by adjusting the control signal, applied to the Jordan control valve, to increase or decrease the total TEB flow as needed.

However, this intended closed-loop control scheme was found to be unstable at much lower gains than were needed to support the desired flow. The instability was due to the highly nonlinear and hysteretic action of the valve (an effect of the high static friction of the valve

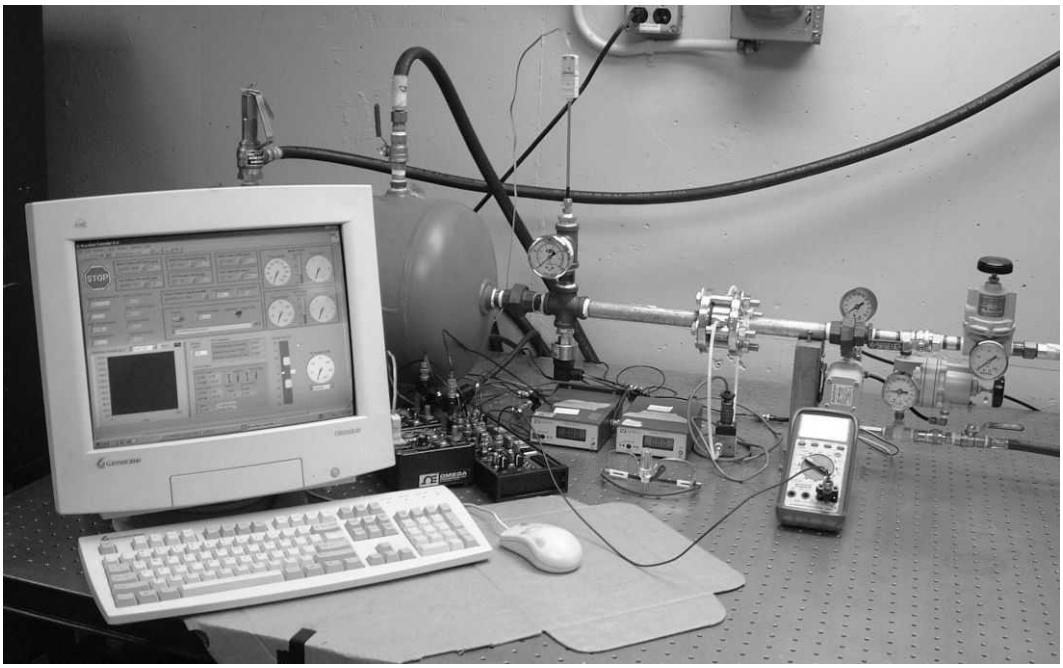

Figure 2.12: Overview of the TEB flow measurement and control station.

stem packing installed to withstand the maximum rated pressure of 5000 psi), and resulted in the valve rapidly alternating between fully-open and fully-closed positions.

While an additional valve "positioner" might have sufficiently linearized the valve action to allow closed-loop operation, it was decided for expediency to simply operate the valve in a manual (open-loop) fashion. This mode of operation involved the same control scheme as listed above, with the exception that the valve control signal was manually adjusted to minimize the error. For all of the TEB cases documented, the flow proportioning error was manually maintained within $\pm$ 5 percent. This level of error was deemed acceptable, since it was equivalent to the basic flow variation between paired holes supplied by a single line.

Since the flow control system, located downstairs from the rig and the rig control room, had to be manually supervised, communication between the flow control operator (the author) and the rig operators was primarily by means of 2-way radio. A picture of the TEB flow control system setup in the downstairs instrumentation room is provided in Figure 2.12.

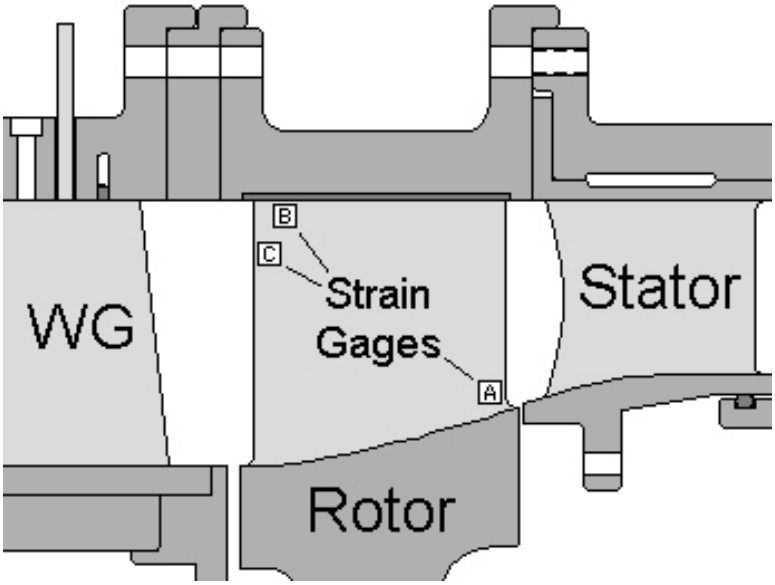

Figure 2.13: Strain gage locations for each of nine SMI fan rotor blades.

2.3 Measurements & Data Analysis

2.3.1 Forced Response

The SMI compressor rig was originally designed to investigate upstream wake influences on stage flow matching [32], and the rig has primarily been used for that and other aerodynamic investigations. However, with the adjustability of the WG forcing function and the addition of rotor-mounted strain gages, the rig has been demonstrated in recent investigations to be quite useful for forced response experiments. Forced response measurements were the focus of the present investigation.

As required for the initial mechanical checkout of the fan rotor, strain gages were surface mounted on the pressure side of nine rotor blades at each of the three locations, which are depicted in Figure 2.13. The locations, one at the trailing edge hub (denoted "A") and two near the leading edge tip (denoted "B" and "C"), were based on the recommendations of Cheatham and Tyner [32] for effective monitoring of key vibration modes.

The strain signals were extracted from the rotor via a slipring. To protect it from overheating at the high rotational speeds of the rig, the slipring was liquid-cooled. The strain signals and other dynamic signals, such as a once-per-revolution (1/Rev) key-phaser, were simultaneously recorded with a high-speed 28-channel analog tape recorder. Data was recorded at a tape speed of 60 inches per second (ips), which provided an effective bandwidth of 40 kHz.

The strain gage bridge circuitry was zero-balanced and calibrated for 10 ksi (69 MPa) per signal volt. Due to limitations of the data system front end, the signals could only be recorded in a DC-coupled manner. The DC-offset (corresponding to the time-mean blade loading) consumed much of the available dynamic range ($\pm$ 5 volts), such that alternating portions of the signal were often clipped due to voltage saturation. Though the mean component of the blade loading is certainly important for HCF considerations, only the alternating component (that is, the forced response) was expected to be substantially affected by the application of TEB flow control. Thus to ensure sufficient dynamic range for quantifying the alternating stress loads, the DC-offset was largely removed by rebalancing the bridge circuitry at 80% rotor speed.

Digitizing of data was performed during playback of the tape after the experiments. Because of the data buffering limit of the analog-to-digital conversion system, and in the interest of limiting file sizes, some effort was spent to see how low the sampling frequency could be while still providing sufficient resolution. A sampling frequency of 40 kHz was sufficient for the intended spectral analysis of the strain data. However, it was found that a higher sampling rate was needed to accurately resolve the 1/Rev key-phaser, required for the "order tracking" data analysis technique described in the following section. A sampling rate of 80 kHz provided sufficient definition of the sharply-rising 1/Rev pulsetrain without causing a buffer overrun. Anti-aliasing filtering was performed with a cutoff frequency of 32 kHz.

All of the selected channels (the 1/Rev and typically 8 responsive strain gage channels)

were digitized simultaneously, as required for the subsequent order tracking, at this higher sampling rate. Each 45-second rotor speed sweep (see Section 2.4.1) was digitized individually as a continuous block, yielding a typical ASCII-text raw data file size of 192 megabytes (MB) for each sweep. Data management was not a trivial matter, as digitizing and writing this volume of data to a high-speed networked hard drive took roughly 30 minutes per sweep. For this reason, less than one-quarter of the recorded rotor speed sweeps and channels were digitized and analyzed. Even this small fraction of the available raw data required 9 gigabytes (GB) of disk space in text form.

2.3.1.1 Order Tracking Analysis

After digitizing, rotor forced response data were post-processed in MATLAB© using engine-order tracking tools developed by the author. The following description is intended to provide an overview of the order tracking technique. Though developed independently, the present approach is equivalent to the computed order tracking technique, as described in more detail by Fyfe and Munck [34].

Order tracking is a very powerful tool for the analysis of rotating machinery. The primary advantage of the approach is that it provides a highly-effective means for extracting signal content that is synchronous, or correlated to rotor speed. Many forcing functions in rotating systems, including the WG and stator aerodynamic forcing functions in the current investigation, are correlated in frequency to *integer* multiples of the shaft speed, called *engine orders*. This fact is of course the basis of the Campbell diagram previously discussed, and illustrated in Figure 1.1.

Since forced response occurs at the same frequencies as the applied forcing functions, its magnitude and phase can be precisely followed, or "tracked", by engine order analysis. As a result, varying shaft speed is readily accommodated, a fact which allowed a wide test range for the present investigation. The order analysis approach is so effective at isolating synchronous signal content that it is also commonly used as a filtering technique for spectral

analysis of *asynchronous* phenomena in rotating environments, such as blade flutter [35].

The primary requirement for performing order analysis is that the data be synchronously sampled. There are several approaches for accomplishing this, including direct synchronous sampling, which typically uses hardware, such as an optical rotary position encoder, to trigger sampling by the analog-to-digital converter (ADC). An alternate approach, and the one presently used, involves the re-sampling of data which was originally sampled in the traditional fixed-frequency manner. The re-sampling approach, though presenting a substantial post-processing load, is often easier to implement and use, as it inherently preserves the time-domain information needed to correlate the data back to actual shaft speed.

To provide a conceptual overview of the re-sampled (or "computed") order tracking approach, the major steps of the process are itemized below. Though some of the details are specific to the current application, the basic approach could be readily adapted to suit other rotating machinery applications.

Summary of Computed Order Tracking Procedure

1. Strain gage signals are simultaneously digitized with the 1/Rev key-phaser signal to allow synchronization to shaft rotary position. A fixed sampling frequency of 80 kHz, sufficiently high to resolve several data points within the leading edge of the 1/Rev pulses, is used.

2. The 1/Rev pulsetrain is interrogated to establish precise "timing" of the start of each shaft revolution in the data file. Pulse leading (rising) edge detection is used, and timing is based on interpolation of the crossing of a reliable amplitude threshold.

3. Using the individual revolution timing data as a framework, a synchronous timing vector is generated by linearly interpolating the desired number of samples per revolution (fixed; in this case, 512) between the start times of each revolution and the successive revolution. Note that this interpolation assumes a high rotational inertia, such that the variation in shaft speed between successive revolutions can be approximated as negligible or linear. This assumption is completely reasonable for the present application, wherein the relative rate of change in shaft speed is quite low (always less than 0.01% speed change per revolution).

4. A corresponding vector of shaft rotational speed is generated for later use by considering the time difference between revolutions. Since the synchronous blade response is primarily a function of rotor speed (and thus only secondarily a function of time), this vector replaces the absolute time scale as the primary independent variable for the order analysis.

5. The strain gage data are then re-sampled by cubic interpolation from fixed time steps to the fixed shaft angle increments represented by the synchronous timing vector. The re-sampled data thus always include the same number of points per revolution, regardless of rotor speed, unlike the original time-sampled data.

6. The re-sampled data are then transformed to the "order" domain by FFT-based spectral analysis. Since the nominal repeating period for the synchronous forced response is a revolution, the complex Fast Fourier Transform (FFT) is computed for successive blocks of re-sampled data, with each data block corresponding to an integer number of revolutions (in this case, 4) that is taken to be quasi-stationary. For efficiency of the FFT computation, the number of revolutions used times the number of samples per revolution should be a power of two (e.g. $4 \times 512 = 2048 = 2^{11}$). Spectral magnitude and phase information are provided by the FFT, with each spectral line corresponding to a fixed engine order, regardless of how rotor speed varies.

7. From this point it is a comparably trivial matter to track the forced response to any particular engine order excitation by simply monitoring the spectral line associated with that engine order. Variation in magnitude and phase of any particular spectral line can be used to identify and quantify speed-related forced response phenomena (notably resonance crossings), as will be demonstrated in Section 3.1.

While the last point of item (6) may not be immediately obvious, it can be clearly understood by considering the analogy between order analysis and traditional time-frequency analysis. In time-frequency analysis, the *frequency* (events per *time*) of each spectral line in the FFT output is *fixed* for a fixed *sampling frequency* (number of sampled points per *time*) and number of points considered in the FFT computation. For the synchronous re-sampling used in order analysis, the *engine order* (events per *revolution*) of each spectral line in the FFT is likewise fixed for a fixed *sampling "frequency"* (number of re-sampled points per *revolution*) and number of points considered in the FFT computation.

The fact that spectral lines become fixed to specific engine orders (which can be easily prescribed to coincide with known synchronous forcing functions) is the basis for the greatly increased forced response tracking precision of order analysis over traditional time-frequency analysis. The re-sampled synchronous forced response signals are still non-stationary, but

they are non-stationary *only with respect to variation in rotor speed*. However, the same variation in rotor speed produces a forced response that, when analyzed from the original time-sampled data, is *non-stationary in both time and frequency*. The resulting frequency resolution error makes time-frequency analysis less accurate for measuring and tracking synchronous content. While increasing the sampling rate can improve the accuracy of the time-frequency approach, order analysis makes clever (and more efficient) use of the fact that the forced response of primary interest occurs at precise and predictable multiples of the shaft speed.

A basic sensitivity study was used to optimize the computed order tracking approach for the present study. Order analysis was compared for a number of different cases, by selectively adjusting the key analysis parameters (including, but not limited to, the interpolation parameters used for the 1/Rev pulse timing and synchronous data re-sampling, as well as the various spectral analysis parameters). The effects of these adjustments on the output of the order analysis was evaluated, and sensitivity to most of the parameter variations was found to be rather small. The final order analysis parameters were then selected to provide the most reliable results.

Computational efficiency was also given consideration in the selection of the various analysis parameters, since post-processing the many large data files by the computed order tracking approach was rather time-intensive. Performing order tracking analysis on a single speed sweep took about 10 minutes using a 1.8GHz Pentium 4 Workstation with 1.5 GB of RAM. It took much longer on a more standard desktop computer (nearly 30 minutes on a 933MHz P3 with 512 MB of RAM), primarily due to heavy reliance on inefficient "virtual memory" (that is, using hard disk space to compensate a shortage of physical RAM memory). Order analysis output files were written in the form of magnitude tracks over the rotor speed range for the first 60 integer orders of each strain gage signal, using only about one-tenth of the disk space required for the raw data.

2.3.1.2 Uncertainty

Precision errors were deemed to be more important than measurement accuracy, since the purpose of the investigation was to make relative response comparisons between different test configurations (rather than to quantify absolute levels of forced response). Accordingly, overall uncertainty was defined in terms of the measured response repeatability, which is discussed in the Results chapter (see Section 3.1.3). The following discussion is limited to the instrumentation- and analysis-related errors, the effects of which are inherently included in the overall repeatability uncertainty reported later.

Excepting the basic digital quantization error, direct quantification of the strain gage measurement error was not feasible. Quantization error, based on one-half of the least significant bit (LSB), was rather small at 0.02 ksi peak-to-peak (just 0.35% of the average measured resonance amplitude).

Using properly normalized data (such as shown later in Figure 3.8) from the *different gage locations* on the *same blade*, it was found that the gages provided very consistent resonance amplitudes (generally within one percent) across the range of TEB. While this is not a reliable means of quantifying measurement uncertainty, the consistency of the gage-to-gage comparison eliminated concern as to whether the gages were capturing the true blade response. This point is generally taken for granted with most measurements. However, due to repeatability issues (see Section 3.1.3) and the unknown impact of a variety of other factors (e.g. slipring noise effects on the as-then-unamplified, and often small, strain signals; speed-related intermittency of some strain signals; propagation of interpolation errors in the order analysis) in the present investigation, it was worthwhile to seek some confirmation of the measurement reliability.

2.3.2 Trailing Edge Blowing

Trailing edge blowing flow was routed to the set of wake generator in the SMI compressor as described in Section 2.2.3. A control scheme was used to maintain, as best as possible, a uniform flowrate to each of the TEB holes being used.

The primary TEB measurement of interest was the total massflow supplied to the wake generator vanes. This data was acquired using an orifice meter (item 2 in Figure 2.8), in conjunction with measurements of the orifice differential pressure and upstream static pressure and temperature.

Some other data were recorded that are not reported with the results. Combined flow to the tip holes of all the WGs was measured, as part of the control system (Section 2.2.3.3), to insure proper proportioning of the tip flow with respect to the other holes. In addition, TEB supply static pressure and temperature were monitored in one of the rig-mounted manifolds. These data were recorded for future consideration of aero-thermodynamic performance of the TEB-equipped stage, an aspect not presently addressed.

2.3.2.1 Data Normalization

With the exception of data presented in Appendix B, TEB flowrates are presented in normalized form. Because the TEB wake-filling concept is based on momentum addition to, and exchange with (i.e. mixing), the wake flow, it is intuitive to normalize the TEB input by the baseline wake momentum deficit, as done by Wo et al. [29]. This, however, requires detailed wake profile measurements unavailable for the broadly varying TEB and wake conditions of the present study.

Taking the viewpoint of the engine designer, it is more useful to consider the blowing input in terms of some relative "expense" to the engine's operation. In extending the present application to a hypothetical engine installation, the compressed air requirement for TEB would most likely be satisfied by bleeding and recirculating a fraction of the compressor

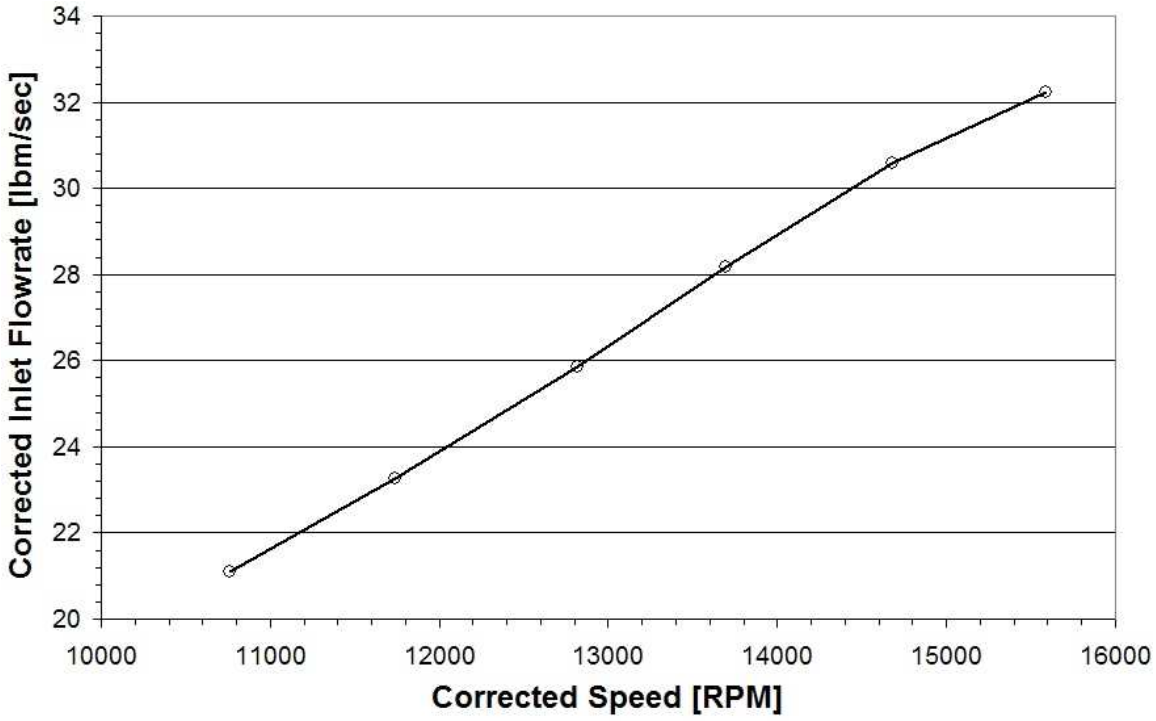

Figure 2.14: Rig inlet flow characteristic for the chosen operating line.

throughflow. Thus, it was deemed most useful to normalize the TEB mass flowrate as a percentage the rig inlet flowrate.

Because forced response data will be presented with respect to various resonance crossings, each occurring at a different rotor speed, the rig inlet massflow *at the particular speed of the resonance* was used as the normalizing factor. The variation of rig inlet flowrate as a function of fan rotor speed is provided in Figure 2.14. Using the steady aerodynamic measurement system described by Gorrell [36, 33], this data was acquired with the rig throttle set to represent the same near-design operating line used for the forced response data collection. The selected operating line is illustrated with respect to a partial compressor map in Figure 2.15 for the 12 WG configuration.

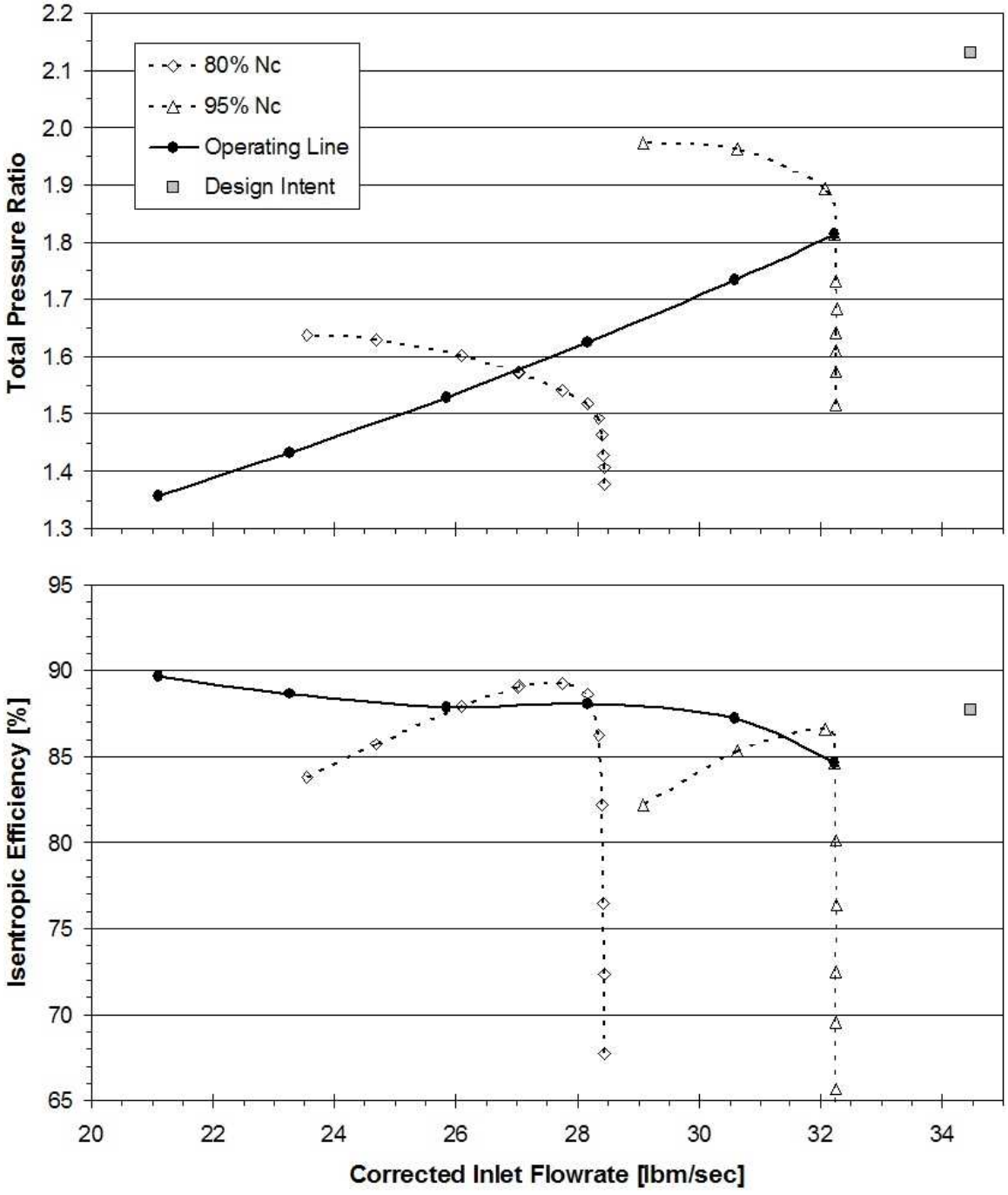

Figure 2.15: SMI fan maps illustrating the selected operating line.

2.3.2.2 Uncertainty

Uncertainty in the TEB massflow measurement was less than ± 1%. However, there was some difficulty in maintaining a completely steady flowrate, particularly at the highest flowrates, over the duration of a given run. The tendency during each 45-second rotor speed sweep was for the TEB flowrate to drop slightly due to the decline in supply pressure as the tuber was slowly depleted.

Had the TEB active control system (see Section 2.2.3.3) worked as intended, such variations would have been virtually eliminated. However, problems with stability of the control system forced the use of manual control. The same highly non-linear valve action (small "jumps" instead of continuous response to the control signal) that had caused the active control instability also meant that very fine manual adjustments could not be made. Despite the resulting tedious task of sometimes making minor adjustments during a given sweep, the massflow was held steady within ± 1% of the mean flowrate, as illustrated for a typical sweep (at a medium flowrate for the tested range) in Figure 2.16. This variation was acceptably small, so the average flowrate from each run was used to represent the entire run.

Thus the *overall uncertainty in the total TEB flowrate was within ± 2%*. Though it was not confirmed by direct measurements, it is believed that the manifold and consistent tubing length resulted in each WG receiving the same amount of TEB flow (i.e. 1/12 of the total flow). However, the reader is reminded that hole-to-hole flowrate variations of a given WG, primarily due to the geometry of the internal passages, were estimated to be up 5%.

2.4 Test Conditions & Procedures

2.4.1 Rig Conditions

Several resonance crossings were identified from the Campbell diagram as being potential HCF drivers for the 12-WG configuration. The fundamental 12E crossing of the first torsional

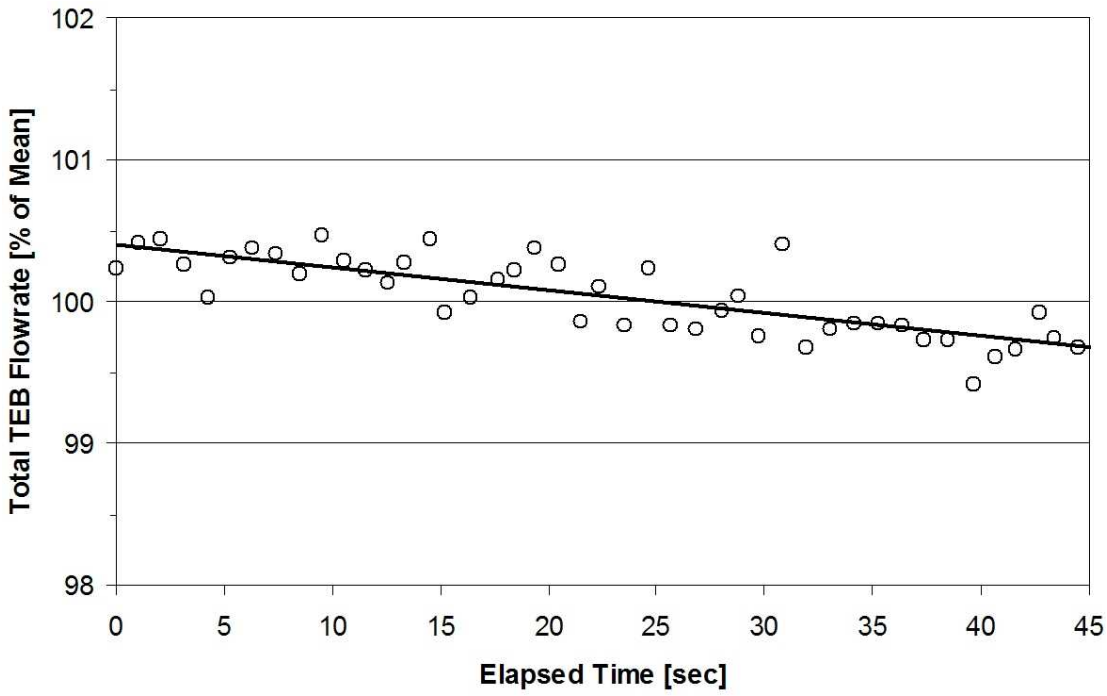

Figure 2.16: Time history of total TEB flowrate for a typical sweep.

mode (1T/12E) near 12,800 rpm was known to be particularly severe. Harmonic crossings were also of interest, including those of the second leading-edge bending mode (LE2B/24E) near 13,600 rpm and the second chordwise bending mode (2C/36E) near 11,600 rpm. These crossings, as well as a pair of Mode 7 crossings, are indicated by circles in the Campbell diagram given in Figure 2.17. To encompass these and various higher order modal crossings, a test range from 11,000 rpm to 16,000 rpm (67 - 97% of design speed) was selected, as indicated in the figure.

The modes corresponding to the circled crossings of Figure 2.17 are illustrated in Figure 2.18. The colors indicate relative local blade deflections for the respective modes, from which the modeshapes can be inferred. The red color represents the highest deflections and white corresponds to negligible deflection. Strain gage locations are also indicated on the blades by the black rectangles; the "A" gage is at the trailing edge hub, the "B" gage is near the leading edge tip, and the "C" gage is located at about 75% span along the leading edge.

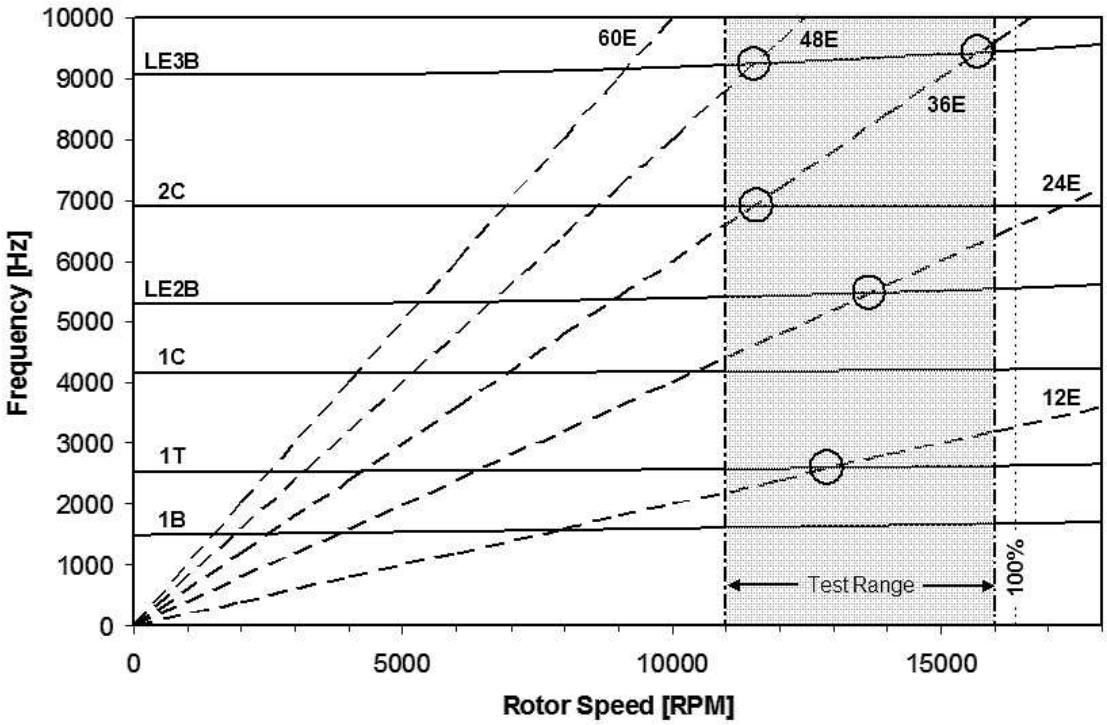

Figure 2.17: Campbell diagram for SMI fan rotor showing test range.

It is important to note that the gages respond to the local blade *strain* (from which the stress in inferred), not the overall deflections. The reader is reminded of this point to avoid confusion, since the deflection contours are provided while the stress contours are not. Damage is most likely to occur where the stresses are highest, which is typically at locations where the deflections are low. For instance, the highest stress for the 1T mode occurs at the trailing edge root, while the deflections there clearly go to zero due to the rigid connection with the disk. Hence, for the 1T mode, the "A" gage is by far the most responsive.

Rotor forced response is expected to be somewhat loading sensitive. However, to limit the overall test matrix, it was decided not to investigate different loading conditions. An unloaded condition (i.e. wide-open throttle) would tend to produce higher responses, but this would not be representative of normal operation. Thus an operating line was selected, based on clean inlet aerodynamic performance mapping, and controlled by an exit flow throttle, to

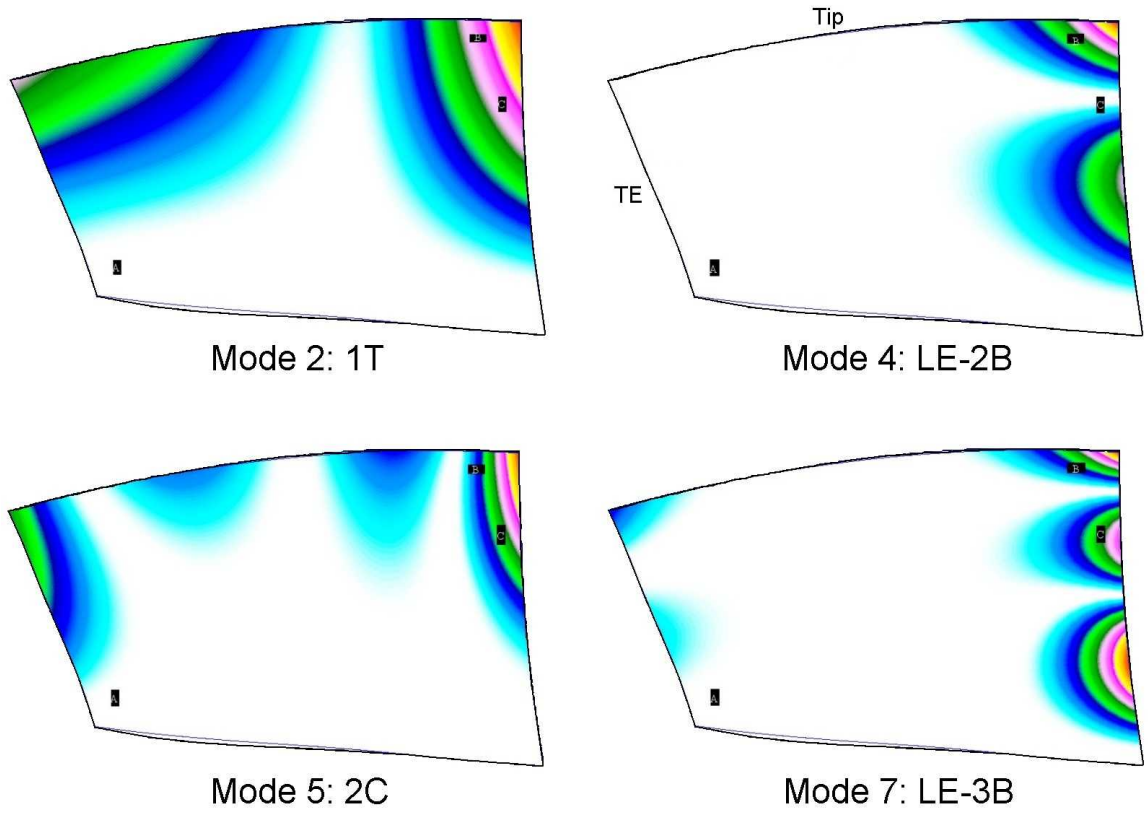

Figure 2.18: Predicted SMI fan vibration modes, colored by displacement (from [37]).

represent near-design loading (again, Figure 2.15).

The loading was set a little below peak-efficiency to maintain an appropriate degree of surge margin at the higher rotor speeds. This operating line was maintained by the same nominal throttle setting for all of the forced response data collection. However, as will be discussed in Section 3.1.3, some forced response repeatability error was found to be introduced by hysteresis effects in adjusting the throttle position. Throttle re-positioning was required every time the rig speed was brought up to the test range from idle.

2.4.2 TEB Conditions

The baseline condition, against which all flow control cases were compared, was with no TEB flow applied to the WGs. To ensure the same nominal baseline forcing function, the same set of WGs (with TEB holes) was used. The presence of the holes was not believed to affect the baseline flow.

As described in Section 2.2.3, two primary TEB variables were available for altering the baseline WG forcing function. The primary control variable was the total TEB flowrate, with a manifold system being used to distribute flow identically to all WGs. As a secondary control variable, the WG-spanwise (that is, radial) TEB distribution could be varied by selectively shutting off any of the four independent supply lines. To limit the test matrix, it was decided to only test a relatively simple set of four distinct spanwise variations, each of which was evaluated over a range of TEB flowrate. These cases are illustrated in Figure 2.19.

The initial case, referred to as *7-hole* or *full-span TEB*, was the most widely tested and involved flow to all seven holes per WG. It is noted that this case does not actually provide complete or uniform spanwise coverage; as shown in Figure 2.19a, roughly 20% of the span near the hub is left unaffected by the 7-hole TEB (or the endwall boundary layers). It is also expected that wake-filling effectiveness is somewhat reduced between the blowing holes as compared to directly downstream of the holes.

It is called "full-span" TEB because it covers as much as of the span as was feasible with the geometric constraints of the TEB plumbing design and WG thickness distribution. Additionally, even if it were feasible, extending the TEB coverage (further towards the hub) was expected to contribute little to any overall forced response reduction, since blade deflections, and hence modal receptivity to input force, approach zero at the fixed hub connection.

The remaining three TEB configurations are collectively referred to as *part-span TEB*. As portrayed in Figures 2.19b-d, these cases are achieved by progressively turning off flow to spanwise pairs of holes, beginning at the hub, thereby providing a wide variation in spanwise

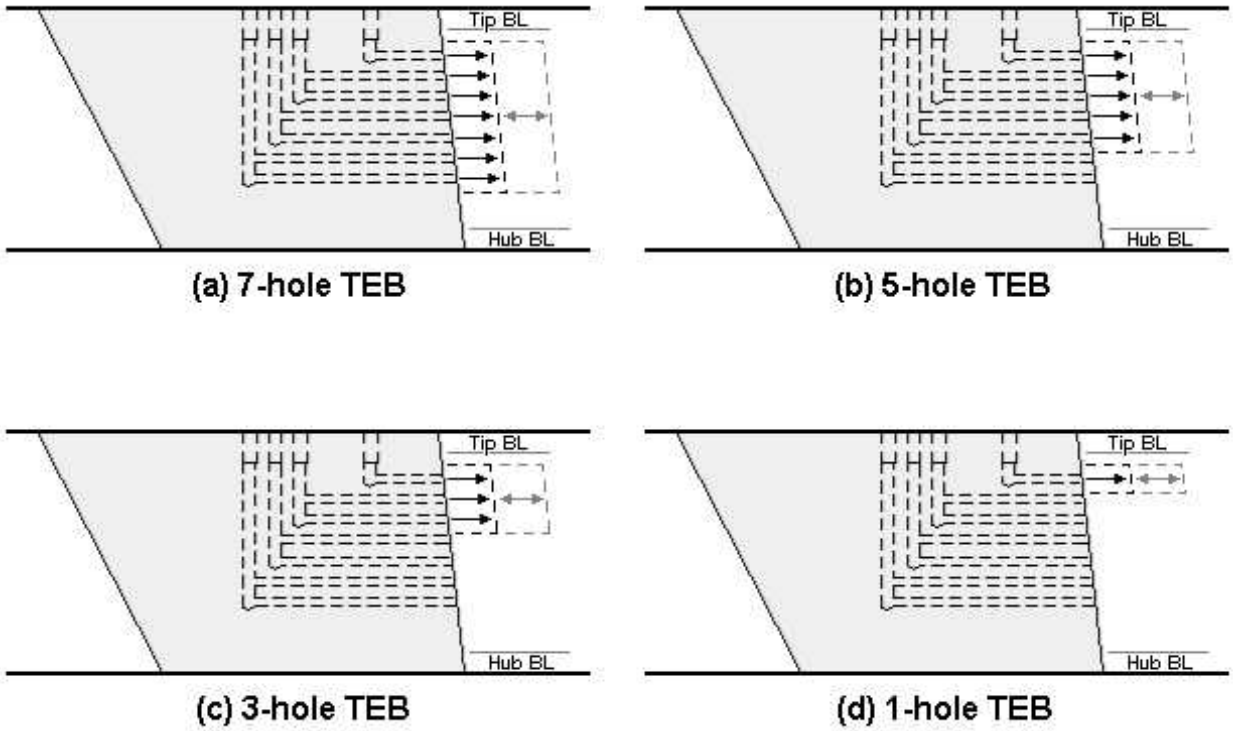

Figure 2.19: TEB test cases, with uniformly-distributed, variable-magnitude flow to different spanwise sectors.

TEB coverage. To maintain a uniform distribution within the sector of TEB application, the same flowrate was supplied to each hole in the sector, but with the total flowrate being variable. Because of resource limitations, the part-span cases were evaluated for a reduced number and range of flowrates (as compared to the full-span configuration).

2.4.3 Test Procedures

After starting the rig, it was run for about ten minutes at idle and again at 80% speed as part of a standard warm-up procedure. Strain gages were monitored to identify any failed (or failing) gages, and data channels were reconfigured as necessary to make sure as many good gages were recorded as possible. The exit flow throttle was then moved to the same nominal position (near-design loading), and the strain gage circuitry was re-balanced at 80% speed

(nominally 13,100 rpm). For an explanation behind this latter step, the reader is referred back to Section 2.3.1.

The rig speed was then brought to 11,000 rpm in preparation for the first speed sweep. One or more baseline (again, no TEB) 45-second speed sweeps were conducted by the rig operator over the test range (11,000 to 16,000 rpm). During this sweep, a second operator recorded the dynamic signals (primarily the strain signals) with the analog tape system while visually monitoring the critical gage responses with oscilloscopes.

After completing the baseline data collection, the TEB flow control system was prepared downstairs from the test cell and the rig control room. This system is described in detail in Section 2.2.3.3. References to item numbers in Figure 2.8 are included below in parentheses to aid explanation of the TEB test procedure.

The appropriate supply lines (4) were opened to match the desired WG spanwise TEB distribution, and the valves corresponding to the desired bank of air cylinders on the tuber were opened to charge the line to the control valve (1). Control voltage (10) was then applied to gradually open the control valve and initiate flow to the wake generator vanes in the rig. The control voltage was slowly increased until the total flowrate, monitored by the LabVIEW^{TM} control system, was close to the desired value. The tip flow was then specified by a regulator (6), which steadily maintained the desired tip flow for moderate fluctuations of the upstream supply pressure. With assistance of an error display on the PC, the control signal was manually adjusted such that the total flow was properly proportioned with respect to the tip flow.

Upon reaching this desired flow setting, a call was given via 2-way radio to the rig operator to initiate a 45-second rotor speed sweep through the test range. At the same time the second test operator began recording the strain gage signals on tape, while the flow control operator (the author) recorded the pertinent TEB data. Two sweeps were typically recorded for redundancy at each TEB setting. Because of the time-intensive nature of the data post-processing, though, typically only one of sweep at each condition was analyzed.

For much of the data collection, the TEB flowrate was adjusted in small increments, which allowed sweeps to be conducted with minimal delay. However, substantial changes in the TEB flowrate or configuration sometimes required a delay between sweeps on the order of 30 minutes (e.g. for changing the internals of the control valve to accommodate a different flow range).

During these extended delays, the rig was either brought down to idle speed, or shut down altogether, either of which required the throttle to be opened to avoid compressor surge. Only after the conclusion of the experiments was it discovered that new baseline data should ideally have been collected after each throttle adjustment (despite the same nominal position setting). It is believed that collection of new baseline data for each respective throttle adjustment would substantially reduce the repeatability uncertainty associated with the normalized TEB forced response measurements (to be discussed in Section 3.1.3).

Chapter 3

Results & Discussion

Before entering into a detailed discussion of the results, it is worthwhile to orient the reader with some introductory comments regarding the approach and scope of the discussion. While the overall applied research program was rather multi-disciplinary, and consequently had many facets and phases, the following discussion is an attempt to concisely focus on the ultimate objective, and primary contribution, of the undertaking. This ultimate objective was, for the first time, to apply a stator wake management scheme in a typical modern transonic compressor, and to document the effects of that scheme on the aerodynamically-forced response of the downstream rotor blades.

As a preliminary step in the program, a wake management scheme suitable for the high-speed compressor application had to be developed. Since no such scheme was found to be documented in the open literature, this development is itself a useful contribution. However, since it was only a supporting element of the overall program, the development took the form of design iterations in a somewhat rudimentary bench test environment, simulative of the specific compressor application. Thus the findings of this developmental phase, though necessary and sufficient for the present application, are neither exhaustive nor of implied applicability to other wake management applications. Accordingly, only a brief discussion of this phase and its results are provided as Appendix A.

3.1 Baseline Forced Response

Two primary forcing functions acted on the rotor blades during the experiments conducted in the SMI transonic compressor rig. An aerodynamic forcing function, comprised of both vortical and potential components, was generated by the 12 wake generator (WG) vanes installed upstream of the rotor. Additionally, an upstream-propagating potential forcing function was generated by the 49-vane stator row installed downstream of the rotor.

The WG and stator forcing functions are synchronous in nature, which means they are directly correlated in frequency to integer multiples of the rotor shaft rotational speed, called engine orders and denoted by "E". The forcing functions are also both composed of an infinite series of harmonics, with respective fundamental 12E and 49E components.

The computed order tracking approach, described in Section 2.3.1.1, was used to extract synchronous magnitude and phase content from the raw signals. While only the harmonic engine orders corresponding to the two known aerodynamic forcing functions (12, 24, 36, 48, 49 and 60E) were of primary interest, all synchronous orders up to 60E were evaluated to check for any additional excitation sources, whether unidentified or assumed negligible (e.g. 6E excitation from the six inlet support struts installed far upstream). It is worth mentioning that turbulent fluctuations around the time-average WG forcing function will spread some energy to non-synchronous frequencies, but this contribution to the overall forced response is very small by comparison and not presently addressed.

The effectiveness of the order tracking technique for extracting and distinguishing synchronous components from the non-stationary strain signals is demonstrated in Figure 3.1. The different lines in the figure represent various harmonics of the known aerodynamic forcing functions, extracted from a single strain gage signal during a single speed run-up at baseline (no TEB) conditions. As is the case for all forced response data presented here, stage loading was set by an exit flow throttle to represent a design operating line. Multiple resonance crossings are clearly characterized by the various peaks in the figure.

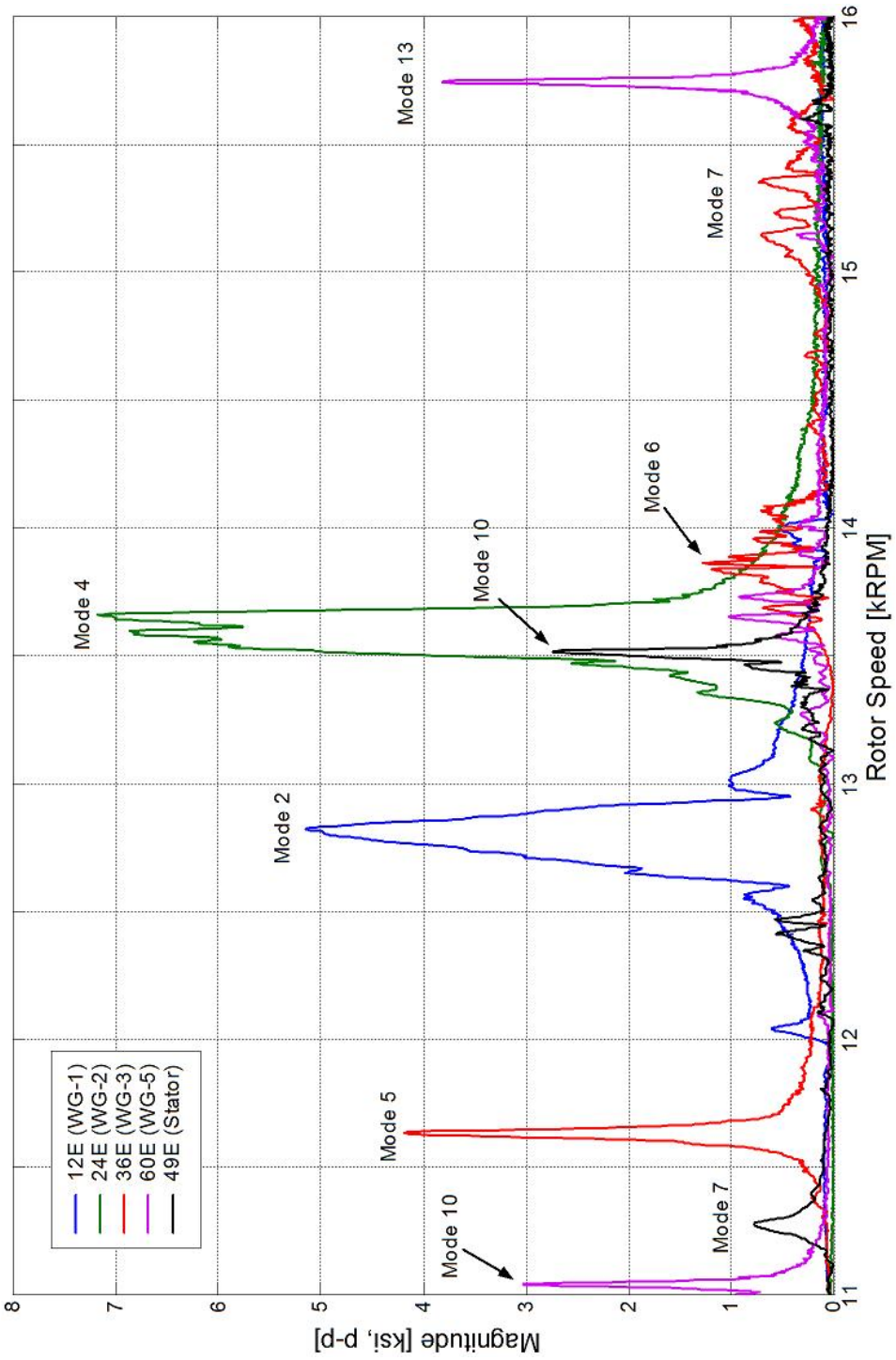

Figure 3.1: Baseline order tracks of a strain gage signal, showing multiple modal resonances due to upstream WG and downstream stator excitations.

Mode identities, as labeled in the figure, were confirmed by mutual comparison of order magnitude and phase tracks with previous modal analysis of the rotor. Although the first torsion response was noted in the previous chapter to be particularly severe, the observant reader may note that it is neither the largest response *in this figure* (denoted as "Mode 2"), nor does it appear to be particularly severe at only about 5 ksi peak-to-peak. However, the figure includes data from the "B" gage location, which is not nearly as responsive as the "A" location for the first torsion mode. For comparison, see the ("A" gage) response of "Blade 22", presented subsequently in Figure 3.2. It is further noted that none of the three gage locations actually coincide with the maximum first torsion stress location, nor is Blade 22 the most responsive (i.e. critical) blade for first torsion.

Cheatham and Tyner [32] documented SMI fan blade modes and frequencies with data from impact testing, finite element analysis, and holography at static (zero-speed) conditions. Using an improved finite element model, Blackwell [37] recently computed the blade modes and frequencies across the operating speed range, to account for blade stiffening due to centrifugal effects. Blackwell's analysis also yielded estimated ratios between the predicted max stress for each mode and the stress predicted at each of the three strain gage locations. Some of these data are included later (in Table 3.1) for comparison with the forced response measurements presently documented.

3.1.1 Blade-to-Blade Response Variability

A large degree of variability was observed between the resonant responses of different blades. This is illustrated in Figure 3.2 for the crossing of the fundamental 12E excitation and the second blade mode, first torsion (hereafter referred to as 1T/12E). The figure includes simultaneous data from the "A" gage location of four blades. The peak amplitude of the maximum responding blade is 55% greater than the mean peak amplitude from the four blades.

While small differences in the mechanical damping properties of the individual blades

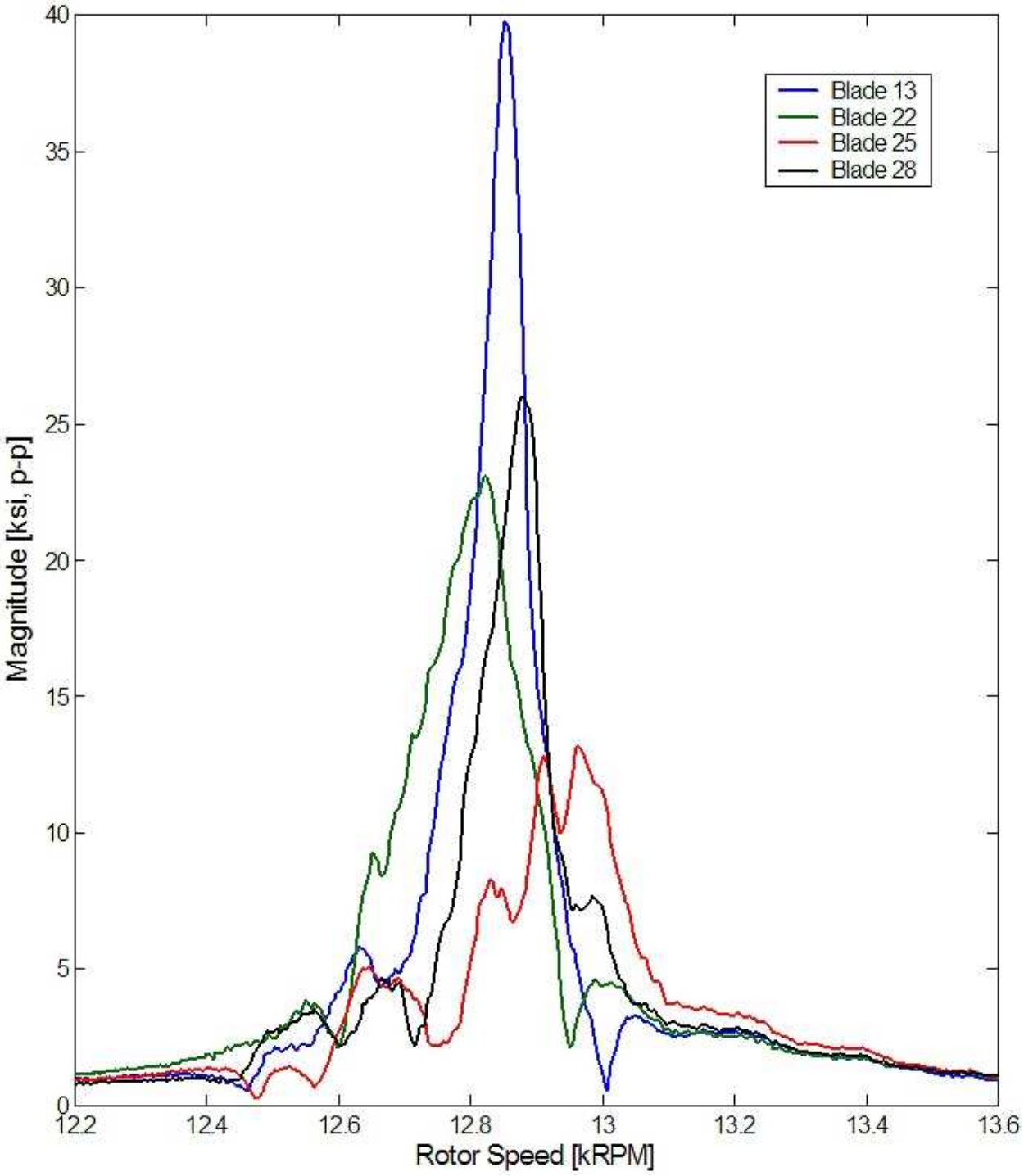

Figure 3.2: Blade-to-blade variability of 1T/12E Response.

may be present, this hardly accounts for the degree of blade-to-blade variability observed in the resonant response. Moreover, aerodynamic damping is generally dominant at resonance for low-aspect ratio bladed disk assemblies, which inherently have very low mechanical damping [2, 38].

Some degree of the blade-to-blade response variation is likely due to error in the positioning of individual strain gages. Because of the large stress gradients near the gage locations for certain modes, small errors in gage positioning could yield significant error in the stress measurement (with respect to the nominal location). However, no gage position certification or modal sensitivity analysis has yet been conducted.

The considerable variation in response is largely attributable to mistuning effects, which have been widely investigated as a typical and important characteristic of bladed disk assemblies. Small differences in blade geometry, owing to machining tolerances and asymmetric wear [39], yield small variations in the natural frequencies of the blades (hence the "mistuned" descriptor) [40]. In addition to this structural mistuning, blade passage deviations can also introduce aerodynamic mistuning.

Because of the integral construction, there is significant coupling between the motions of the disk and its blades. Consequently, energy associated with the resonance of one blade may be structurally transmitted to another blade with a slightly different natural frequency. Aerodynamic coupling also plays a substantial, if not dominant [38], role.

Depending on the mistuning pattern (i.e. the degree of variation and circumferential sequencing of the blade natural frequencies), the inter-blade phase angle (a function of the number of blades and the order of the excitation) and the mode in question, the response of a particular blade may be preferentially amplified or attenuated. Many studies have been dedicated to the analysis of mistuning patterns and their effects, including prediction of the maximum responding blade [41, 38], and even the use of intentional mistuning patterns as a passive means of vibration mitigation [39].

As discussed by Rao [3], the mistuned blade interactions are generally quite complex.

Mistuned response phenomena typically include, as noted in the present investigation, resonance peak splitting and the appearance in one blade's response of multiple distinct peaks related to the natural frequencies of other blades on the disk. In the interest of thorough and accurate mistuning analysis, Rao stressed the importance of knowing all of the blade natural frequencies.

That substantial mistuning effects were observed in the present rotor response is not surprising. After all, a real rotor blisk, manufactured in typical fashion and with inherent blade geometry variations, was used. The measured response variability is also consistent with results from a numerical study by Kahl [38]. Using a basic structural model with coupled aerodynamic forces, Kahl evaluated the 1T response of 500 randomly mistuned permutations of a transonic compressor blisk rotor. Only a small fraction of the cases yielded any reduction in response (compared to the tuned case), while as much as *40% increase* in response was noted.

Thus the large and complex measured blade-to-blade response variability underscores the strong, and seemingly unavoidable, role that mistuning plays in the current generation of high-speed compressors. Although it is not the purpose of this document to discuss the mistuning effects in depth, it is nonetheless important to make some mention of these effects, as they necessarily influenced the approach to data reduction and presentation, as discussed in the following sections. Additionally, mistuning effects have some role in the experimental repeatability (see Section 3.1.3).

3.1.2 Maximum Resonant Response

3.1.2.1 Critical Blade Selection

Since the high amplitudes associated with resonant vibration are the primary contributor to high-cycle fatigue, it is logical to focus attention on the data available at resonance crossings. In view of the large blade-to-blade response variability discussed in Section 3.1.1, it was

decided to primarily present results for the maximum responding blade, hereafter referred to as the "critical" blade, for each measured modal crossing. The blade number identified as critical can and does vary depending on the mode in question, but it does not depend on which of the relative gage location compared. In some cases, amplitude results are also presented in a multiple-blade-average form, based on all available measurements for a given modal crossing and relative strain gage location.

It is important to note that the critical blade is not necessarily the blade most likely to experience an HCF failure, nor is the maximum stress location on the failing blade necessarily the location where the failure will originate. More specifically, fatigue damage (e.g. crack propagation) will occur anywhere the overall stress (from applied and induced forces) exceeds the local material limits, which can be substantially reduced by a variety of factors (e.g. stress concentrations resulting from the basic geometry, material flaws, impact damage, or thermal gradients). A fatigue failure will first occur, often catastrophically, when and where the ultimate residual strength is reduced by cumulative fatigue damage below the instantaneous applied load.

Moreover, since measurements are not available for all blades, there is no guarantee that the identified "critical" blade is in fact the maximum responding blade. Nonetheless, given the available measurements and the impracticality, even impossibility, of accurately quantifying the influence of the various stress-amplifying factors on a per-blade basis, the most logical approach is to concentrate attention on the blade with the highest measured response.

3.1.2.2 Quantification of Peak Crossing Amplitude

For crossings exhibiting a sharp, single-peaked response (e.g. modes 2, 5, 10/60E and 13 in Figure 3.1), quantification of the peak amplitude is a simple matter, at least with the resolution afforded by the order tracking technique. However, for some crossing responses on various blades, complex phenomena, such as peak splitting or multiple distinct peaks, are

observed (e.g. modes 4 and 7/36E in Figure 3.1).

These phenomena, attributable to the mistuning effects discussed in Section 3.1.1, make selection of the peak crossing amplitude a less straight-forward task due to the multiplicity of local maxima. Since the amplitude of the alternating blade stress is of primary significance to HCF, and for obvious convenience, the convention used for the present work was to define the resonant amplitude as simply the highest amplitude anywhere within the modal crossing region (as opposed to including any consideration of phase, which was often complicated by the mistuning effects).

In keeping with the convention most commonly used in fatigue analysis, amplitudes of the measured alternating stress components are given in peak-to-peak (p-p) form (except as indicated in Appendix B). Though normally used in fatigue analysis to account for non-zero mean stress contributions, the "R-factor" (ratio of maximum to minimum stress) is not included in the present work, since the mean stresses were not documented. This is not to imply in the least that the mean stresses are inconsequential to the fatigue life; however, for simplicity, the mean component was ignored since it is principally unaffected by the unsteady aerodynamic forcing functions.

3.1.2.3 Summary of Critical Blade Response

Though not obvious from the gage location represented in Figure 3.1, the largest response amplitude in the test range occurred for "Mode 2", i.e. at the 1T/12E crossing. This resonance is represented for multiple blades in Figure 3.2. The highest measured, or critical, 1T response (Blade 13) reached 39.7 ksi (274 MPa) p-p at the "A" gage location.

Based on stress ratios obtained from the finite element analysis of Blackwell [37], this corresponds to a maximum alternating stress amplitude on the blade of 191.5 ksi (1322 MPa) p-p. Even without considering the addition of mean stresses or any strength-reducing factors (e.g. elevated temperature, stress concentrations, etc.), this large response amplitude exceeds the titanium alloy's endurance limit (from [42, 43]) by 10%, thereby indicating the strong

possibility of an HCF failure being prompted by baseline 1T/12E damage accumulation.

Other modal crossings, corresponding to higher harmonics of the WG excitation, were in general of much lower magnitude than the 1T/12E crossing. However, some higher mode crossings, such as third leading-edge bending (LE-3B/36E) and second trailing-edge bending (TE-2B/60E), were surprisingly responsive. In light of the cumulative nature of fatigue damage, their contribution should not be ignored. The critical blade responses at these and other crossings are summarized in Table 3.1.

Though not surprising, it is worth noting that the 49E potential excitation was generally found to be weaker in effect than the viscous excitation originating upstream of the rotor (see modes 7, 9 and 10 in Table 3.1). When a comparison for the same mode could be made, the response to the fundamental stator excitation was typically of the same order as that produced by the fourth (48E) or fifth (60E) WG harmonics, which contain less energy than the WG fundamental (12E). This finding suggests the importance of considering multiple harmonics of vortical forcing functions in the aeromechanical design of turbomachinery.

Table 3.1: Summary of baseline resonance data for maximum responding (critical) blade.

Blade Mode		Impact Frequency Data [1]		Excitation		Crossing	Mode Crossing Frequency [Hz]			Critical	Crit. Blade Stress [ksi, p-p]	
Number	Shape	Mean [Hz]	Std. Dev.	Order	Source	RPM	Measured	Predicted [2]	Error [%]	Blade/Gage	at Gage	Max [2]
2	1T	2538	28	12	WG-1	12854	2571	2405	-6.4	13 / A	39.7	191.5
4	LE-2B	5285	95	24	WG-2	13568	5427	5144	-5.2	28 / C	7.4	22.2
5	2C	6902	96	36	WG-3	11602	6961	6872	-1.3	13 / B	4.6	8.6
6	2B-LE	8375	113	36	WG-3	13836	8302	7928	-4.5	10 / C	1.9	6.3
7	LE-3B	9060	183	49	Stator-1	11274	9207	9350	1.6	10 / C	3.0	5.0
7	LE-3B	9060	183	48	WG-4	11456	9165	9355	2.1	10 / C	2.2	3.6
7	LE-3B	9060	183	36	WG-3	15392	9235	9435	2.2	10 / C	18.0	30.1
8a [3]	1C-2B	—	—	48	WG-4	12120	9696	9653	-0.4	10 / B	1.8	2.7
8b [4]	1C-2B	10085	153	48	WG-4	12850	10280	—	—	10 / B [6]	1.5	—
8b [4]	1C-2B	10085	153	49	Stator-1	12468	10182	—	—	28 / B	4.4	—
8c [5]	—	—	—	48	WG-4	12926	10341	—	—	28 / A	8.0	—
9	3C	10815	177	49	Stator-1	13160	10747	11013	2.5	10 / B	3.4	5.2
9	3C	10815	177	48	WG-4	13436	10749	11013	2.5	10 / B	5.2	7.8
10	TE-2B	—	—	60	WG-5	11042	11042	11220	1.6	22 / B	3.0	41.2
10	TE-2B	—	—	49	Stator-1	13514	11036	11226	1.7	22 / B	2.7	37.1
12	LE-4B	13489	210	60	WG-5	13460	13460	14499	7.7	10 / C	4.8	12.1

[1] Blade impact frequency data from Cheatham and Tyner (1991).

[2] Frequencies and gage / max stress ratios based on NASTRAN finite element model of Blackwell (2002).

[3] Unresolved mode, supported by Blackwell (2002).

[4] Unresolved mode, supported by impact tests and holography of Cheatham and Tyner (1991).

[5] Unresolved mode, which shows significant "A" gage response at a frequency not noted by Blackwell or Cheatham and Tyner.

[6] Not the highest responding blade, but shown for distinction of apparent modes 8a and 8b

3.1.3 Repeatability and Uncertainty

Since direct comparisons were to be made between the different flow control cases and baseline data, overall uncertainty was deemed to be best quantified in terms of *precision errors* (that is, repeatability). In any case, repeatability errors proved to be much larger than the instrumentation errors previously discussed. Thus repeatability in resonance crossing amplitude was used to quantify overall uncertainty in the rotor forced response measurements.

The primary contributor to the repeatability errors was found to be the lack of precise control of exit throttle position, which is used to set the aerodynamic loading of the compressor. Though the throttle was always set to the same nominal position to provide loading representative of a design operating line, the position control was a manual open-loop type, with significant hysteresis effects.

It is clear that aerodynamic performance is quite sensitive to loading (the very reason compressor performance is "mapped" by varying the throttle), and special care is accordingly given to throttle positioning when taking aerodynamic measurements. However, it was not expected that the forced response would be particularly sensitive to the throttle position, so no special attention was given to minimizing the position hysteresis each time a throttle adjustment was made (e.g. whenever returning to test speed from start-up or idle).

The *different-series* repeatability (that is, using data from independent throttle adjustments) is shown for the 1T/12E crossing in Figure 3.3. The different series correspond to measurements acquired on three different days, with data shown for the critical blade at the "B" gage location (note that this response is much less than that presented in Figure 3.2, because this gage location is much less sensitive to 1T than the "A" location). The rotor speed corresponding to the resonance peak of each series varies only about 0.1%. However, the peak response amplitude is seen to vary about 15%. Though not shown, the variation on a non-critical blade was lower at 6.5%. That the percent response variation is exaggerated on the critical blade is a further indication of the nonlinear mistuning effects. Conversely, considering rotor speed sweeps within the same throttle adjustment, *same-series* repeatability

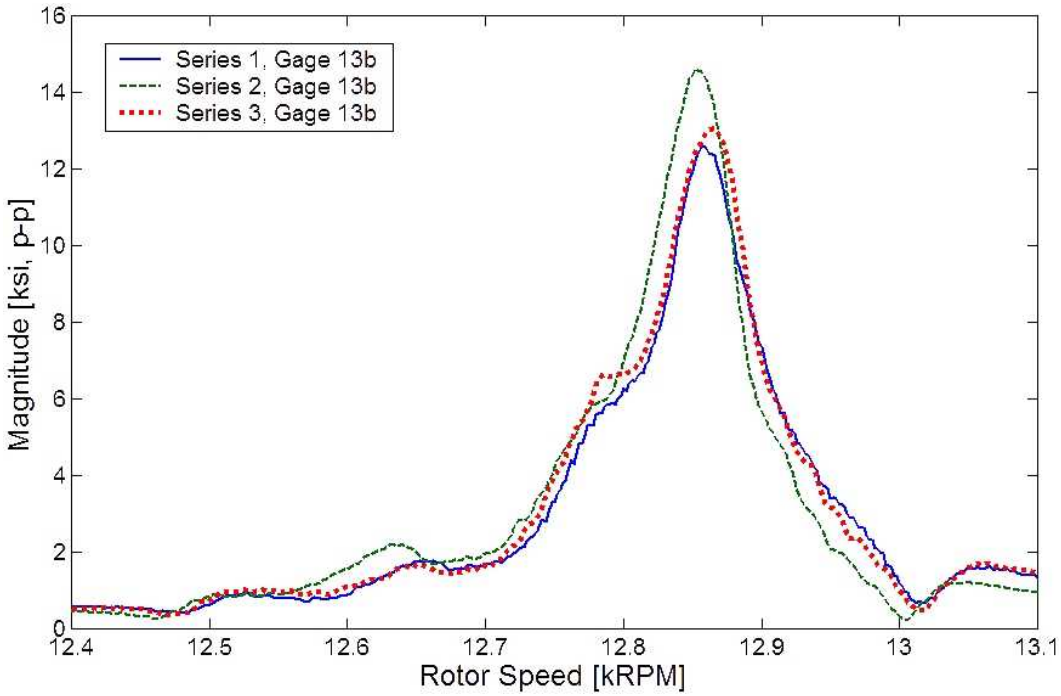

Figure 3.3: *Different*-series critical 1T/12E repeatability, for three different days.

of resonance crossing amplitude for various modes was found to be within ± 3 percent.

The sensitivity of response amplitude to rotor speed sweep rate and direction was evaluated, as illustrated for the 1T/12E crossing in Figure 3.4. While desirable for minimizing the data storage and post-processing requirements, very fast sweep rates may not allow the blades to reach maximum resonant response before the excitation frequency has moved far from that corresponding to the resonance. Indeed the fastest sweep rate (that is, 5000 rpm in 0.4 sec) was found to be inaccurate for defining the true maximum resonant response. Strong same-series response repeatability is illustrated by the excellent agreement between the two slower sweep rates, which also lends confidence that the maximum resonant response, independent of sweep rate, has been captured. The intermediate sweep rate was thus deemed acceptable, and a slightly slower nominal sweep rate of 111 RPM/second was used for all of the subsequent forced response measurements.

Because forced response data was collected over multiple days, it was unavoidable that

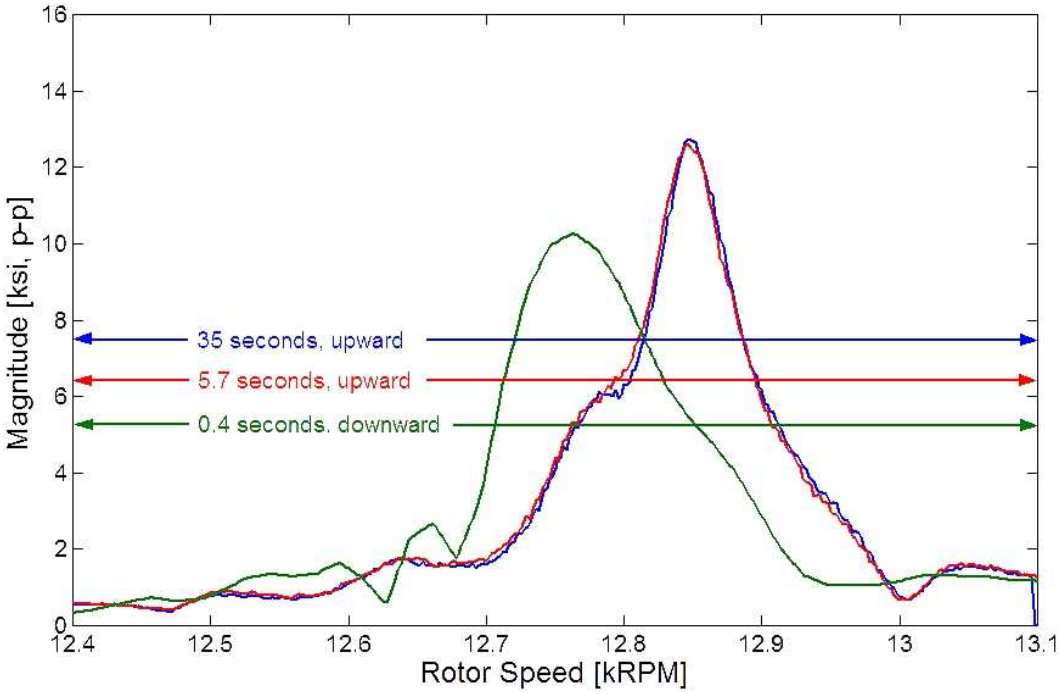

Figure 3.4: *Same*-series critical 1T/12E repeatability, for three different sweep rates.

different-series comparisons would have to be made. To minimize errors when making such comparisons, much of the TEB forced response data, presented in the following section, are normalized by baseline data from the same series. However, it was not yet known at the time of the experiments just how sensitive the response can be to small throttle adjustments. Consequently, some throttle adjustments were made during the data collection *without* acquiring new same-series baseline data.

The effects of this throttle position oversight are unfortunately interspersed in the results comparisons, and it becomes quite cumbersome to try to distinguish between the varying uncertainties (of same-series and different-series data). Thus to simplify the discussion, overall uncertainty for *all* of the normalized forced response data is collectively, and more conservatively, based on the different-series repeatability, which is *estimated to be* $\pm$ *8 percent*. While this uncertainty could likely be reduced in future experiments (by closer attention to throttle position effects), it does not change the overall conclusions of the present study.

3.2 Trailing Edge Blowing Effects on Forced Response

The trailing edge blowing (TEB) flow control technique was applied to a set of 12 wake generator (WG) vanes installed in the SMI transonic compressor rig. The goal of this undertaking was to manipulate the baseline aerodynamic forcing function produced by the WGs, and thereby to attenuate the forced vibratory response of the downstream fan rotor. While no measurements were made of the forcing function itself in the closely-coupled compressor environment, the rotor response was directly measured with blade-mounted strain gages to assess the effects of forcing function manipulation by the various TEB conditions.

While forced response measurements were collected for multiple blades and across a wide speed range, the effects of TEB are primarily documented with respect to the critical blade. Critical blades were identified based on the maximum baseline response, and are listed in Table 3.1. The same criteria were used for selecting the resonant peak amplitude in the TEB cases as in the baseline case (Section 3.1.2).

As illustrated in Figure 2.19, four distinct spanwise TEB configurations were used, with each being evaluated over a range of TEB flowrate. Data was primarily collected for the 7-hole configuration, referred to as full-span TEB, the effects of which are discussed in Section 3.2.1. The remaining three TEB configurations, shown in Figures 2.19b-d and collectively referred to as part-span TEB, provide a wide variation in the extent of spanwise TEB coverage. The effects of part-span TEB on forced response are discussed in Section 3.2.2.

3.2.1 Effects of Full-Span TEB

Using the approach described in Section 2.4.3, data was collected for each flow control setting over a wide speed range with one fundamental and numerous harmonic resonance crossings. Total flowrate for full-span TEB ranged from 0.32% to 1.01% of the rig's *design* flow capacity. The reader should note that TEB flowrates are *hereafter normalized by the rig flow at the speed corresponding to each respective resonance crossing*, as discussed in Section 2.3.2.1.

The overall test domain is shown most clearly by the response surface provided in Figure 3.5. The figure documents the response of the first-torsion (1T) critical blade over the entire test range of rotor speed and TEB flowrate. The surface itself is built from 12E order tracks of repeated speed sweeps, each with successively incremented full-span TEB flowrate. Again, TEB flowrates are normalized as a percentage of the rig flow at the resonance crossing speed (in this case, about 12,850 rpm). The figure is discussed further in the following section.

3.2.1.1 Reduction of Resonant Response

The baseline (e.g. 0% TEB flowrate) response is shown in the foreground of Figure 3.5, with the 1T/12E resonant response of 39.7 ksi (274 MPa) peak-to-peak (p-p) clearly dominant. As TEB is applied and progressively increased, the 1T/12E response is seen to decline sharply. Eventually, for TEB flow above 1.1%, the response is seen to begin to increase, a trend which is discussed in more detail in Section 3.2.1.2. Minimal baseline response is seen away from resonance and, correspondingly, the effect of TEB is less noticable.

While the response surface demonstrates the benefit of the computed order tracking technique for isolating synchronous excitations, it does not demonstrate very effectively the resolution that the technique can provide. This is shown more clearly in Figure 3.6, which compares selected slices of the response surface data to provide a more detailed view of the local effects at resonance.

Application of increasing TEB flowrate is shown to progressively attenuate the first torsion response. Using a total of 1.07% of the rig inlet flow at the crossing speed, the 1T response was limited to 5.8 ksi (40MPa) p-p on this blade, a reduction of 85% ($\pm$ 8% as determined earlier).

A secondary peak is also seen to emerge (near 12,750 rpm) when TEB is applied. This peak is also attenuated, though initially not as sharply as the primary peak, such that the secondary peak becomes dominant for the 0.86% TEB case. Thus, despite the associated shift

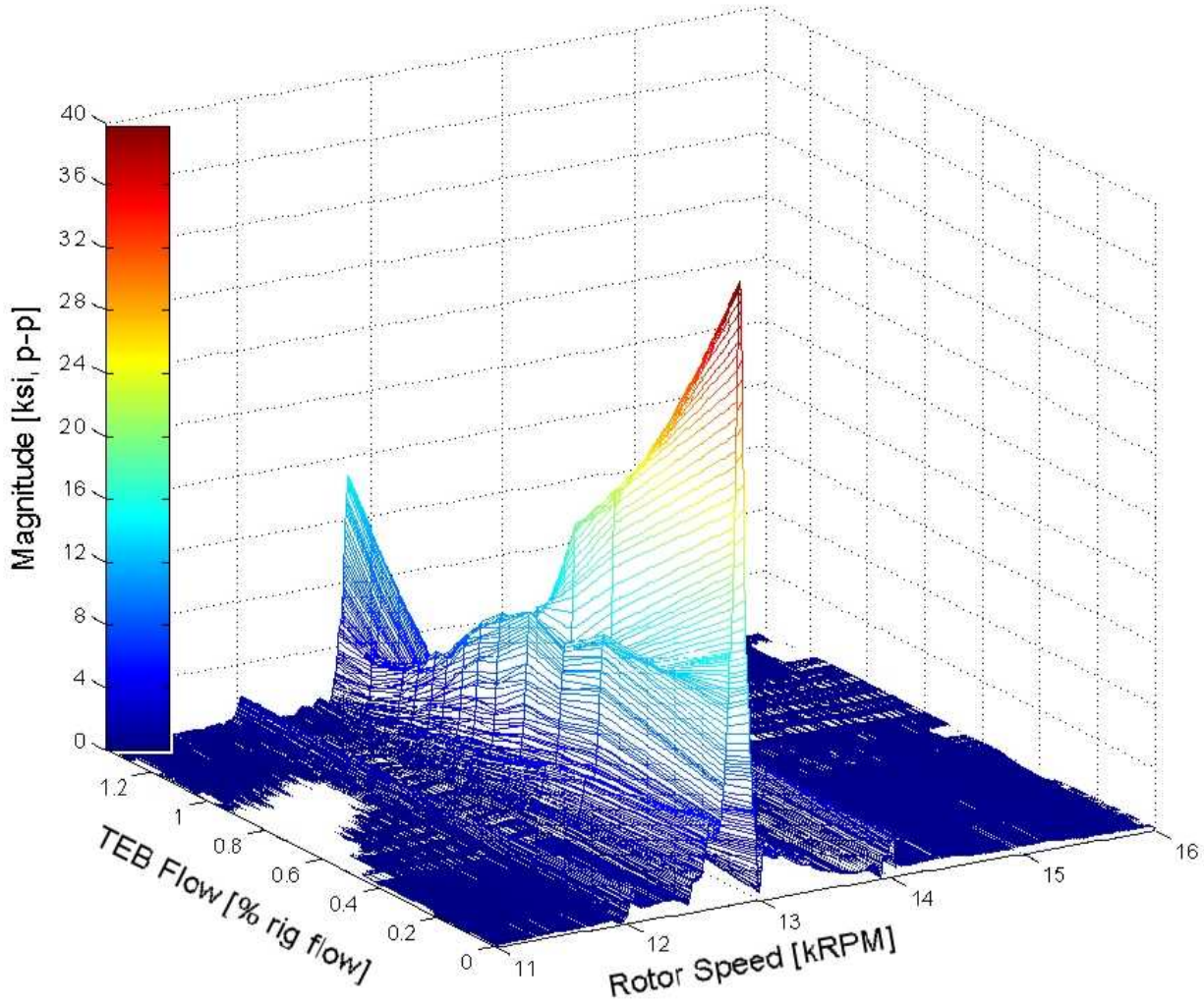

Figure 3.5: 12E response surface for entire full-span TEB test domain.

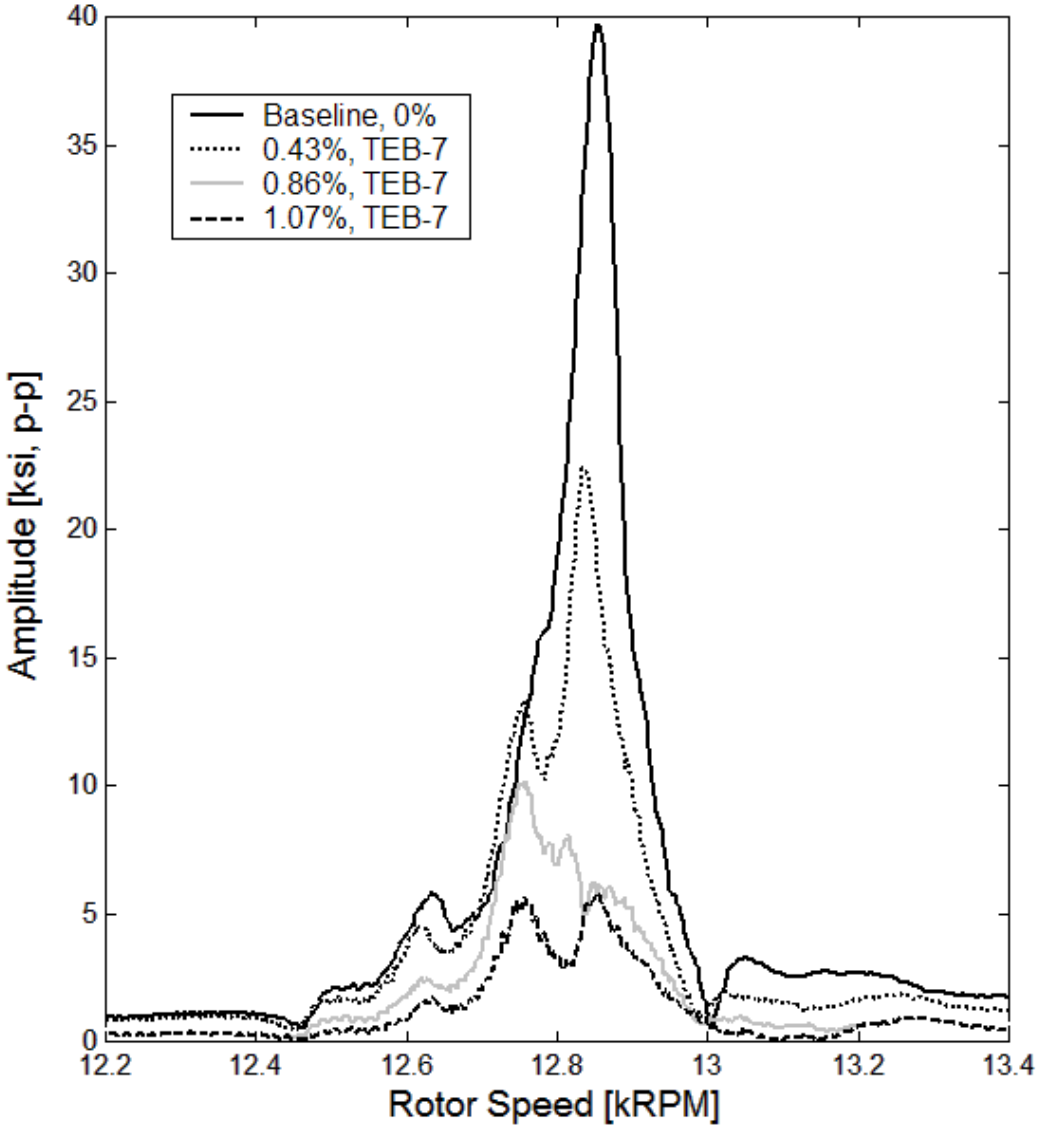

Figure 3.6: Order tracks showing full-span TEB effects on critical blade 1T/12E resonant response.

in rotor speed, the secondary peak is used at this TEB condition to quantify the resonance crossing amplitude (per the convention established in Section 3.1.2).

A similar multi-peak characteristic was often observed for other blades and at other modal crossings, such as shown for the second leading-edge bending (LE-2B/24E) critical blade response in Figure 3.7. The figure shows the effects of full-span TEB flowrate, again normalized by the rig flow at the crossing speed. The baseline response clearly shows multiple peaks, all of which are attenuated by TEB, but generally still visible. This multi-peak behavior, like the large blade-to-blade response variability discussed in Section 3.1.1, is believed to be caused by the complex coupled interaction between nearby mistuned blades. A maximum reduction in response amplitude of 94% was achieved using 0.8% of the rig flow for TEB. For TEB flow at 1.0%, the response is seen to have begun increasing.

Resonant amplitude data from four blades were normalized and averaged for the 1T/12E and LE2B/24E crossings, as presented in Figures 3.8 and 3.9, respectively. Amplitudes are normalized by the baseline crossing amplitude for each respective gage used in the average, while TEB flowrates are normalized by the corrected rig inlet flow for the speed at which the respective crossing occurs. In addition to the four-blade-average data, the critical blade data is shown. Bars are included to illustrate the range of responses for the measured blades.

Based on the four-blade-average data, the maximum attenuation at the 1T/12E crossing was 76% using 1.07% of the rig flow for TEB. A maximum average attenuation of 89% was achieved at the LE2B/24E crossing using 0.74% of the rig flow. For both crossings it is noted that more maximum attenuation occurs on the critical blade than the other blades used in the average. Table 3.2 summarizes the maximum reductions by full-span TEB in *critical* blade response at these and other resonance crossings. In most cases the 60% attenuation goal established for the National HCF Program [1] was exceeded.

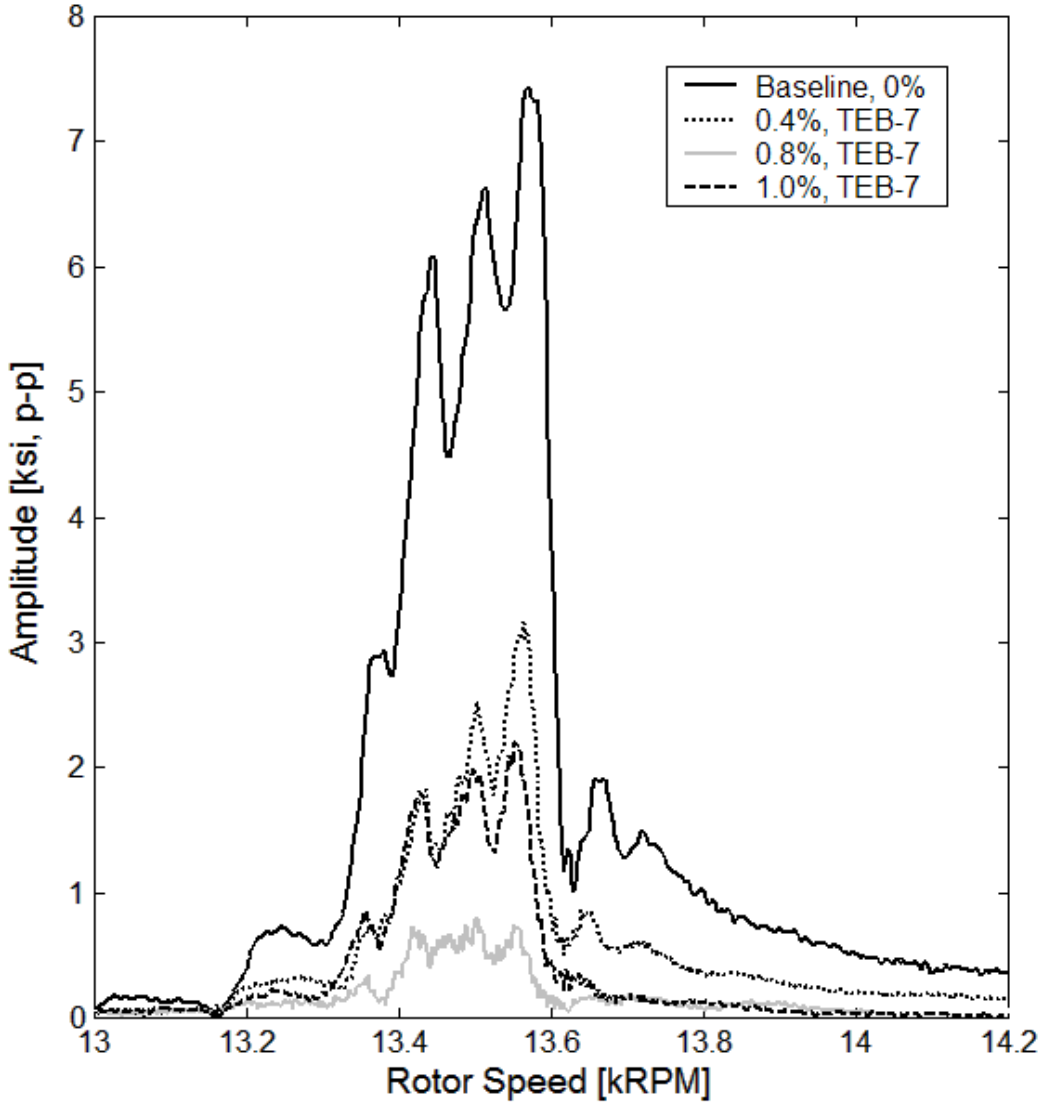

Figure 3.7: Order tracks showing full-span TEB effects on critical blade LE-2B/24E resonant response.

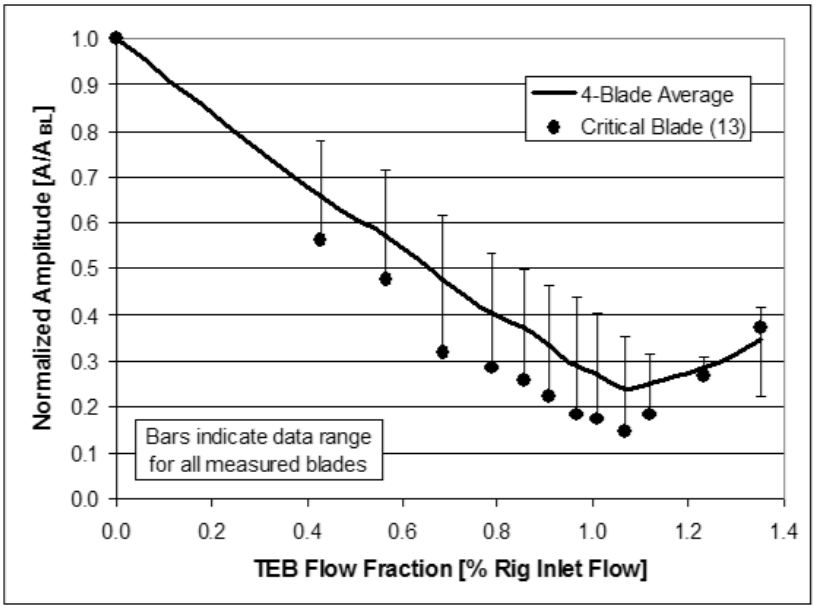

Figure 3.8: Effect of full-span TEB flowrate on 1T/12E resonant response.

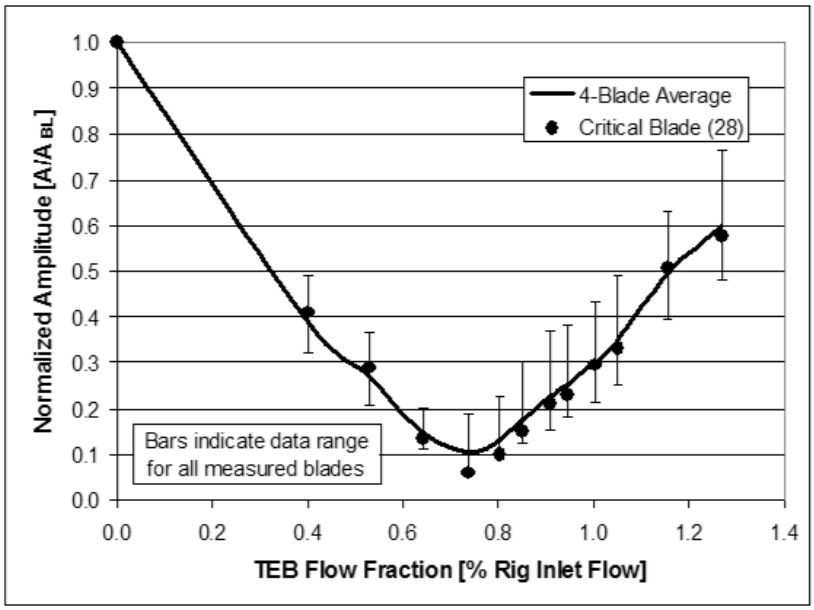

Figure 3.9: Effect of full-span TEB flowrate on LE2B/24E resonant response.

Table 3.2: Summary of maximum reductions in critical blade resonant response by full-span TEB.

Blade Mode		Excitation		Critical	Baseline Crit. Gage	Max Reduction w/ Full-Span TEB		% Reduction using
Number	Shape	Order	Source	Blade/Gage	Response [ksi, p-p]	Reduction [%]	Flowrate [% rig]	0.8% Full-Span TEB
2	1T	12	WG-1	13 / A	39.7	85	1.07	72
4	LE-2B	24	WG-2	28 / C	7.4	94	0.74	89
5	2C	36	WG-3	13 / B	4.6	82	0.64	58
6	2B-LE	36	WG-3	10 / C	1.9	49	0.77	49
7	LE-3B	49	Stator-1	10 / C	3.0	32	0.91	27
7	LE-3B	48	WG-4	10 / C	2.2	85	0.49	47
7	LE-3B	36	WG-3	10 / C	18.0	54	0.78	54
8b [1]	1C-2B	49	Stator-1	28 / B	4.4	0	—	—
8c [2]	—	48	WG-4	28 / A	8.0	87	0.78	85
9	3C	49	Stator-1	28 / B [3]	2.7	Amp. [4]	—	Amp. [4]
9	3C	48	WG-4	28 / B [3]	4.0	71	0.64	65
10	TE-2B	60	WG-5	22 / B	3.0	36	0.50	22
10	TE-2B	49	Stator-1	22 / B	2.7	Amp. [4]	—	Amp. [4]
12	LE-4B	60	WG-5	10 / C	4.8	62	0.85	59

[1] Unresolved mode, supported by impact tests and holography of Cheatham and Tyner (1991).

[2] Unresolved mode, which shows significant "A" gage response at a frequency not noted by Blackwell or Cheatham and Tyner.

[3] Not the highest responding blade; shown due to unavailability of critical blade data

[4] Crossing response was amplified under the tested TEB conditions.

3.2.1.2 Response Saddle Behavior

As illustrated in Figures 3.5, 3.8 and 3.9, the resonant response amplitude exhibits a saddle-shaped trend over the range of TEB flowrate. For increasing TEB flow, resonant response is attenuated until a minimum crossing response is achieved, at what is considered the optimal flowrate for that particular resonance crossing. If flow is further increased beyond this saddle point, referred to as "overblowing", the crossing response begins to increase. In the event of substantial overblowing, the response can exceed that of the baseline case.

This inflection behavior, which was generally noted for all the measured crossings, is expected. For effective TEB application along the entire span, the saddle point (i.e. the *forced response* optimum) occurs at the TEB flowrate (and spanwise distribution) where the amplitude of the offending forcing function harmonic passes through an overall spanwise minimum. To the aerodynamicist, this condition corresponds conceptually to the original wake velocity deficit being "filled", or to the flowfield being as circumferentially uniform as possible (referred to as the *aerodynamic* optimum). For increasing TEB flowrate, the original wake velocity deficit is replaced with a surplus, such that the forcing function passes its minimum amplitude and experiences a phase reversal. This crossover is accordingly noted in the blade response, which likewise begins to increase in amplitude for overblowing. Thus the overall TEB flowrates leading to the *forced response* and *aerodynamic* optima are expected to be effectively the same.

Emphasis is placed on the word "entire" because this is an idealized goal for effective reduction of the near-wake. To promote more effective mixing (i.e. momentum exchange) with the wake flow, discrete TEB holes are presently used instead of spanwise slots. Discrete holes, though, have the disadvantage of reduced wake-filling effectiveness *between* holes. Slots could potentially provide more consistent filling along the span, but it can be rather difficult to implement a flow control blade that actually achieves the desired blowing distribution with slots, as suggested by the efforts of Wo et al. [29]. It is perhaps easier, though hardly trivial, with discrete holes. Moreover, it may be impractical to extend either holes or slots all

the way to the endwalls to provide wake management across the entire span. In the present TEB design, not including any reduced effectiveness between the holes, about 30% of the span was largely unaffected by TEB.

Without accurate predictions, correlations, or a sophisticated real-time measurement capability to assist an integral TEB flow control system, it would be difficult to closely match the optimal flowrates (in either the structural or aerodynamic sense) in an operational flight engine. Thus, as addressed in the following section, *robustness of the TEB scheme at non-optimal conditions is highly desirable*. It is accordingly noted from Figures 3.8 and 3.9 that substantial attenuation in resonant amplitude, roughly proportional to the TEB flowrate, is achieved at sub-optimal flowrates. This point should not be lost on the designer seeking an appropriate balance among forced response mitigation, ease of control and overall engine performance.

3.2.1.3 Robustness of Full-Span TEB

The effect of full-span TEB on response amplitude is shown in Figure 3.10 for multiple WG-induced resonance crossings documented in the test range. By stacking so many data series together, the robustness of the full-span TEB case is demonstrated. *All* of the mode crossings are seen to be attenuated for some range of TEB. Specifically, for a flowrate ranging from 0.5 to 0.9% of the rig flow (normalized with respect to each crossing), the response at all crossings is reduced by at least 32%. Moreover, *for the most responsive crossings, indicated by the heavy solid lines and symbols, the response reduction was at least 50% over the same flowrate range*. While greater reductions in the high 1T/12E response are achieved at higher flowrates, the response at other crossings (e.g. Mode 5 / 36E) begins to be amplified due to substantial overblowing.

The observant reader might recall, and even raise objection, that many of the resonance amplitudes presented in the figure were small in the absolute sense (see Table 3.1), and hence present little concern for fatigue damage. However, it should be stressed that the designer

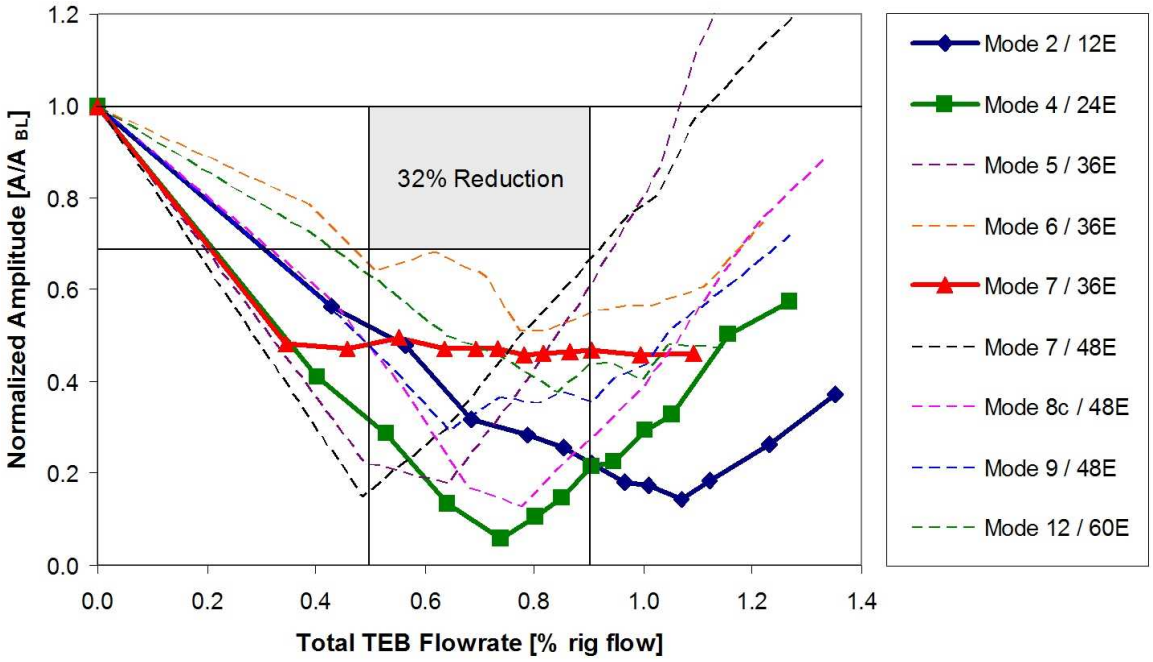

Figure 3.10: Effect of full-span TEB flowrate on multiple resonance crossings, showing region of substantial attenuation.

does not generally know before build (or even extensive field service) which modes will be most responsive, or which ones may become problematic. As a prime example, the fact that the third WG harmonic (36E) crossing of Mode 7 generated a substantial response is rather surprising. Also, many of the low amplitude modes in the present investigation are likely to be much more responsive under fundamental excitation (as opposed to the higher WG harmonics of this study), as may be presented in a different compressor (or the current one with more upstream vanes installed).

In addition to the modal- and flowrate-robustness illustrated in the figure, it is also clear that the *optimal* TEB flowrate varies for the different modal crossings. Since the crossings occur at different speeds, it was a point of interest to see if optimal TEB flowrate could be better correlated as a function of rotor speed. Such a correlation would be rather convenient, as it would make implementation of a basic TEB control system relatively easy. Thus, for the available family of resonance crossing minima, the corresponding full-span TEB flowrate

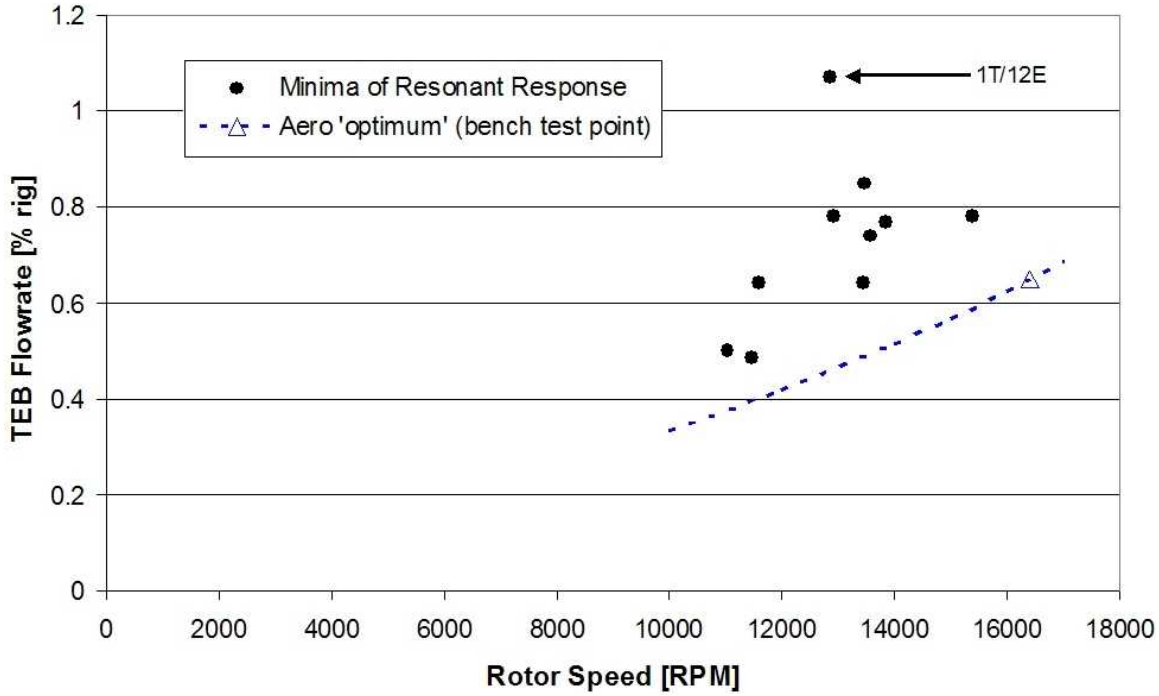

Figure 3.11: Comparison of optimal full-span TEB flowrates based on resonance crossing data and aerodynamic estimates.

was plotted against the speed at which the crossing occurred, as provided in Figure 3.11. The data in the figure is widely scattered, without a clearly-defined trend with relation to rotor speed.

A single data point, based on the TEB bench test measurements described in Appendix A, is plotted in the same figure. This point provides an approximate reference for aerodynamically-optimal TEB (that is, best wake-filling). The associated curve is an estimated variation in aero-optimal flowrate with rotor speed, based on the reference measurement and momentum balance between the wake and the TEB flow. It is assumed that the blowing holes are choked (always the case for the present investigation) and that the WG drag coefficient is a constant. While the drag coefficient is typically a strong nonlinear function of the Reynolds number (which scales with rotor speed), the depicted speed range corresponds to Reynolds numbers for which the drag coefficient is estimated to be relatively

constant. There does appear to be a similarity of the aerodynamic characteristic's slope and that of the scattered response minima.

For TEB application over the *entire* span, a more defined trend with respect to rotor speed would generally be expected, and this trend should be roughly coincident with the aerodynamically-optimal TEB characteristic as described previously. However, *all* of the forced response minima are seen to require *more* flow than was estimated to be aerodynamically-optimal.

It is noted that exact agreement with the bench test data is not expected for several reasons. First, the precise definition of an aerodynamic optimum is itself subjective, and this issue is only made more difficult by the relatively coarse spatial and TEB flowrate resolution of the bench test data. Second, the bench tests do not include the rotor-shock passing effects present in the rig tests, effects which were noted by [24] to substantially increase IGV wake depth; in other words, the aerodynamic optimum is expected to be different with and without periodic shock interaction.

Thirdly, for TEB application on anything *less* than the entire span (which is always the case in the present investigation, as described in the last section), it will generally require a higher flowrate than is aerodynamically optimal to reach a minimum in forced response. This point can be interpreted as a need to overblow (in the aerodynamic sense, i.e. a velocity surplus with respect to the mainstream flow) in one spanwise sector to compensate for the underblowing (i.e. the velocity deficit) that remains in the sector(s) without flow control. In other words, simply removing the baseline forcing function in one sector by optimal wake-filling will not necessarily coincide with the minimum forced response, because significant forcing is still present elsewhere on the span.

The robustness of the full-span TEB is further demonstrated by Figure 3.12, which summarizes the maximum response reductions for various modal crossings. Additionally, data are presented for reductions at a constant prescribed TEB flowrate of 0.8%. It is clear from Figure 3.11 that 0.8% is not likely to be the best overall TEB schedule, as it does not

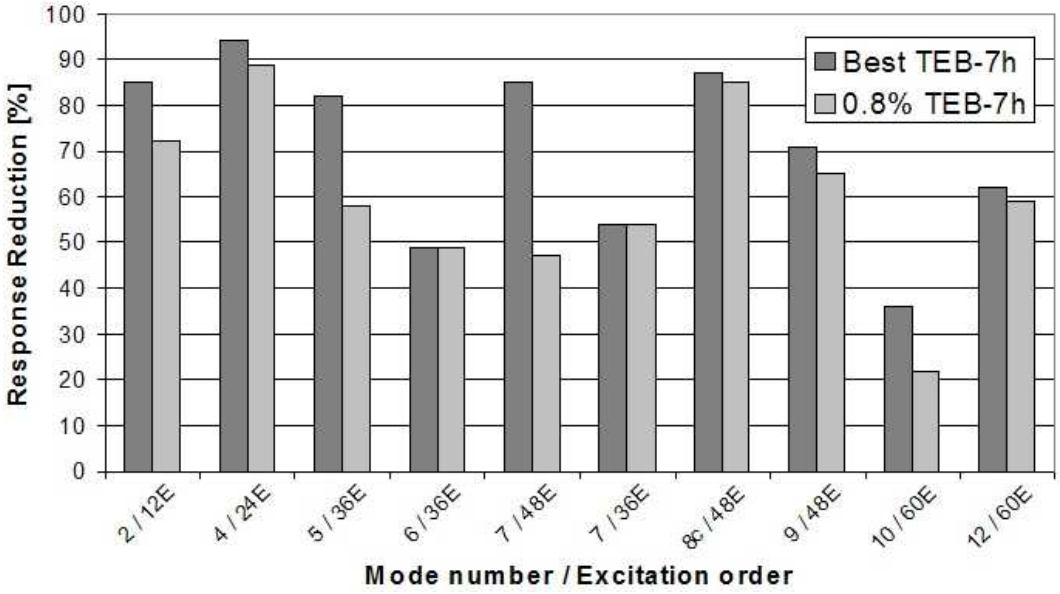

Figure 3.12: Comparison of resonant response reductions by optimal and prescribed full-span TEB.

match the sloping trend of the scattered minima; in fact, this prescribed flowrate corresponds to significant overblowing for most of the modes. Nonetheless it is evident from Figure 3.12 that, *even for a poorly chosen TEB schedule, substantial reductions are still achieved for all of the modes* (at least 55% of the maximum reduction).

3.2.2 Effects of Part-Span TEB

It is useful at this point to remind the reader of the primary motivation behind the part-span aspect of the investigation. It was desired to see if substantial forced response mitigation could be achieved with reduced air consumption, by concentrating TEB near the tip, where blade deflections, and hence modal receptivity to force input, are generally the greatest. More specifically, it was conjectured that blowing near the tip might, on a per-massflow basis, be more efficient than full-span blowing. To this end, several additional flow control cases with reduced spanwise TEB coverage, as depicted and labeled in Figures 2.19b-d, were evaluated.

The effect of the various TEB cases on the 1T/12E resonant response are compared in Figure 3.13. As in the previous plots of this type, response amplitude is again normalized by the baseline (no TEB) response, while the *total* TEB flowrate is presented as a percentage of the rig inlet flowrate at the crossing speed. The figure shows that the normalized response tends to level off (i.e. approach its minimum) at progressively lower values for increasing spanwise TEB coverage. In other words, greater peak reductions are achieved as more of the span is covered by TEB. This is not a surprising trend, since the first torsion mode is generally receptive to a force input along the entire span. Thus the greater the spanwise extent of the forcing function mitigation, the greater the potential net reduction can be.

A second point of interest in the figure is that the different spanwise cases appear to collapse toward a single common characteristic for sub-optimal flowrates. That the different characteristics seem to collapse together indicates that there is *no evident benefit (or penalty) in concentrating the TEB input near the tip for the first torsion mode.* In other words, roughly the same amplitude reduction as in the part-span cases can be achieved by distributing the same total flow over more of the span.

The same type of plot is provided for the LE-2B/24E crossing in Figure 3.14. Like the case of the 1T/12E crossing, there again seems to be no particular advantage for the available data of concentrating the blowing at the tip (though it is noted that extension of the 5-Hole data to lower flowrates might show some improvement in reduction-per-unit-massflow over the 7-Hole case).

Different trends, however, are noted in Figure 3.15 for the response at the 36E crossing of the second chordwise bending mode (2C/36E). For this specific mode (mode 5), it is first of all clear that tip blowing is much more effective on a per-massflow basis than full-span blowing (i.e. both the 1-Hole and 3-Hole characteristics pass closer to the origin than the 7-Hole characteristic does). In addition, similarly large attenuation, about 80%, is achieved with *each* of the different spanwise TEB cases. Thus for this particular resonance crossing, tip blowing appears to be distinctly advantageous.

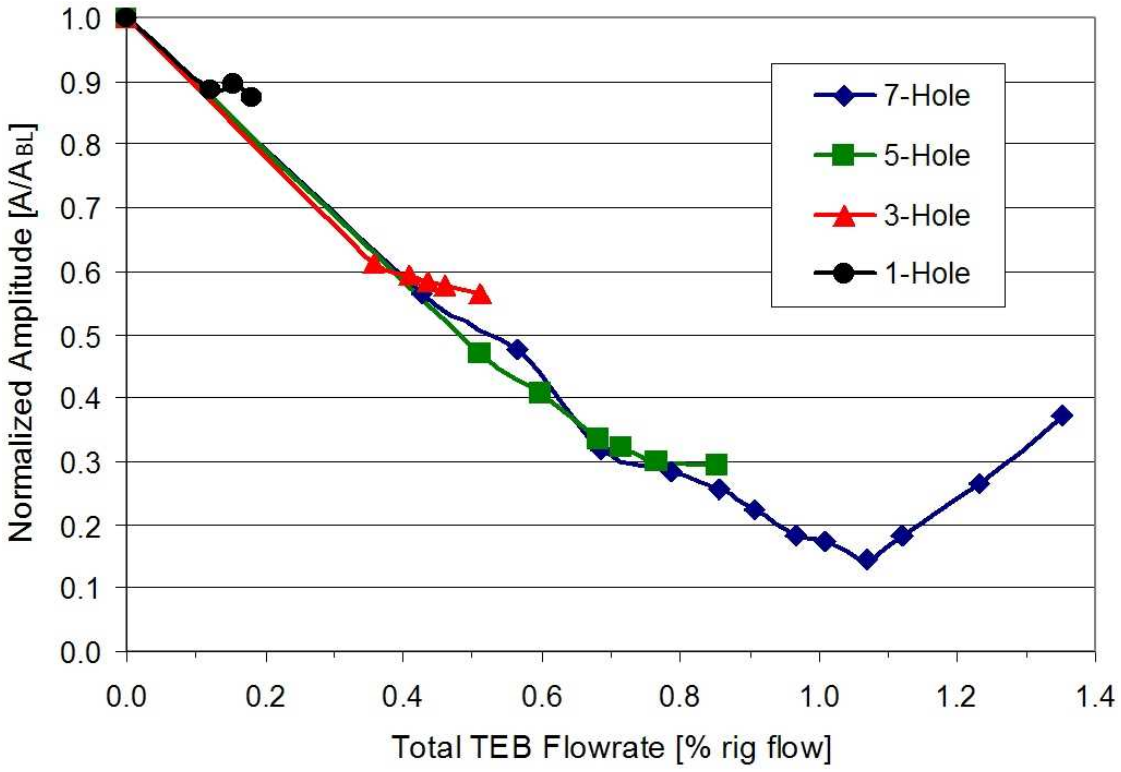

Figure 3.13: Effect of spanwise TEB coverage and flowrate on 1T/12E response.

The same 2C/36E data are compared in a slightly different manner in Figure 3.16. Instead of using the total TEB flowrate, data are plotted in terms of the TEB flowrate *per hole*, revealing an important feature. Though the saddle points (i.e. minima) are not fully characterized with the available data, it is nonetheless clear that they occur at different flowrates for each of the spanwise TEB cases. The flowrate-per-hole corresponding to the respective response minima consistently increases for decreasing spanwise TEB coverage.

An estimate of the aerodynamically-optimum TEB flowrate-per-hole (i.e., that yielding the minimum local flowfield nonuniformity) is included in the figure. This value is approximately constant in the spanwise direction, since the WG wakes are predominantly two-dimensional. Based on the previous discussion (Section 3.2.1.2), it might be expected that response minima would occur at a similar flow-per-hole as this aerodynamic optimum.

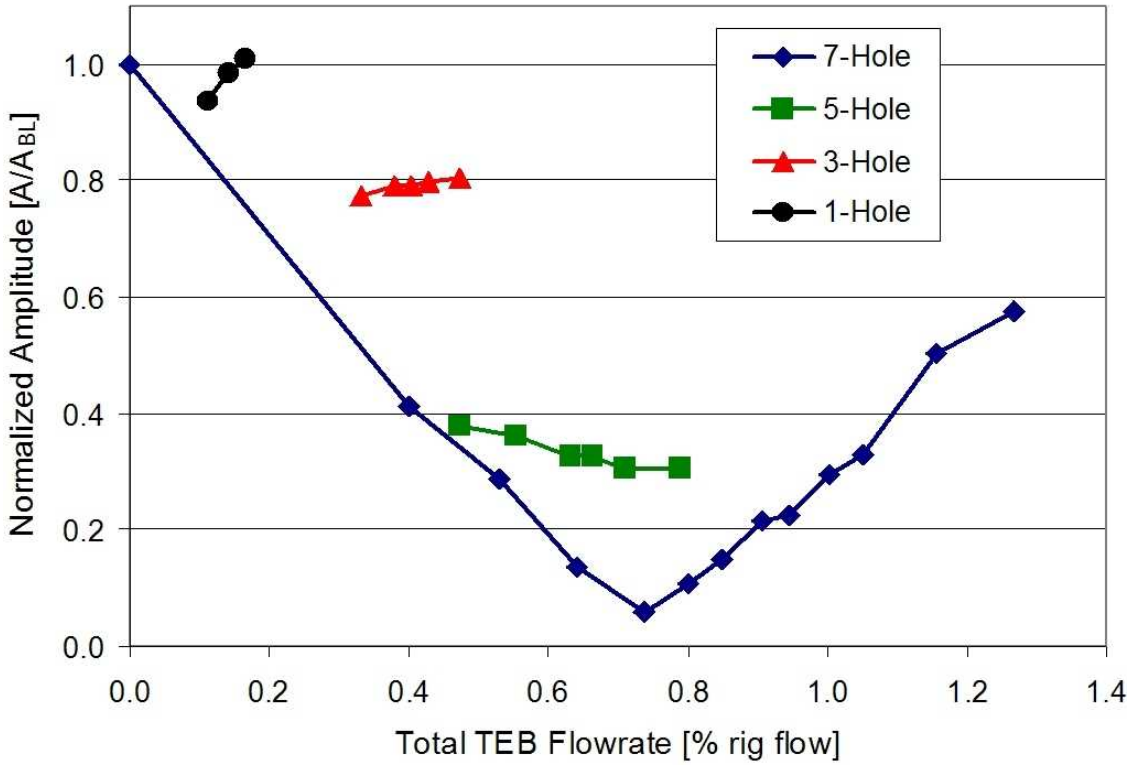

Figure 3.14: Effect of spanwise TEB coverage and flowrate on LE-2B/24E response.

However, in each case *more flow is required per hole* to minimize the response than aerodynamically estimated, *up to about 4 times as much* for the 1-Hole case.

The overall modal robustness of the different part-span TEB cases can be evaluated from Figures 3.17 - 3.19. The figures include normalized response data from multiple modal crossings for the 5-Hole, 3-Hole and 1-Hole test cases, respectively.

In the case of 5-Hole TEB, it is evident that large reductions are still achieved for some of the modes (e.g. modes 2, 4, 5 and 8c). However, unlike the full-span case, other modes are not substantially attenuated. This increased mode-to-mode variability in response reduction indicates *less modal robustness with decreased TEB coverage.*

Reductions for the 3-Hole TEB case are seen to be diminished, with only mode 5 experiencing more than 50% response attenuation. In addition, several modes (e.g. 6, 7 and

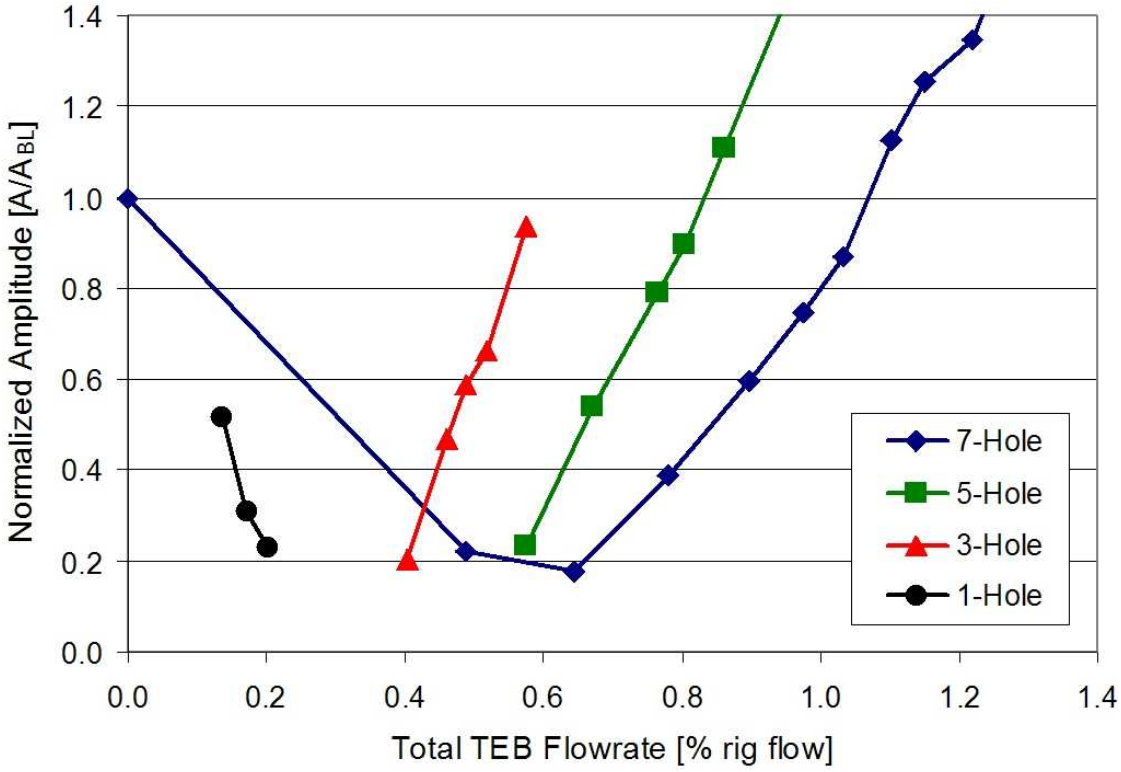

Figure 3.15: Effect of spanwise TEB coverage and flowrate on 2C/36E response.

12) are shown to experience amplification over the baseline response for all of the flowrates tested. While some attenuation may be achieved at lower flowrates for these modes, it can be inferred from the slope of the available data that any potential reductions will be minimal.

In applying 1-Hole (tip-only) blowing, the general part-span trend is continued. Modal response reductions are seen to be further diminished on average. With the exception of mode 5, responses are generally concentrated around the baseline, illustrating that tip-only blowing was found to be largely ineffective. More modes are also shown to be amplified than in the TEB cases with greater spanwise coverage.

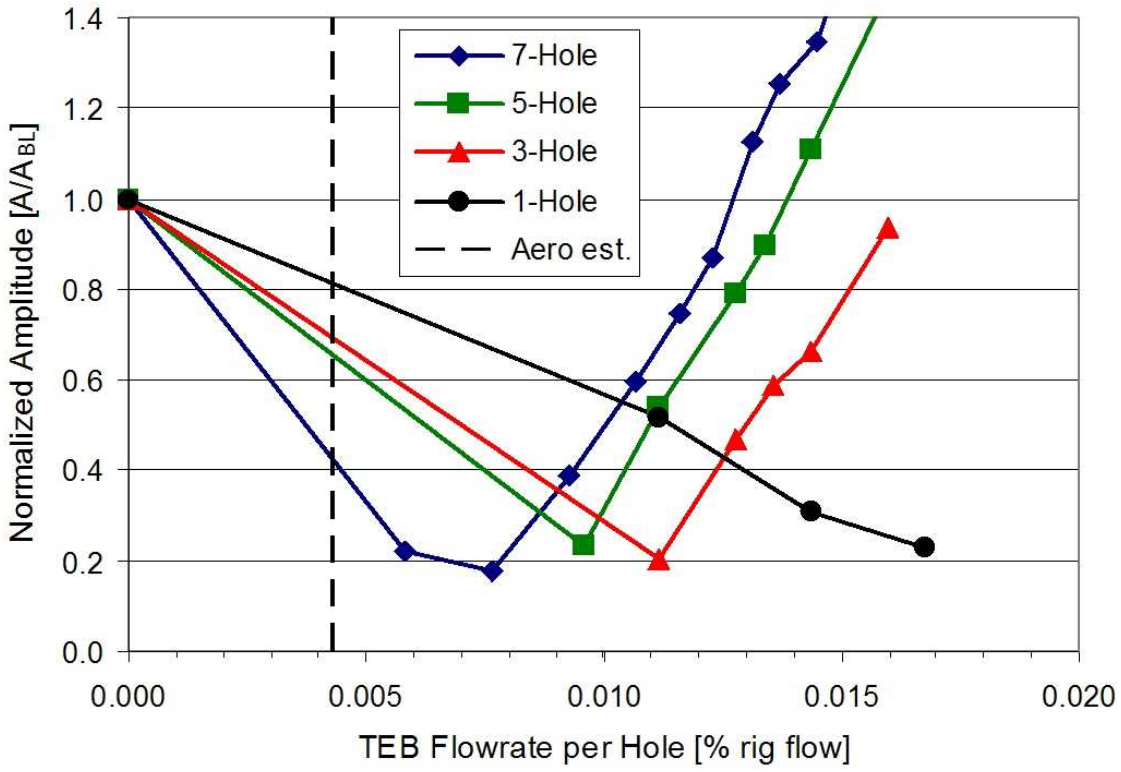

Figure 3.16: Effect of spanwise TEB coverage and flowrate *per hole* on 2C/36E response.

3.2.3 Summary of TEB Effects

The best reductions achieved by the different TEB cases for each modal crossing are summarized in Figure 3.20 and Table 3.3. It is important to note that, while the values presented correspond to the *best* reductions achieved within the limited range of tested flowrates, they are not necessarily the *maximum* reductions that may be achieved with a broader flow range.

These data summarize the key findings regarding TEB effects on forced response. It is again shown that substantial reductions in forced response, roughly 50% or better, are achieved for every measured crossing by full-span TEB. The flow required to minimize the forced response at all crossings was somewhat greater than that based on basic aerodynamic estimates. However, the *modal-robustness of full-span TEB* suggests that the aeromechanical designer might be able to rely heavily on aerodynamic estimates (e.g. CFD or cascade

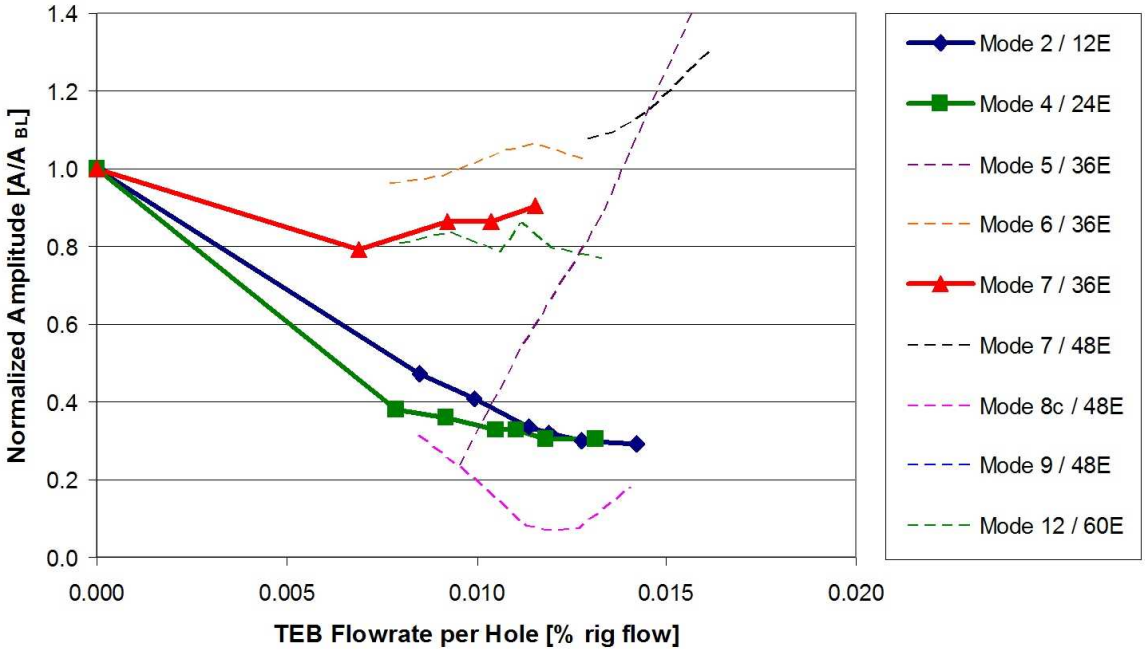

Figure 3.17: Effect of 5-Hole TEB flowrate on multiple resonance crossings.

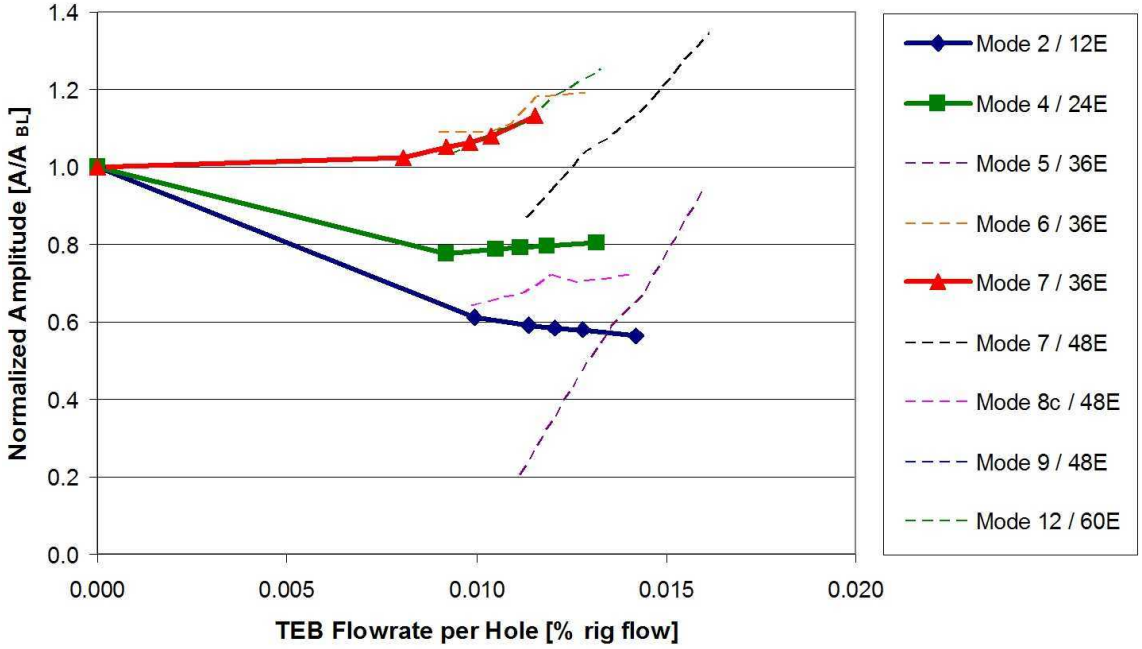

Figure 3.18: Effect of 3-Hole TEB flowrate on multiple resonance crossings.

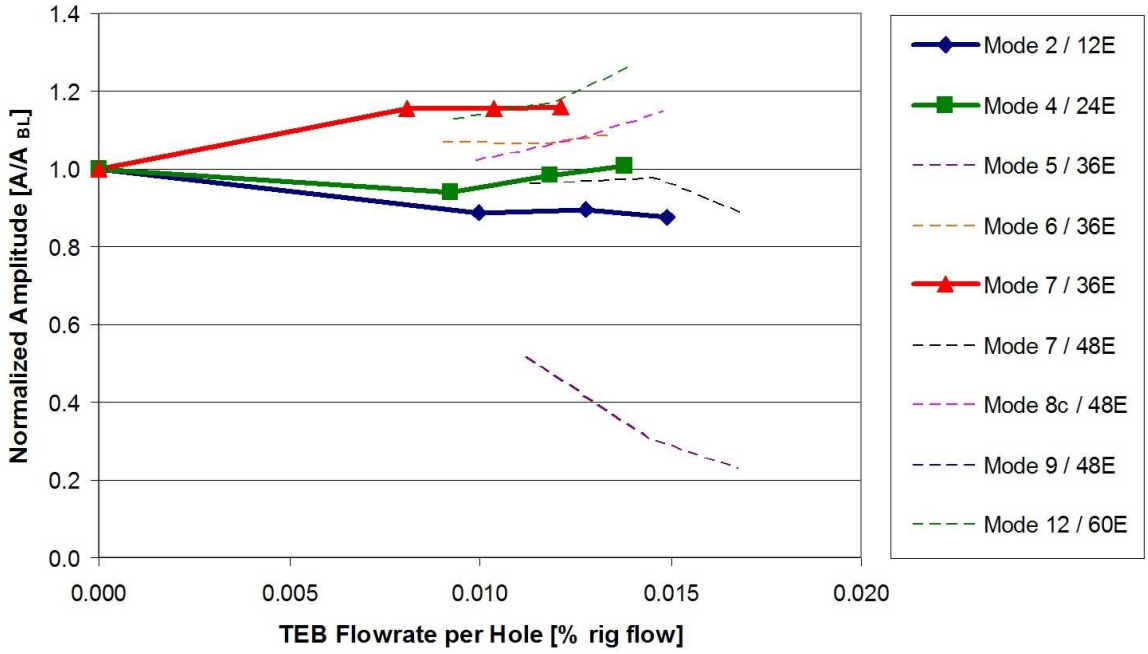

Figure 3.19: Effect of 1-Hole TEB flowrate on multiple resonance crossings.

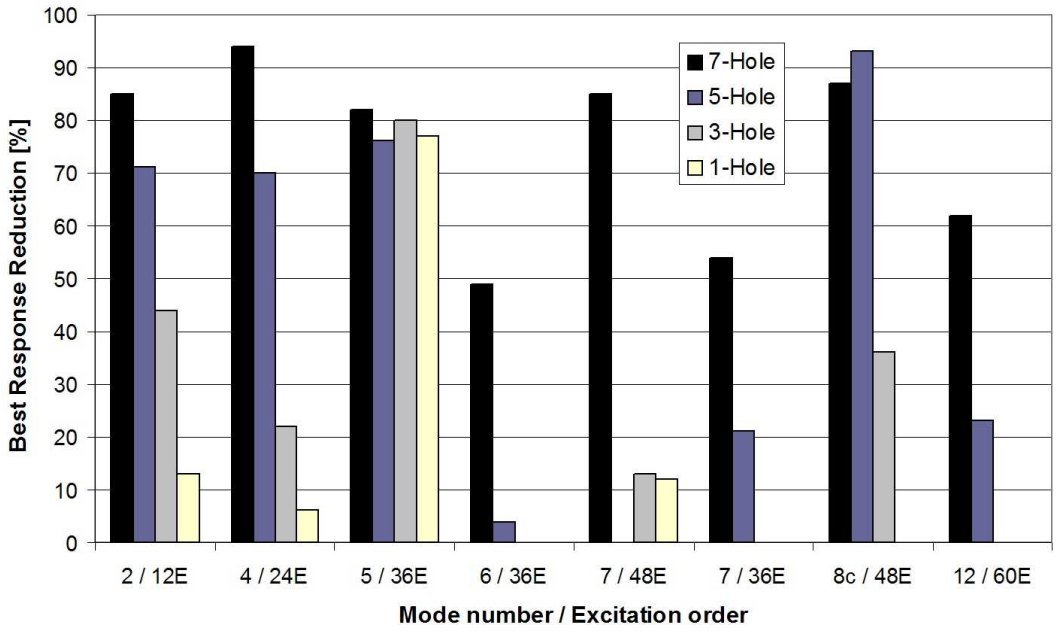

Figure 3.20: Comparison of best resonant response reductions by various spanwise TEB configurations.

testing) of full-span wake management schemes.

The figure indicates that *response reductions are generally diminished for decreasing spanwise TEB coverage*. Although part-span TEB is highly effective in certain cases (again, notably for mode 5, or 2C), *individual modal sensitivities to the spanwise TEB distribution are found to play a significant role*. The mode-specific sensitivities lead to large variability of part-span TEB effectiveness, including the amplification of some modes. As such part-span TEB is found in to be *less modally-robust* than full-span TEB.

The general implication of this reduced robustness is that it makes the design-space more challenging. If a designer has assurance that attention can be limited to select modes, there may be merit in tailoring the TEB distribution based on the specific spanwise sensitivities of those modes. Such tailoring could include more complex distributions than those presently evaluated. However, such assurance is generally not available, and in either case, care must be taken to avoid adversely affecting other modes by part-span blowing.

Table 3.3: Summary of best reductions in critical blade resonant response by each spanwise TEB case.

Blade Mode		Excitation		Critical	Best Response Reduction [1] and Total TEB Flowrate for Spanwise TEB Cases							
					7-Hole		5-Hole		3-Hole		1-Hole	
Number	Shape	Order	Source	Blade / Gage	% Red.	% Flow	% Red.	% Flow	% Red.	% Flow	% Red.	% Flow
2	1T	12	WG-1	13 / A	85	1.07	71	0.85	44	0.51	13	0.18
4	LE-2B	24	WG-2	28 / C	94	0.74	70	0.79	22	0.33	6	0.11
5	2C	36	WG-3	13 / B	82	0.64	76	0.57	80	0.40	77	0.20
6	2B-LE	36	WG-3	10 / C	49	0.77	4	0.46	Amp. [4]	—	Amp. [4]	—
7	LE-3B	49	Stator-1	10 / C	32	0.91	19	0.83	12	0.41	Amp. [4]	—
7	LE-3B	48	WG-4	10 / C	85	0.49	Amp. [4]	—	13	0.41	12	0.20
7	LE-3B	36	WG-3	10 / C	54	0.78	21	0.41	Amp. [4]	—	Amp. [4]	—
8b [2]	1C-2B	49	Stator-1	28 / B	0	—	Amp. [4]	—	Amp. [4]	—	Amp. [4]	—
8c [3]	—	48	WG-4	28 / A	87	0.78	93	0.71	36	0.36	Amp. [4]	—
9	3C	49	Stator-1	28 / B [5]	Amp. [4]	—	N / A	—	N / A	—	N / A	—
9	3C	48	WG-4	28 / B [5]	71	0.64	N / A	—	N / A	—	N / A	—
10	TE-2B	60	WG-5	22 / B	36	0.50	N / A	—	64	0.42	N / A	—
10	TE-2B	49	Stator-1	22 / B	Amp. [4]	—	Amp. [4]	—	Amp. [4]	—	Amp. [4]	—
12	LE-4B	60	WG-5	10 / C	62	0.85	23	0.80	Amp. [4]	—	Amp. [4]	—

[1] Best reduction measured for tested flow range and resolution, but not necessarily best reduction achievable.

[2] Unresolved mode, supported by impact tests and holography of Cheatham and Tyner (1991).

[3] Unresolved mode, which shows significant "A" gage response at a frequency not noted by Blackwell or Cheatham and Tyner.

[4] Crossing response was amplified under the tested TEB conditions.

[5] Not the highest responding blade; shown due to unavailability of critical blade data

3.3 Additional Discussion

This section provides limited discussion on some secondary, yet relevant, aspects of the present investigation. These topics are presented in no particular order.

- Significant TEB sensitivity is only expected for resonance crossings involving excitation orders associated with the wake forcing function directly modified by TEB. Correspondingly, resonance amplitudes from crossings of the 49E order, an excitation produced by the potential field of the 49 downstream stator vanes, were not expected to be affected by the application of TEB.

  However, as indicated in Table 3.3, it was noted with some surprise that the LE-3B/49E crossing amplitude was attenuated by as much 32% with full-span TEB, and to a lesser degree by part-span TEB. Conversely, some 49E crossings were amplified by up to 15%. The baseline amplitudes for the 49E crossings were relatively small, so this unexpected finding does not appear to be consequential in terms of HCF for the present study. However, it is indicative that the convecting wake flow (and manipulation thereof by TEB) affects the development of the downstream stator potential field.

- Since only basic spanwise TEB cases were evaluated, it is unclear whether more complex spanwise distributions could be used to target specific modes in a more efficient manner. An evaluation of the spanwise modal forces, as produced by both the wake forcing function and a particular TEB distribution, would likely shed light on this potentially fruitful direction.

  However, the aeromechanical designer generally does not have the luxury of knowing the critical mode in advance. Thus a more promising avenue would be to use such modal force analysis (or comparably expensive aeroelastic modeling) as a tool in the optimization of a robust TEB scheme (i.e. one of low modal and flowrate sensitivity), with combined objectives of minimizing air consumption, system complexity and

manufacturing expense.

- Pressure ratios (manifold total / wake static) of roughly 3 to 6 were typically used for blowing in the experiments (with even higher ratios having been employed for the highest flowrates). Because the plumbing was designed for installation ease and experimental flexibility rather than for minimizing pressure losses, it should be noted that these ratios are not representative of requirements for engine implementation. A pressure ratio of 2-3, typically achieved within two high-speed stages, should be adequate for implementing an efficient TEB plumbing design.

Chapter 4

Summary & Conclusions

For the first time an inlet guide vane (IGV) wake management scheme was employed for forced response mitigation in a modern transonic compressor. Viscous wake propagation into downstream blade rows is known to be the dominant forcing function, and is a primary cause of high-cycle fatigue (HCF) failures of rotor blades in aircraft engines. With the continual efforts to push performance to higher levels while minimizing engine weight, HCF has become a chronic problem in modern turbomachinery design, particularly for compressor rotors of bladed-disk construction.

An IGV trailing edge blowing (TEB) flow control system was designed and implemented in such a compressor to reduce the wake forcing function. Despite deep wakes, close blade row spacing and strong shock effects from the downstream transonic fan, the TEB technique was successfully demonstrated. The details of the TEB-affected compressor flowfield were not investigated; instead, the effectiveness of the TEB approach was judged directly from the measured vibratory response of the fan blades.

Forced response data were collected for a wide rotor speed range and numerous TEB conditions, using variable TEB flowrate and spanwise distribution. Data were analyzed by order-tracking tools, then evaluated in terms of critical blade response at various resonance crossings.

The following conclusions were reached in the course of this investigation:

1. Substantial reduction in near-wake strength was found to be feasible by TEB at higher flow speeds than previously documented (based on aerodynamic surveys in a high-speed wind tunnel).

2. Despite the closely-coupled blade rows, including strong shock interaction, inlet guide vane TEB was also found to be *quite effective for reducing IGV wake-induced blade response* of a modern transonic fan. Resonant response reductions as high as 94% were documented.

3. A broad response valley was generally noted for varying TEB flowrate. Significant reductions could thus be achieved for a *robust range of TEB flowrates* (see also Item 4). In addition, reductions for sub-optimal TEB (i.e. underblowing) were roughly proportional to the applied flowrate.

4. For application over the majority of the IGV span, TEB was also found to be *modally-robust*, as resonant amplitudes of all documented modal crossings were attenuated substantially. Maximum reductions were typically 50% or more. Moreover, all modal responses were reduced at least 32% for the broad TEB flow range of 0.5 to 0.9% of the rig inlet flow.

5. The optimal TEB flowrates for the various modal resonance crossings did *not* correlate very closely with rotor speed. However, due to the flowrate robustness noted above, even a non-ideal full-span TEB schedule maintained most of the realizable reduction at all crossings. Thus, it may be feasible to apply a passive full-span TEB schedule, based on aerodynamic analysis over the operating range.

6. Reduced spanwise TEB coverage was found to be *less modally-robust* than full-span TEB, due to individual modal sensitivities. Some modal responses were still substantially attenuated by part-span TEB, while the response of other modes was largely

unaffected or, in some cases, amplified by part-span TEB.

7. In only one case (second-chordwise mode) was part-span TEB found to be clearly more effective on a per-massflow basis than full-span TEB. In this case it was also found that, for reducing spanwise coverage, much higher flowrate-per-hole was required (to minimize forced response) than had been aerodynamically estimated.

8. Thus, with the exception of the case noted in the previous item, tip blowing was generally *not* found to be beneficial in terms of specific reductions (that is, reduction-per-massflow). In other words, there was *no clear advantage in concentrating TEB flow near the tip* as opposed to distributing the same flow over more of the span. For this reason, and that of modal-robustness, *full-span TEB appears to be the more promising direction to follow* for forced response reduction.

9. TEB from the upstream IGVs was surprisingly noted to have some effect on rotor blade response to the *downstream* stator potential forcing function. The effect ranged from 32% reduction to 15% amplification, indicating some alteration of the stator potential field by TEB.

Much promise is thus demonstrated in the use of trailing edge blowing for mitigation of rotor forced response in modern compressors. A number of areas, however, would benefit from further study. Some suggestions for future work are listed in the following items:

1. As follow-on work, it would be interesting to use the present forced response measurements as a benchmark for evaluation of computational modeling. A truly coupled aeroelastic simulation (i.e. one with blade modal deformation) of the present test case is probably not feasible in the immediate future. However, an unsteady simulation of the wake/TEB/transonic rotor interactions could be decomposed and evaluated in terms of the forcing functions applied to the rotor. Comparison with the experimental

data would allow a qualitative assessment of the suitability of current computational tools for predicting wake and flow control effects on blade forcing.

2. Most of the important wake-rotor interaction physics (e.g. deep wakes, close spacing, shock effects) were included in the present investigation. However, a basic upstream vane geometry was used, which did not include the effects of flow turning and diffusion typically found in compressor stator vanes. These effects, particularly at off-design operating conditions, make it more challenging to design a robust wake management scheme for curved airfoils. Notable work has been done previously in this area by Waitz et al. [13] and Carter et al. [23], but efforts (both computational and experimental) to apply flow control to realistic turbomachinery blades should no doubt continue.

3. The interaction physics mentioned in the last item were not closely investigated in the present study. Detailed inter-bladerow flowfield data, whether from experiments (e.g. Particle Image Velocimetry, or PIV, measurements) or unsteady computational simulation, would shed some much needed light on the mechanisms and dynamics of the unknown interaction of the TEB with the baseline shock-wake interaction.

4. More data and analysis are needed for the evaluation (and optimization) of aero- and thermodynamic performance of turbomachinery systems with flow control technology. The potential for improvements in both aerodynamic performance (e.g. blade loading, loss coefficient, stall margin) and durability (through forced response reduction) bear closer investigation, and should be balanced with costs, such as compressor bleed, to system-level performance.

5. Some investigation of multi-bladerow TEB effects on forced response and performance is warranted. This, among other benefits, may shed some light on the phenomenon presently noted: there was some effect of upstream TEB on rotor response to the forcing function from the downstream stators.

6. For implementation of active wake management technology in real aircraft engine applications, there ideally should be a reliable means of non-intrusively sensing its effectiveness (whether based on vibration, aerodynamic or other metrics). Substantial progress has been made in sensing technology, such as the Non-intrusive Stress Measurement System (NSMS), but more work needs to be done to transition these technologies from the research lab to production flight engines. Even with effective sensing (or passive scheduling, if feasible), work remains in developing control elements suitable for engine application. The plumbing and control system presently developed (and effective in the lab) would have to be greatly simplified and compacted to be practical for flight use.

Bibliography

[1] Garrison, B., Editor, 2001. "High Cycle Fatigue (HCF) Science and Technology Program 2000 Annual Report". Tech. Rep. AFRL-PR-WP-TR-2001-2010, Air Force Research Lab, WPAFB, OH.

[2] Fleeter, S., 1996. "Real Forcing Functions for Turbomachine Forced Response Analysis". *Proceedings of the ASME Aerospace Division,* **52** , pp. 335–342.

[3] Rao, J. S., 1991. *Turbomachine Blade Vibration*. John Wiley & Sons, New York.

[4] Manwaring, S. R., and Wisler, D. C., 1993. "Unsteady Aerodynamic and Gust Response in Compressors and Turbines". *J. of Turbomachinery,* **115** , pp. 724–40.

[5] Cumpsty, N. A., 1989. *Vibration and Noise - Compressor Aerodynamics*. Longman Scientific and Technical, Harlow, England.

[6] Campbell, Wilfred, 1924. "Protection of Steam Turbine Disk Wheels from Axial Vibration". *Transactions of the ASME,* **46** , pp. 31–160.

[7] Kielb, B., 1999. "Forced Response Design Analysis-1". In *Aeroelasticity in Axial Flow Turbomachines*, VKI Lecture Series 1999-05. von Karman Institute.

[8] Cross, C. J., and Fleeter, S., 1999. "Shunted Piezoelectric Control of Airfoil Vibrations". *ASME Paper 99-GT-385* .

[9] Duffy, K. P., Bagley, R. L., and Mehmed, O., 2000. "On a Self-Tuning Impact Vibration Damper for Rotating Turbomachinery". *Paper AIAA-2000-3100* .

[10] von Flotow, A., Tappert, P., and Mercadal, M., 2001. "HCF Active Control: An Active Wake Management Implementation Manual". *Proceedings of the 6th National Turbine Engine High Cycle Fatigue (HCF) Conference* .

[11] J. R. Fagan, Jr., and Fleeter, S., 1988. "Nonuniform Upstream Airfoil Spacing Effects on Rotor Blade Noise Generation and Forced Response". *Proceedings of Noise-Con 88 (National Conference on Noise Control Engineering)* , pp. 143–48.

[12] Hsu, S. T., and Wo, A. M., 1998. "Reduction of Unsteady Blade Loading by Beneficial Use of Vortical and Potential Disturbances in an Axial Compressor with Rotor Clocking". *J. of Turbomachinery,* **120** , pp. 705–13.

[13] Waitz, I. A., Brookfield, J. M., Sell, J., and Hayden, B. J., 1996. "Preliminary Assessment of Wake Management Strategies for Reduction of Turbomachinery Fan Noise". J. of Propulsion and Power, **12** (5) , pp. 958–66.

[14] Naumann, R. G., 1992. Control of the Wake from a Simulated Blade by Trailing-Edge Blowing. Master's thesis, Lehigh University, Bethlehem, Pennsylvania. Dept. of Mechanical Engineering.

[15] Corcoran, T. E., 1992. Control of the Wake from a Simulated Blade by Trailing-Edge Blowing. Master's thesis, Lehigh University, Bethlehem, Pennsylvania. Dept. of Mechanical Engineering.

[16] Park, W. J., and Cimbala, J.M., 1991. "The Effects of Jet Injection Geometry on Two-Dimensional Momentumless Wakes". *J. of Fluid Mechanics,* **224** , pp. 29–47.

[17] Leitch, T. A., 1997. Reduction of Unsteady Stator-Rotor Interaction by Trailing Edge Blowing. Master's thesis, Virginia Polytechnic Institute & State University, Blacksburg, Virginia. Dept. of Mechanical Engineering.

[18] Saunders, C. A., 1998. Noise Reduction in an Axisymmetric Supersonic Inlet using Trailing Edge Blowing. Master's thesis, Virginia Polytechnic Institute & State University, Blacksburg, Virginia. Dept. of Mechanical Engineering.

[19] Rao, N. M., 1999. Reduction of Unsteady Stator-Rotor Interaction by Trailing Edge Blowing Using MEMS Based Microvalves. Master's thesis, Virginia Polytechnic Institute & State University, Blacksburg, Virginia. Dept. of Mechanical Engineering.

[20] Feng, J., 2000. *Active Flow Control for Reduction of Unsteady Stator-Rotor Interaction in a Turbofan Simulator*. PhD thesis, Virginia Polytechnic Institute & State University, Blacksburg, Virginia. Dept. of Mechanical Engineering.

[21] Sutliff, D. L., Tweedt, D. L., Fite, E. B., and Envia, E., 2002. "Low-Speed Fan Noise Reduction with Trailing Edge Blowing". *AIAA Paper 2002-2492* .

[22] Vandeputte, T. W., 2000. Effects of Flow Control on the Aerodynamics of a Tandem Inlet Guide Vane. Master's thesis, Virginia Polytechnic Institute & State University, Blacksburg, Virginia. Dept. of Mechanical Engineering.

[23] Carter, C. J., Guillot, S. A., Ng, W. F., and Copenhaver, W.W., 2001. "Aerodynamic Performance of a High-Turning Compressor Stator with Flow Control". *AIAA Paper 2001-3973* .

[24] Kozak, J. D., 2000. *Steady and Unsteady Aerodynamic Investigation of Inlet Guide Vane Trailing-Edge Blowing Flow Control in a F109 Turbofan Engine*. PhD thesis, Virginia Polytechnic Institute & State University, Blacksburg, Virginia. Dept. of Mechanical Engineering.

[25] Morris, R. J., Benedict, B. K., and Cowles, B. A., 1998. "Active Structural Control for Gas Turbine Engines". *ASME Paper 98-GT-514* .

[26] Benedict, B. K., 2001. Personal communication, Pratt & Whitney.

[27] Gorrell, S. E., 2002. Personal communication, U.S. Air Force Research Lab, Propulsion Directorate.

[28] Koch, P. J., Probasco, D. P., Wolff, J. M., Copenhaver, W. W., and Chriss, R. M., 2001. "Transonic Compressor Influences on Upstream Surface Pressures with Axial Spacing". J. of Propulsion and Power, **17** (2) , pp. 474–6.

[29] Wo, A. M., Lo, A. C., and Chang, W. C., 2002. "Flow Control via Rotor Trailing Edge Blowing in Rotor/Stator Axial Compressor". J. of Propulsion and Power, **18** (1) , pp. 93–9.

[30] Bailie, S. T., Ng, W. F., Wicks, A. L., and Copenhaver, W. W., 2002. "Effects of Flow Control on Forced Response and Performance of a Transonic Compressor". *ASME Paper GT-2002-30008* .

[31] Law, C. H., and Wennerstrom, A. J., 1989. "Two Axial Compressor Designs for a Stage Matching Investigation". Technical Report AF-WAL-TR-89-2005, Aero Propulsion and Power Directorate, Wright Laboratory, WPAFB, OH.

[32] Cheatham, J. G., and Tyner, T. M., 1992. "Stage Matching Investigation". Technical Report WL-TR-91-2098, Aero Propulsion and Power Directorate, Wright Laboratory, WPAFB, OH.

[33] Gorrell, S. E., 2001. *An Experimental and Numerical Investigation of Stator-Rotor Interactions in a Transonic Compressor*. PhD thesis, Iowa State University, Ames, Iowa.

[34] Fyfe, K. R., and Munck, E. D. S., 1997. "Analysis of Computed Order Tracking". Mechanical Systems and Signal Processing, **11** (2) , pp. 187–205.

[35] Kurkov, A. P., 1981. "Flutter Spectral Measurements Using Stationary Pressure Transducers". Journal of Engineering for Power, **103** (2) , pp. 461–67.

[36] Gorrell, S. E., Copenhaver, W. W., and Chriss, R. M., 2001. "Upstream Wake Influences on the Measured Performance of a Transonic Compressor Stage". J. of Propulsion and Power, **17** (1) , pp. 43–8.

[37] Blackwell, C. M., 2002. Personal communication, U.S. Air Force Research Lab, Propulsion Directorate.

[38] Kahl, G., 2003. "Mistuning and Coupling Effects in Turbomachinery Bladings". *Proceedings of the 10th Int'l Symposium on Unsteady Aerodynamics, Aeroacoustics & Aeroelasticity of Turbomachinery (ISUAAAT)* . September 8-11, Duke University, Durham, NC.

[39] Jones, K., and Cross, C., 2002. "Reducing Mistuned Bladed Disk Forced Response Below Tuned Resonant Amplitudes". *Proceedings of the 7th National Turbine Engine High Cycle Fatigue (HCF) Conference* . Palm Beach Gardens, FL.

[40] Kurkov, A. P., 1981. "Measurement of Aerodynamic Work During Fan Flutter". *Fluid/Structure Interactions in Turbomachinery* , pp. 9–18. Presented at the Winter Annual Meeting of the ASME, Washington, D.C.

[41] Kenyon, J. A., and Griffin, J. H., 2002. "Maximum Mistuned Forced Response Demonstrated on Experimental Bladed Disk". *Proceedings of the 7th National Turbine Engine High Cycle Fatigue (HCF) Conference* . Palm Beach Gardens, FL.

[42] Kalpakjian, S., 1997. *Manufacturing Processes for Engineering Materials*, Third ed. Addison-Wesley, Reading, Massachusetts.

[43] Hibbeler, R. C., 1994. *Mechanics of Materials*, Second ed. Prentice Hall, Englewood Cliffs, New Jersey.

Appendix A

Parametric Study of Trailing Edge Blowing

The first phase of the overall research program was a parametric investigation of the TEB technique on isolated airfoils similar to those to be used in the rig tests. This initial phase was conducted at Virginia Tech in a small-scale wind tunnel, as illustrated in Figures A.1 and A.2. While the transonic rotor shock and potential field effects were not included, the tunnel flow conditions were otherwise comparable to those expected in the subsequent rig application (Mach number ranging from 0.5 to 0.6). Several TEB design parameters (discrete blowing hole diameter, shape and spacing) were evaluated for wake-filling effectiveness at the same relative axial station as the rotor leading edge (LE) in the rig experiments.

After the TEB concept was validated and its design refined through experimental iterations in the wind tunnel, the final TEB configuration was incorporated into a flow control system for a set of inlet guide vanes (IGVs). The details of the TEB geometry are provided in Figure A.3. This system was then implemented in the SMI transonic compressor rig at the Air Force Research Laboratory (AFRL). In this rig, experiments were undertaken to measure the effects of TEB flow control on rotor blade forced response, as documented in the preceding document.

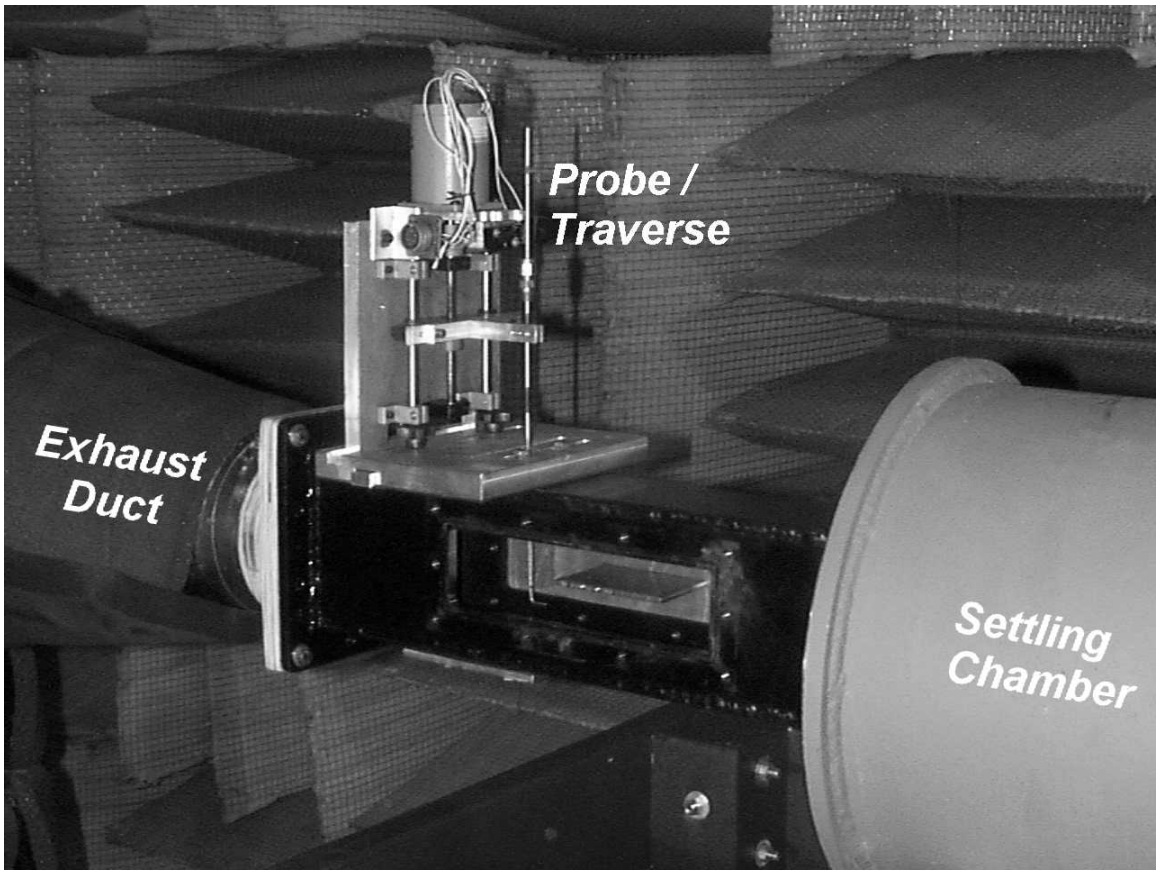

Figure A.1: High-Speed Small Scale (HSSS) wind tunnel with probe traverse assembly mounted on top and side window panel removed.

Wake profiles were measured for the final TEB-equipped vanes at an inlet Mach number of 0.53 (corresponding to 100% rig design speed). Figure A.4 illustrates the location, relative to the isolated vane, of the various Pitot-static probe measurements. The wake profile data are presented in terms of normalized velocity in Figures A.5 and A.6. The total massflow used for this single-vane case was 0.0182 lbm/second, which for 12 vanes corresponds to 0.65% of the rig flow. About 95% of the baseline momentum deficit (of the portion of span with TEB holes) was eliminated by this TEB condition.

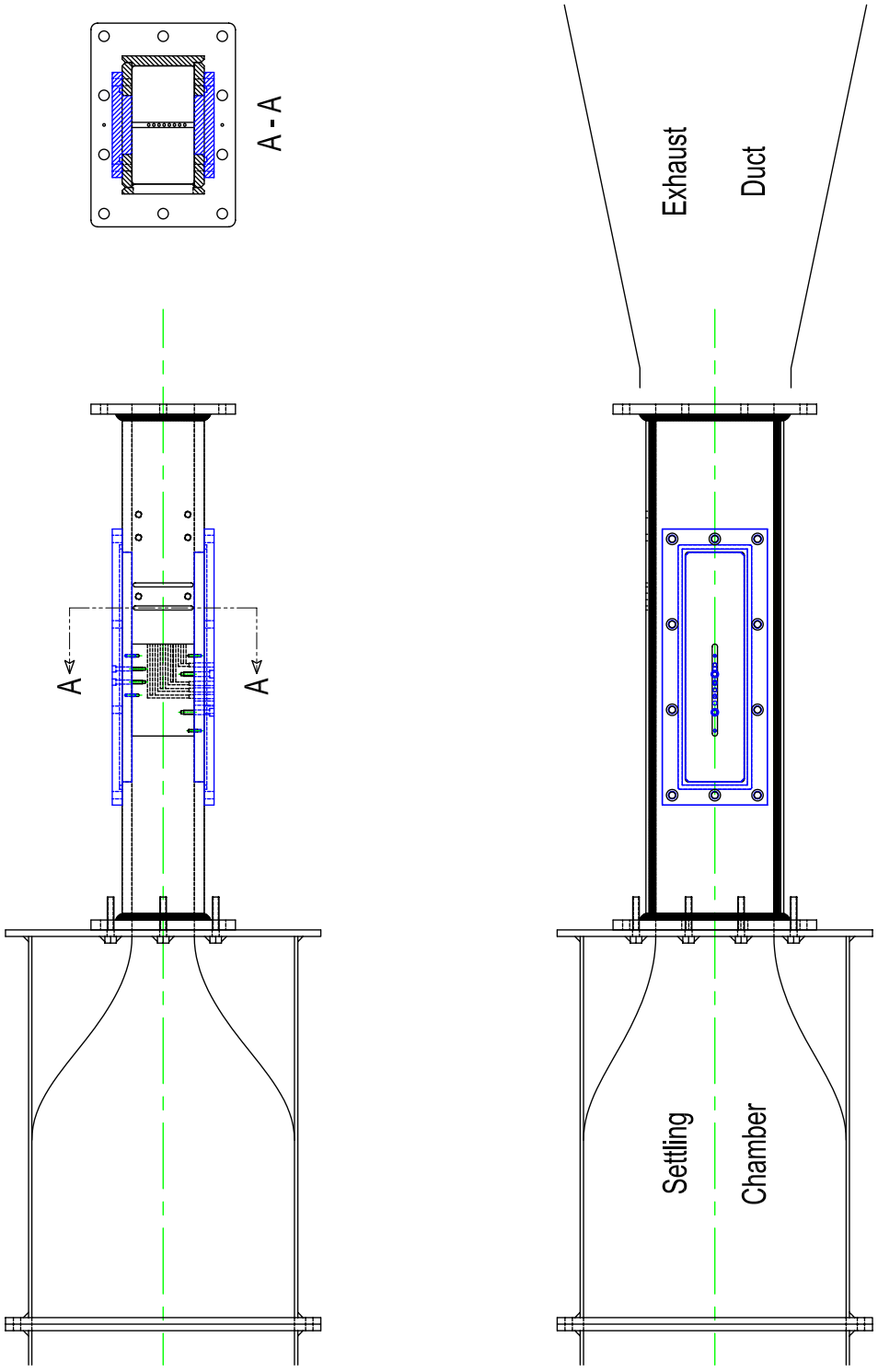

Figure A.2: Drawing of HSSS blowdown wind tunnel.

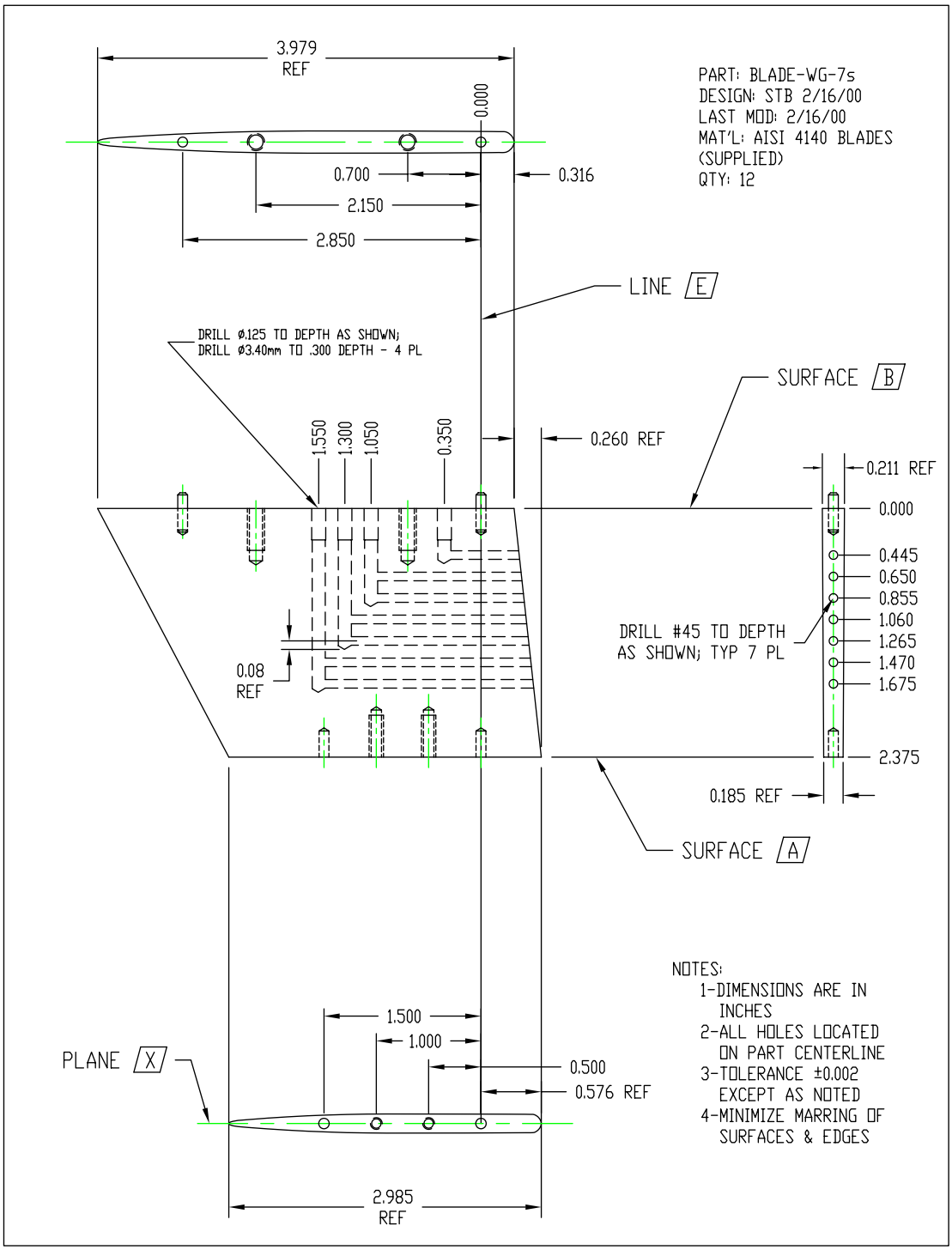

Figure A.3: Drawing of wake generator with 7-Hole TEB design.

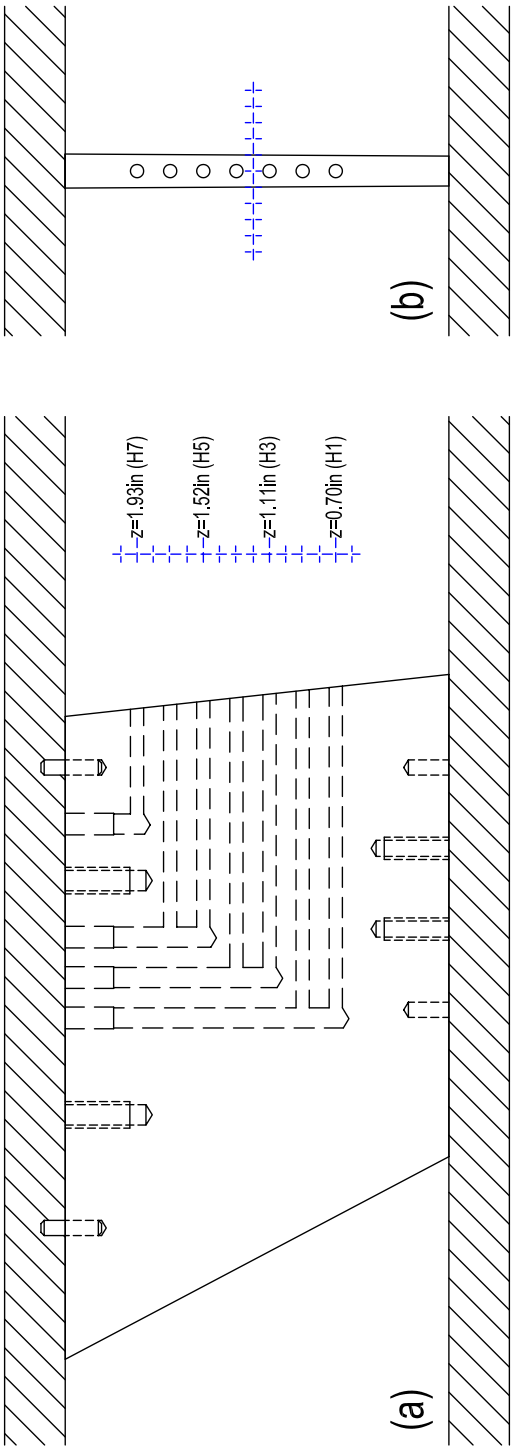

Figure A.4: Pitot-static measurement grid, shown relative to TEB-equipped WG vane in (a) the axial and spanwise directions and (b) the pitchwise direction.

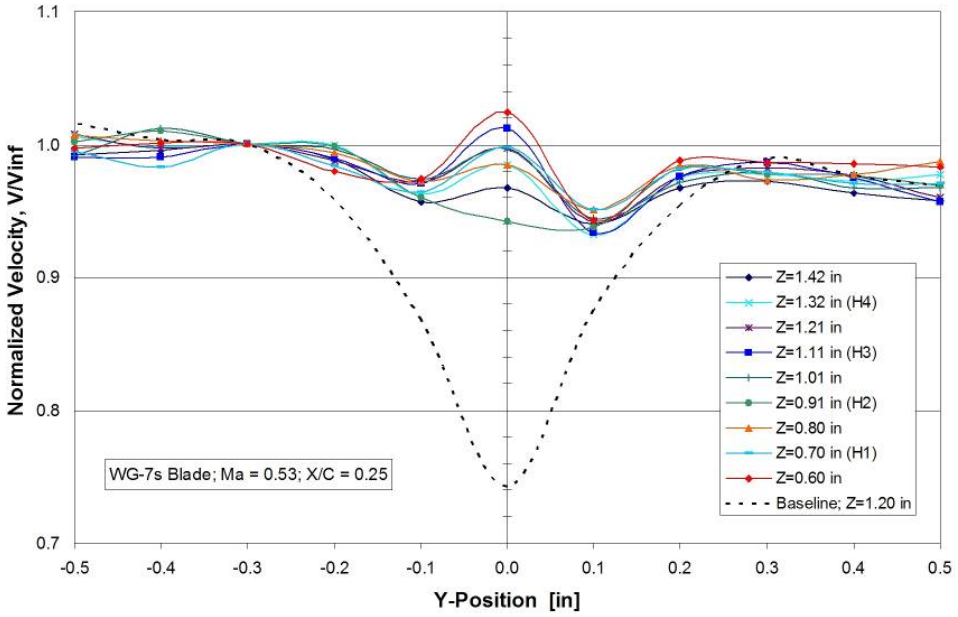

Figure A.5: Wake profiles measured 0.25 chords downstream of holes 1-4 of the final TEB-equipped WG vane.

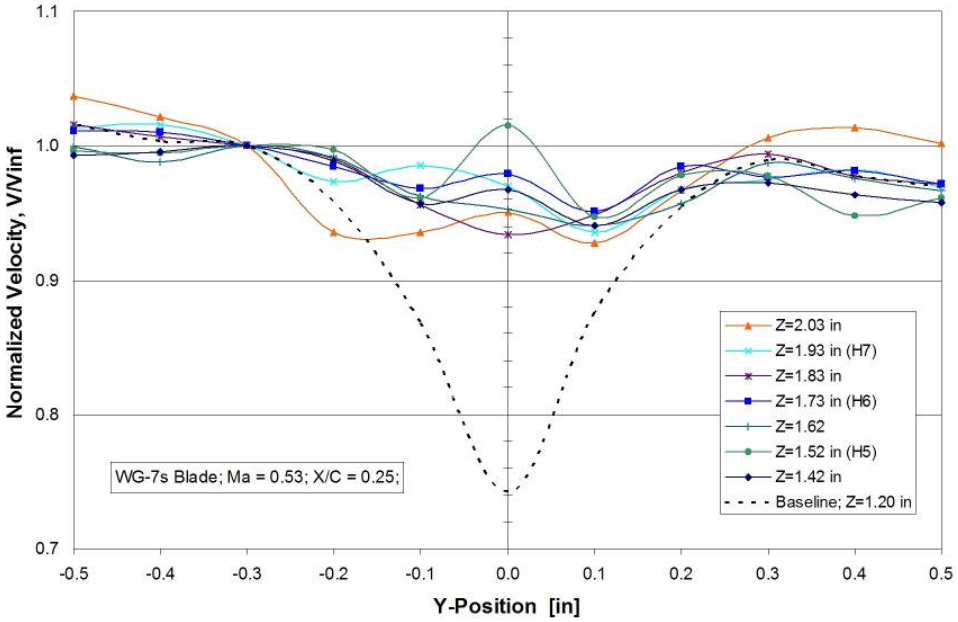

Figure A.6: Wake profiles measured 0.25 chords downstream of holes 5-7 of the final TEB-equipped WG vane.

Appendix B

Forced Response Data

This appendix provides a summary cross-section of the forced response data, presented in the form of order track plots. Baseline data are provided, as well as data from the various TEB configurations and selected flowrates corresponding to each configuration. To limit the overall volume presented, a number of intermediate flowrate cases are omitted. In most cases results are only provided from six strain gages (selected based on reliability and to cover most of the critical crossings). Since multiple plots are provided as part of a common figure, the reader should be aware of the format for the labels, provided at the top of each plot, used to distinguish the various data. The following label, from Figure B.6(a), is provided as an example: *020813-sweep11a-7h-50g / Gage = sg13a*.

The first two items ("020813" and "sweep11a") are only of consequence to the researchers. They identify the date and sweep number, respectively, for cross-referencing with the rig test log and analog tape record. The next two items are of relevance to the reader, as they identify the TEB configuration ("7h" indicates that all 7 TEB holes were used) and the total flowrate ("50g" indicates 50 grams/second) used for TEB, which was distributed evenly to all twelve wake generator vanes. The final (and most significant) entry defines the strain gage from which the plotted data were acquired; "sg13a" corresponds to the *A-location* gage (refer to Figure 2.13) of Blade 13, which incidentally is the critical (highest responding) blade for the

fundamental first torsion resonance crossing. For a summary of the critical blades/gages for the other various resonance crossings, the reader is referred back to Table 3.1.

Unlike the results presented in the body of the document, this appendix provides the data in a raw form. TEB flowrates are presented in grams-per-second, while strain gage response magnitudes are given in volts (zero-to-peak). The gages were calibrated for 10 ksi per signal volt; hence a multiplying factor of 20 is required to reach ksi, peak-to-peak as presented previously.

The data presented herein are divided into the following sections:

- B.1: Baseline Order Track Plots
- B.2: 7-Hole TEB Order Track Plots
- B.3: 5-Hole TEB Order Track Plots
- B.4: 3-Hole TEB Order Track Plots
- B.5: 1-Hole TEB Order Track Plots

B.1 Baseline Order Track Plots

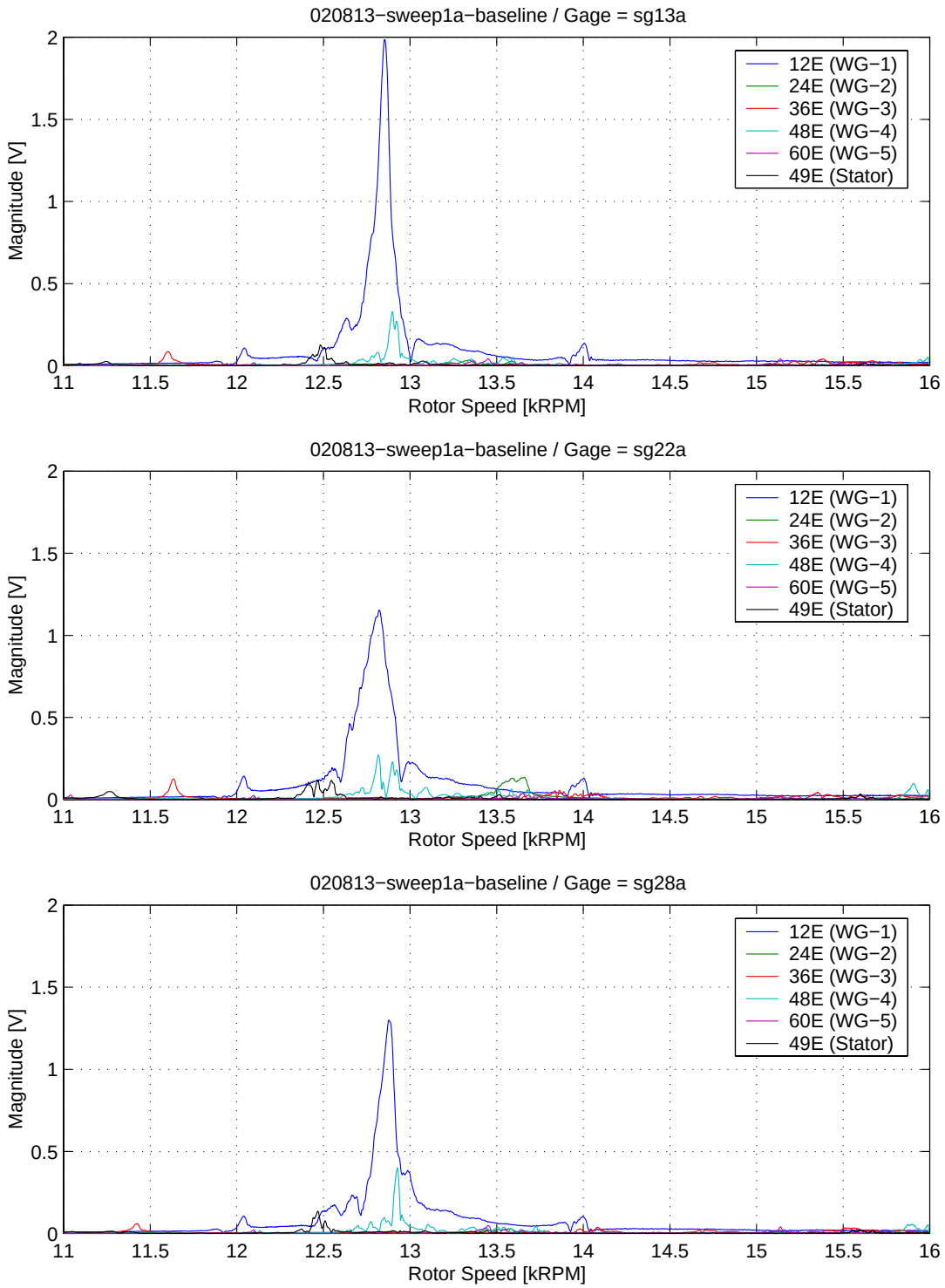

Figure B.1: Baseline order tracks for evaluating 7-Hole TEB (selected "A" gages).

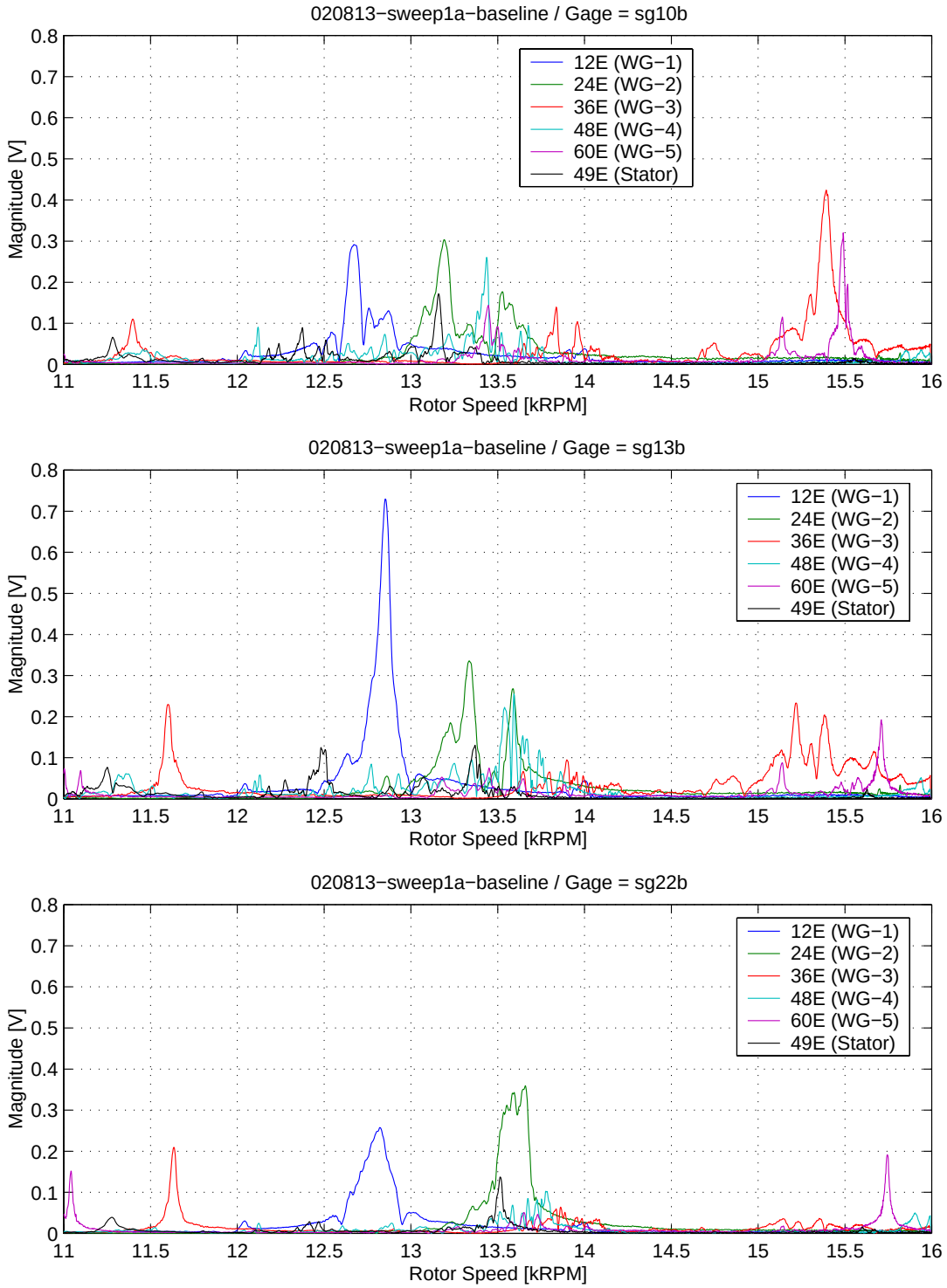

Figure B.2: Baseline order tracks for evaluating 7-Hole TEB (selected "B" gages).

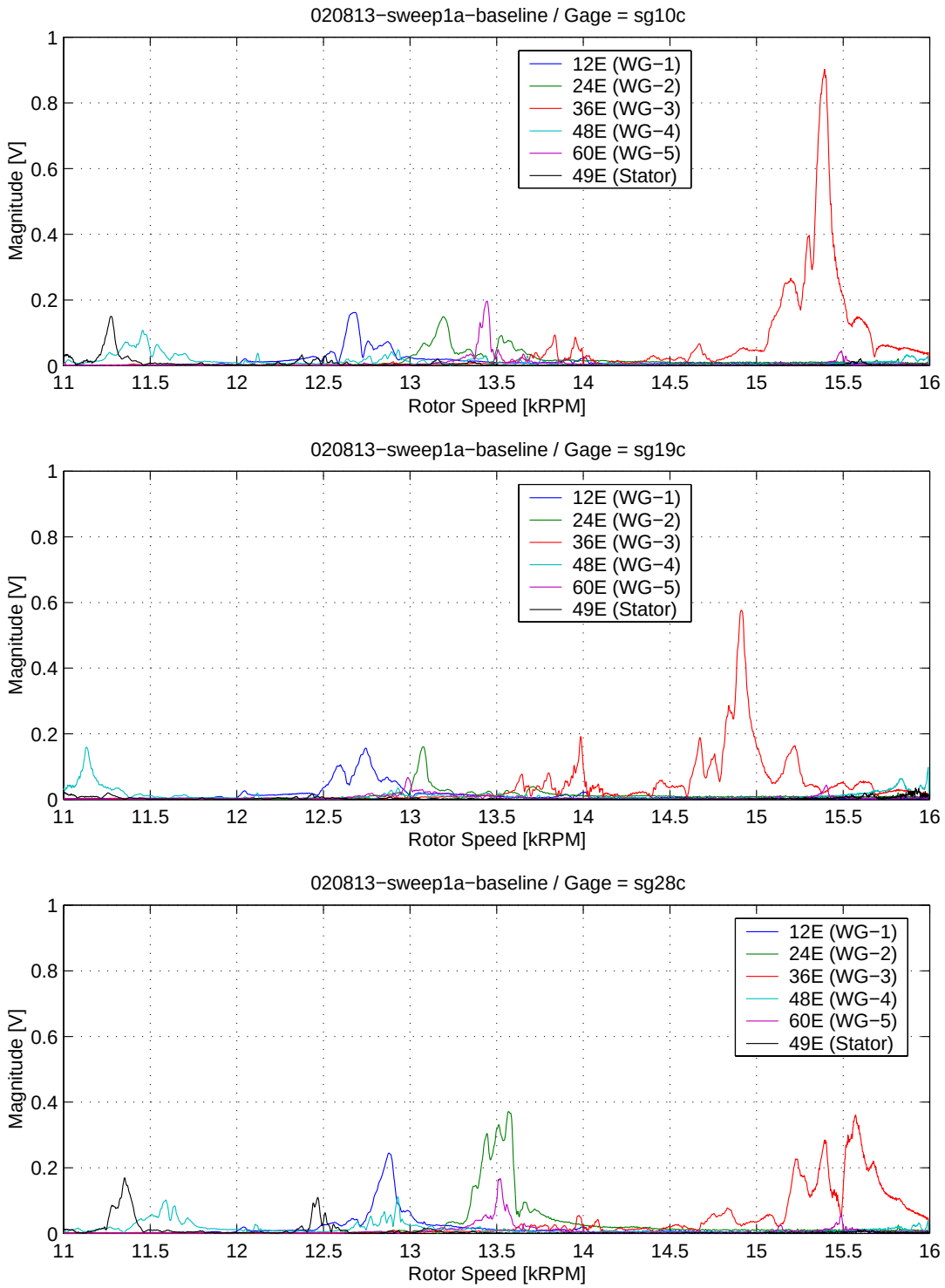

Figure B.3: Baseline order tracks for evaluating 7-Hole TEB (selected "C" gages).

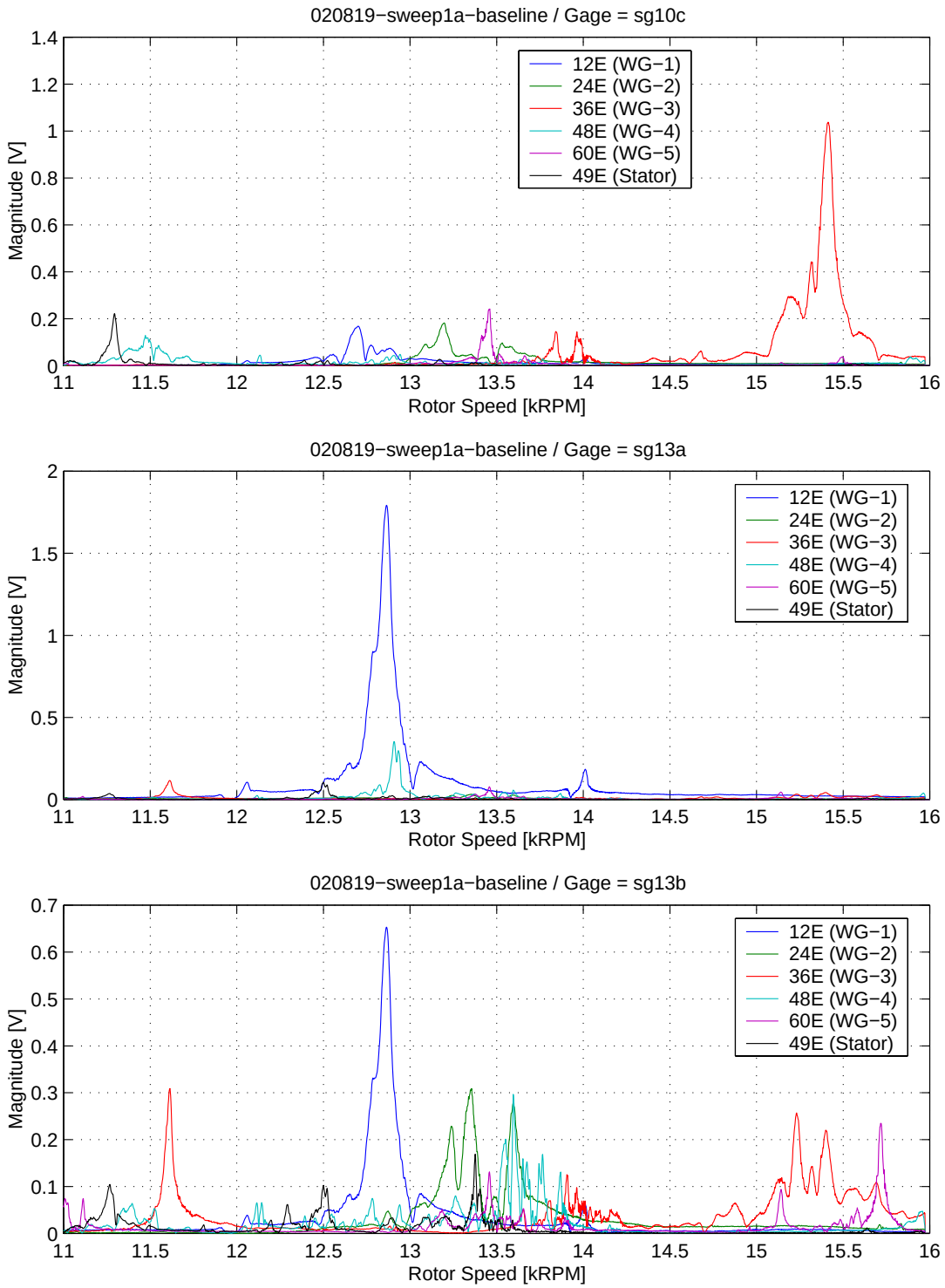

Figure B.4: Baseline order tracks for evaluating part-span TEB (page 1 of 2).

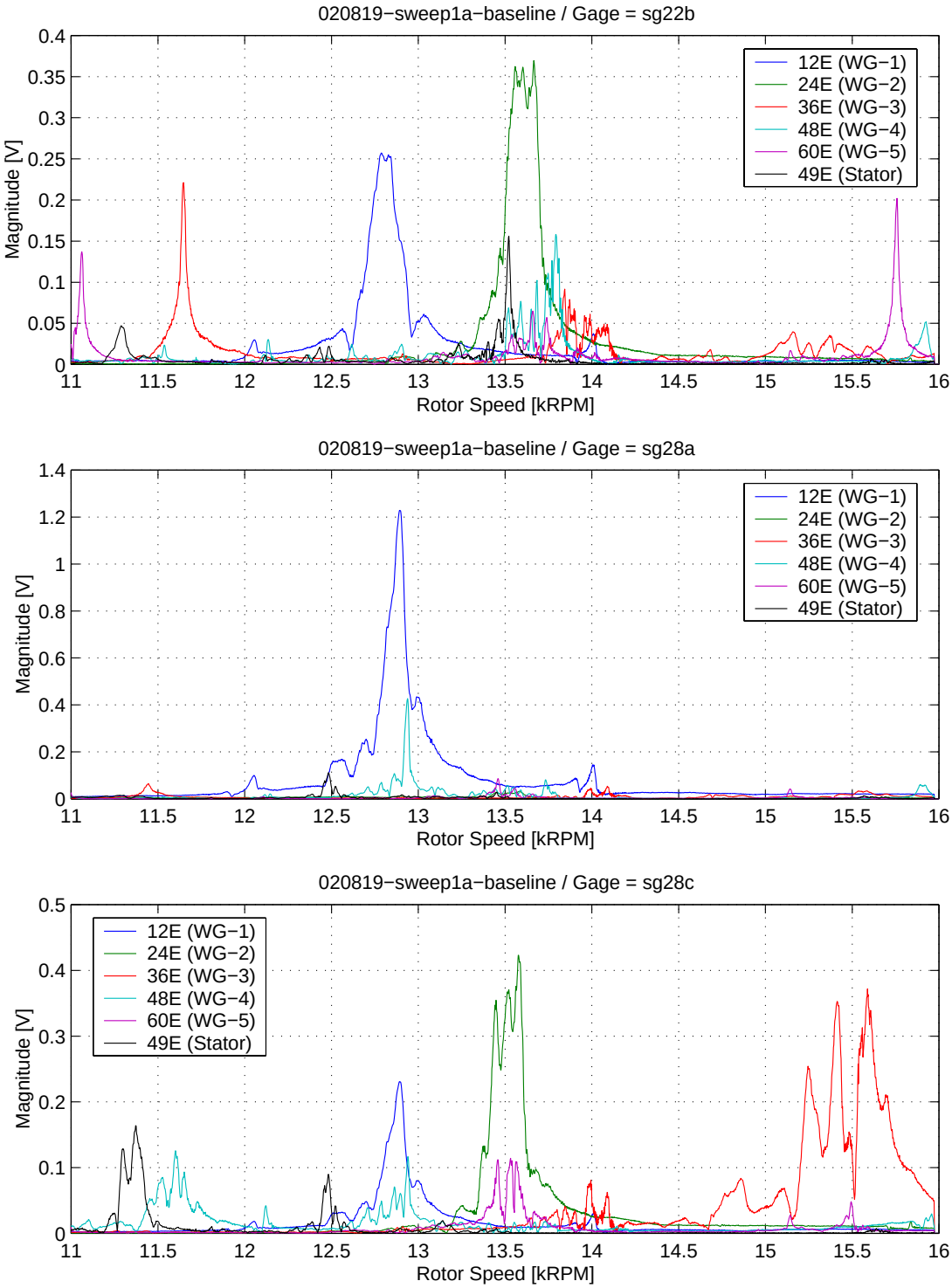

Figure B.5: Baseline order tracks for evaluating part-span TEB (page 2 of 2).

B.2 7-Hole TEB Order Track Plots

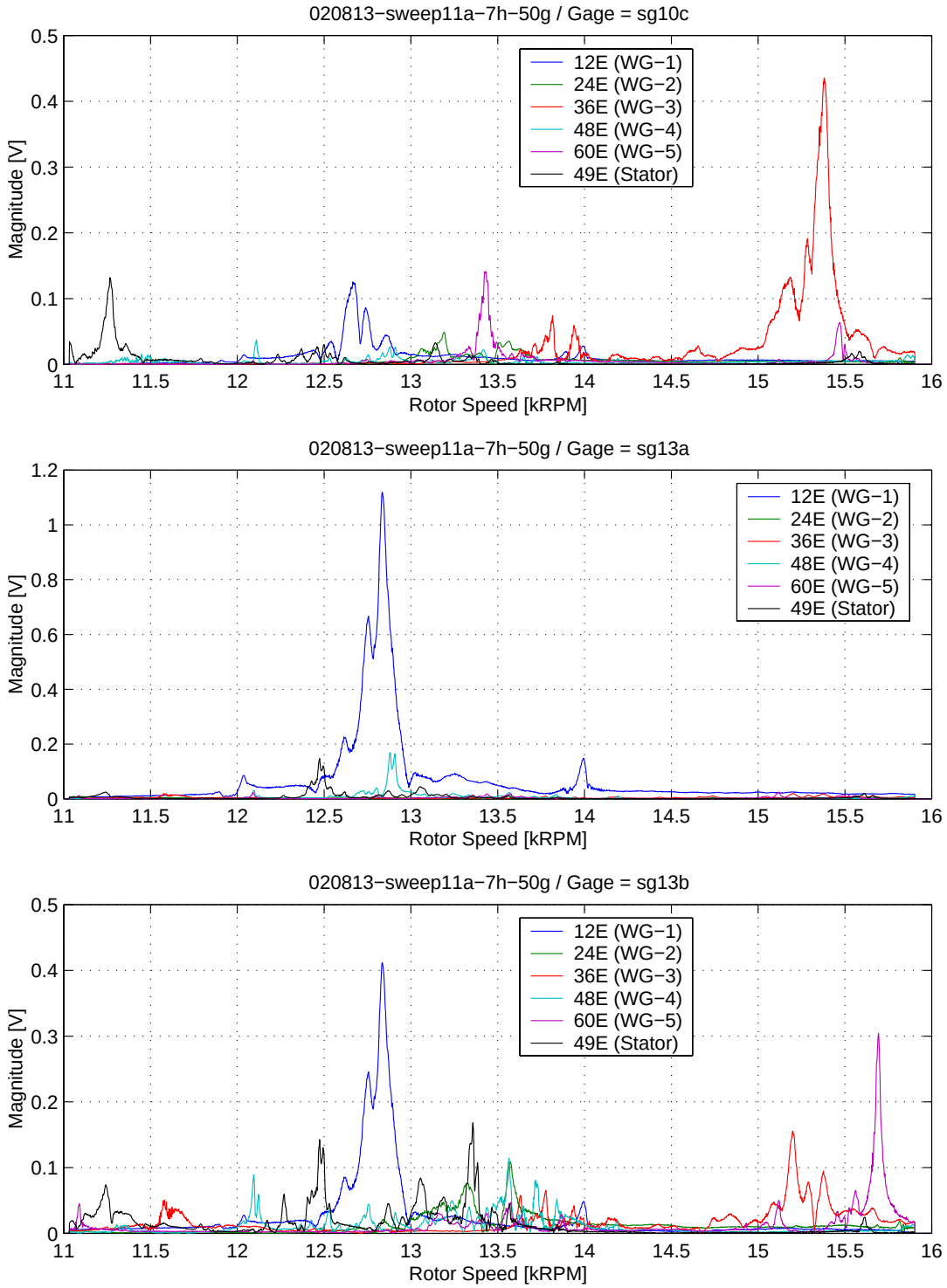

Figure B.6: Order tracks with 7-Hole TEB at 50 g/s (page 1 of 2).

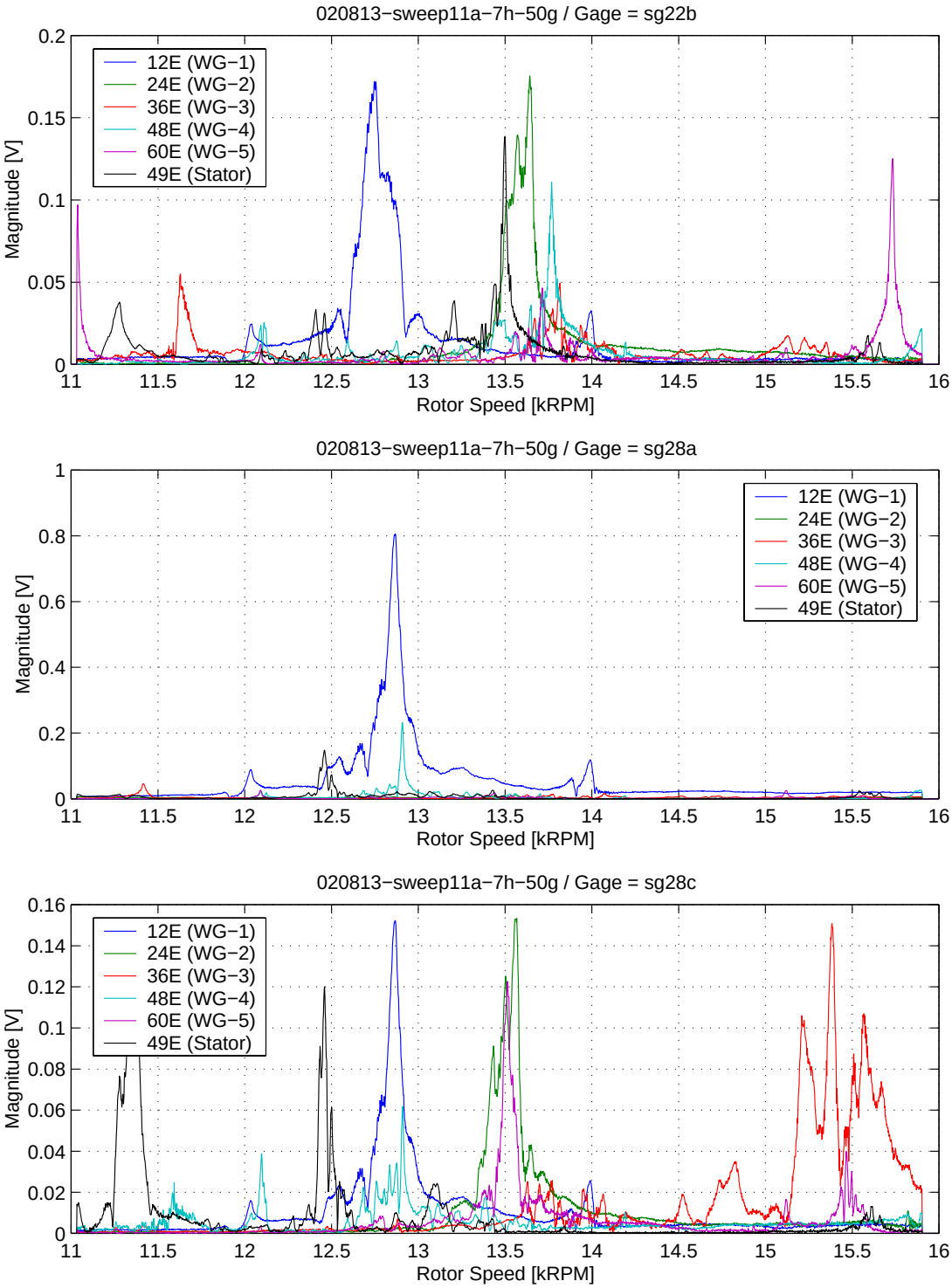

Figure B.7: Order tracks with 7-Hole TEB at 50 g/s (page 2 of 2).

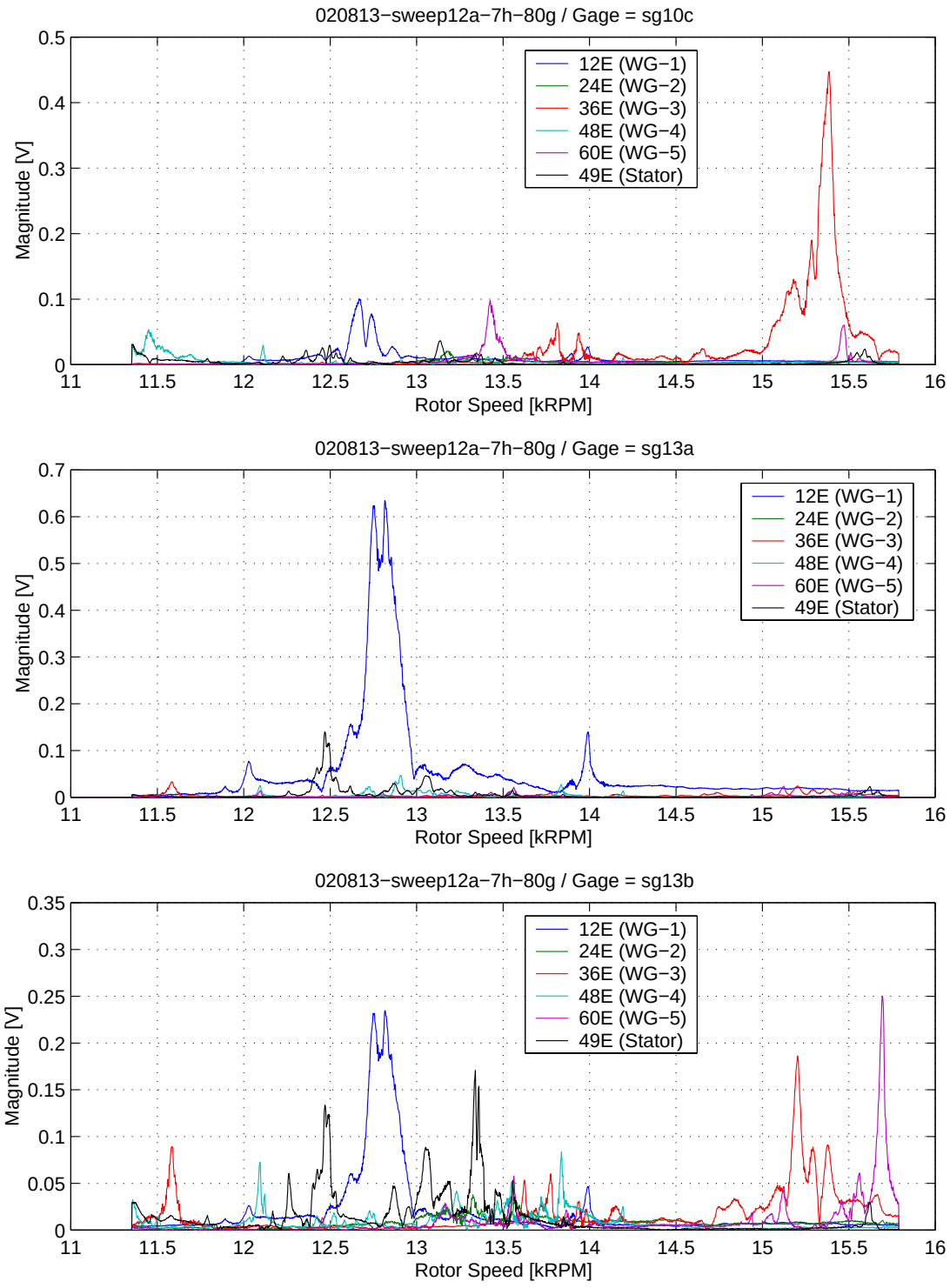

Figure B.8: Order tracks with 7-Hole TEB at 80 g/s (page 1 of 2).

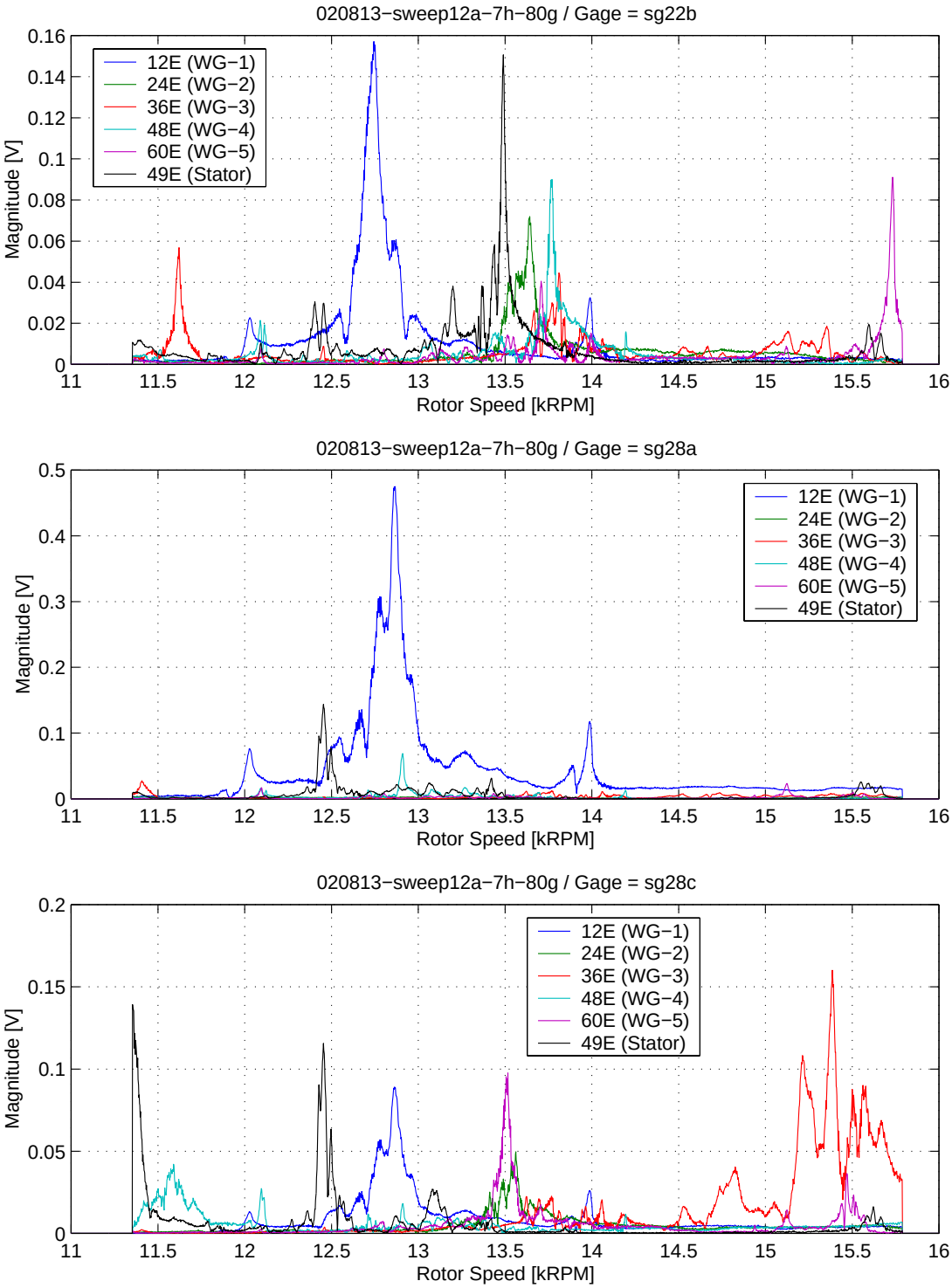

Figure B.9: Order tracks with 7-Hole TEB at 80 g/s (page 2 of 2).

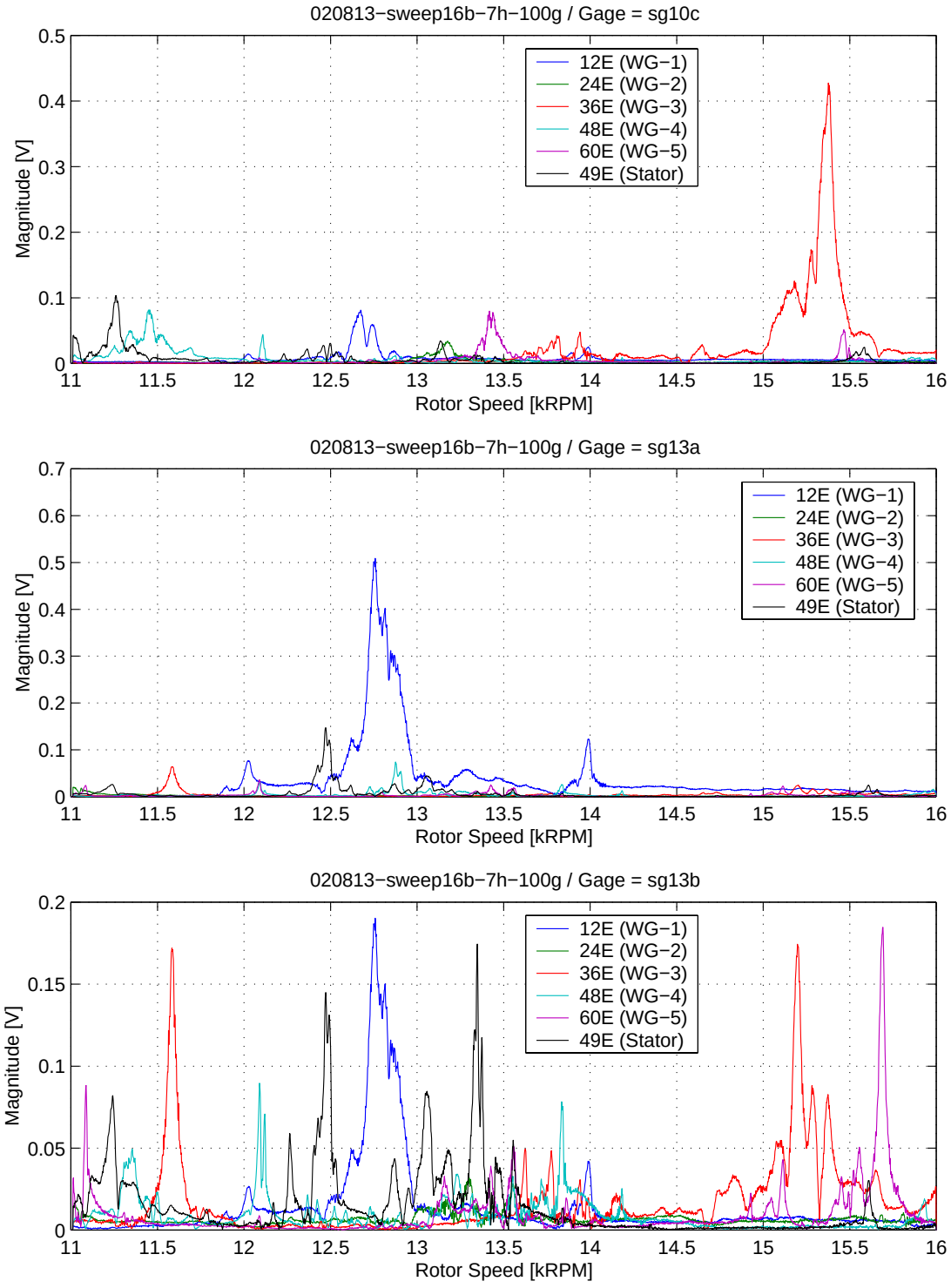

Figure B.10: Order tracks with 7-Hole TEB at 100 g/s (page 1 of 2).

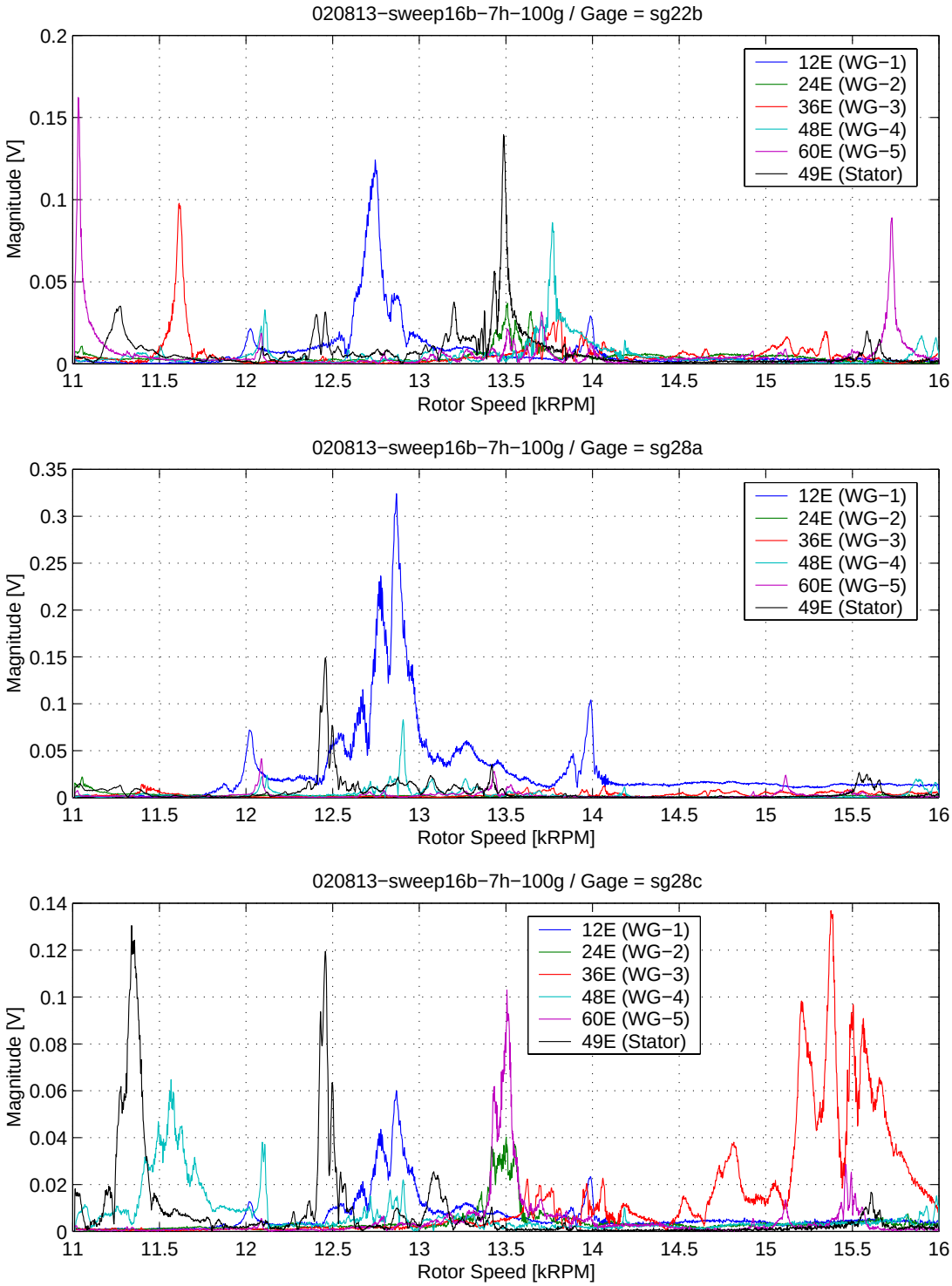

Figure B.11: Order tracks with 7-Hole TEB at 100 g/s (page 2 of 2).

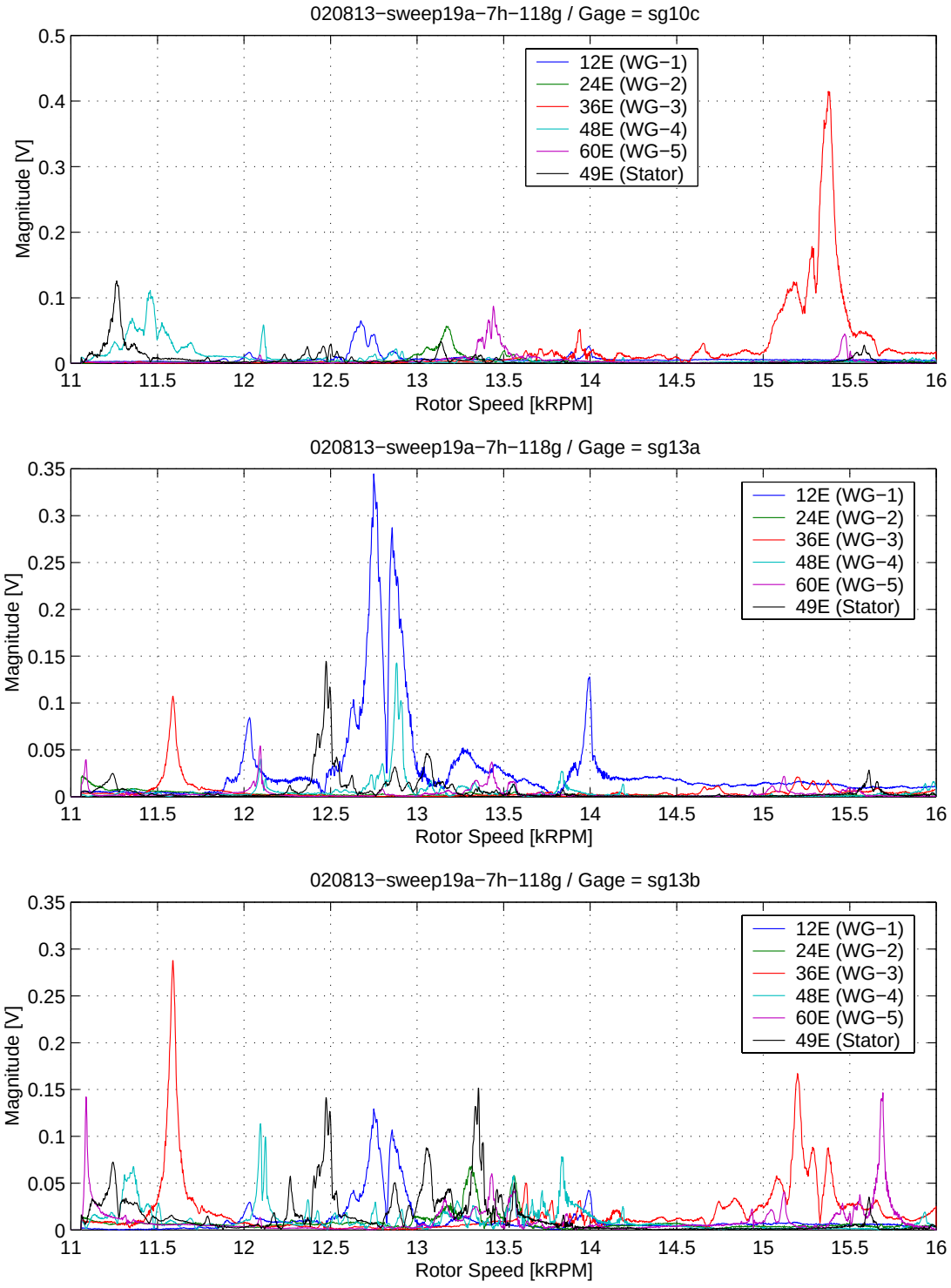

Figure B.12: Order tracks with 7-Hole TEB at 118 g/s (page 1 of 2).

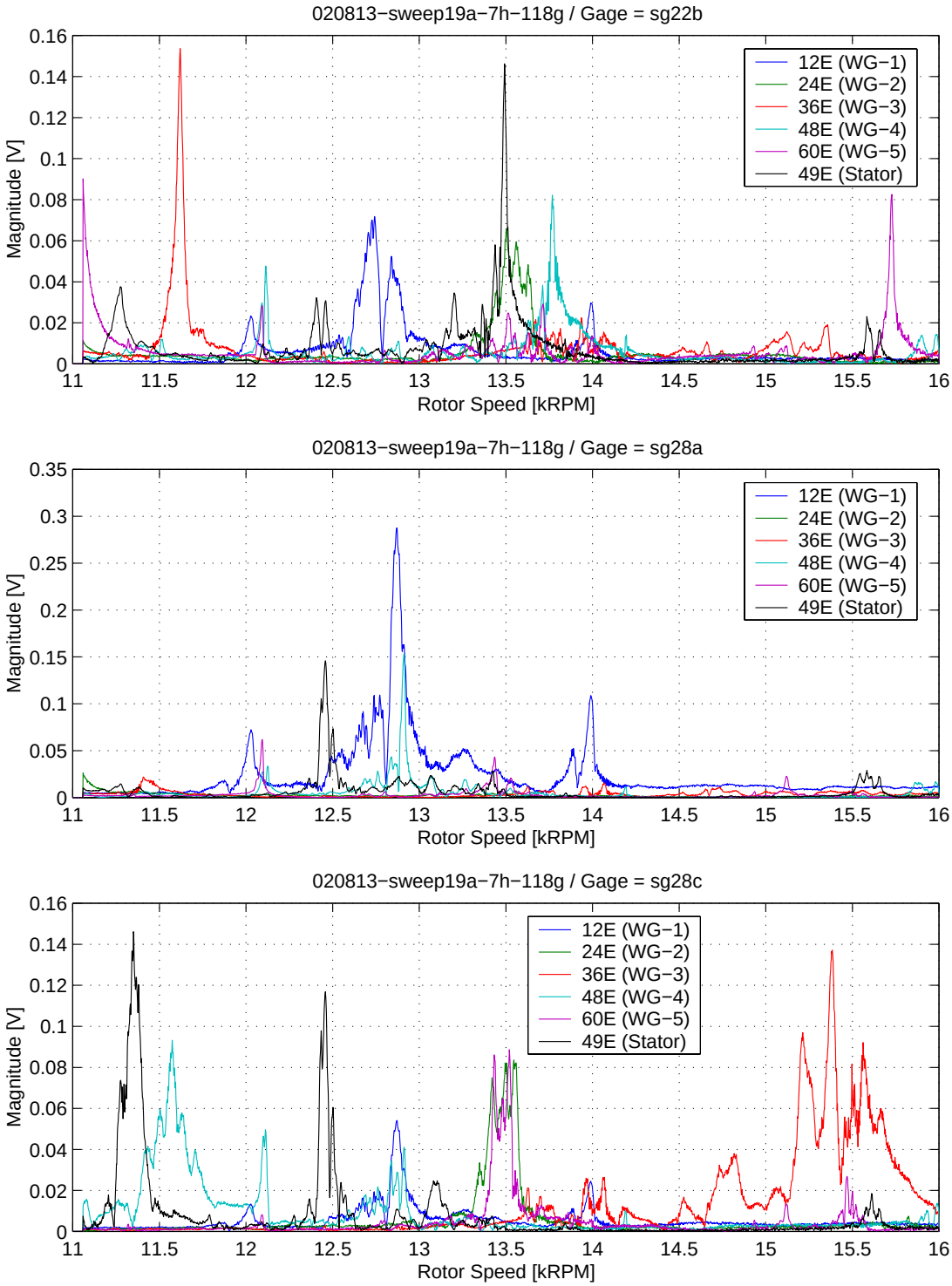

Figure B.13: Order tracks with 7-Hole TEB at 118 g/s (page 2 of 2).

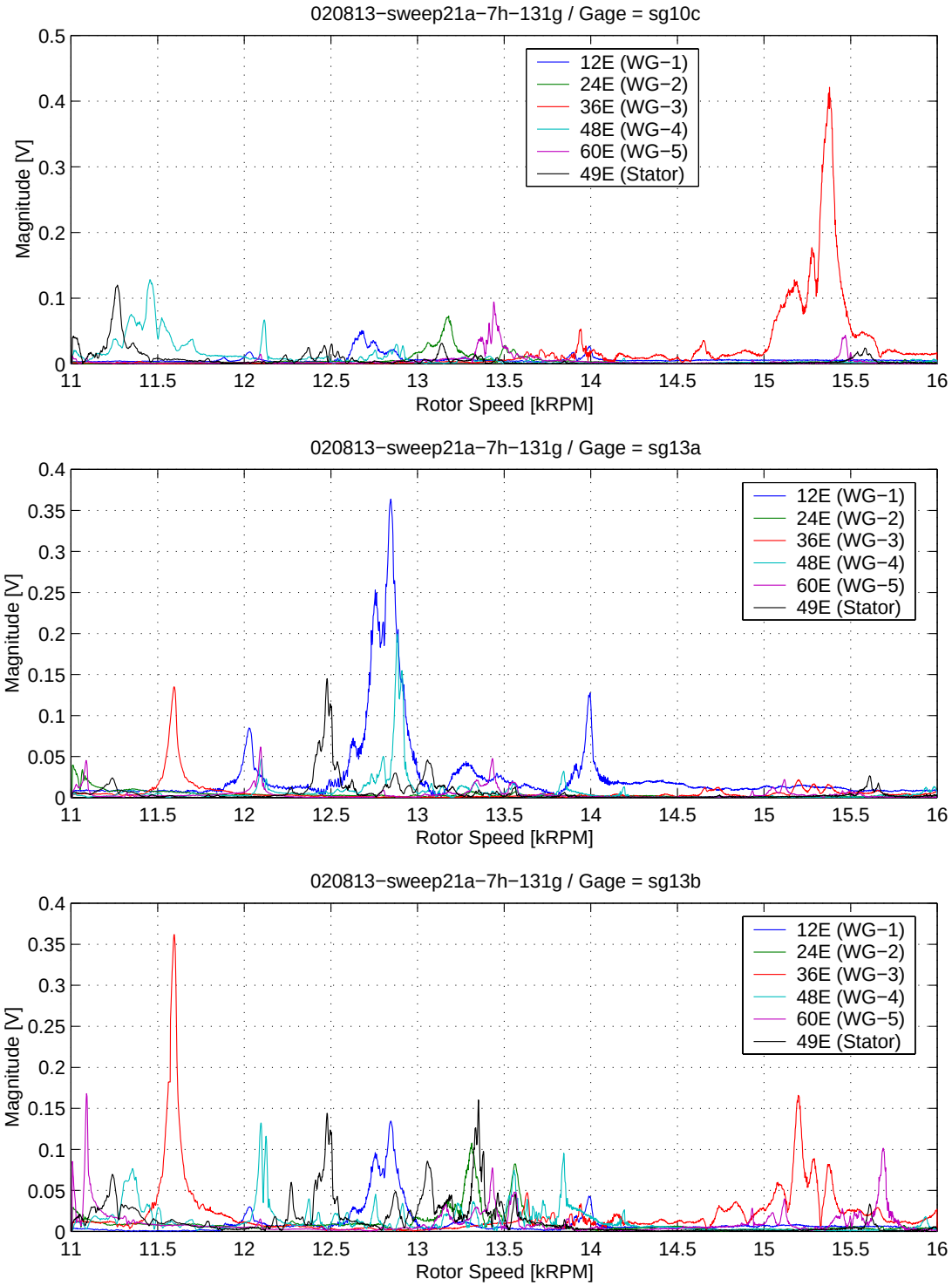

Figure B.14: Order tracks with 7-Hole TEB at 131 g/s (page 1 of 2).

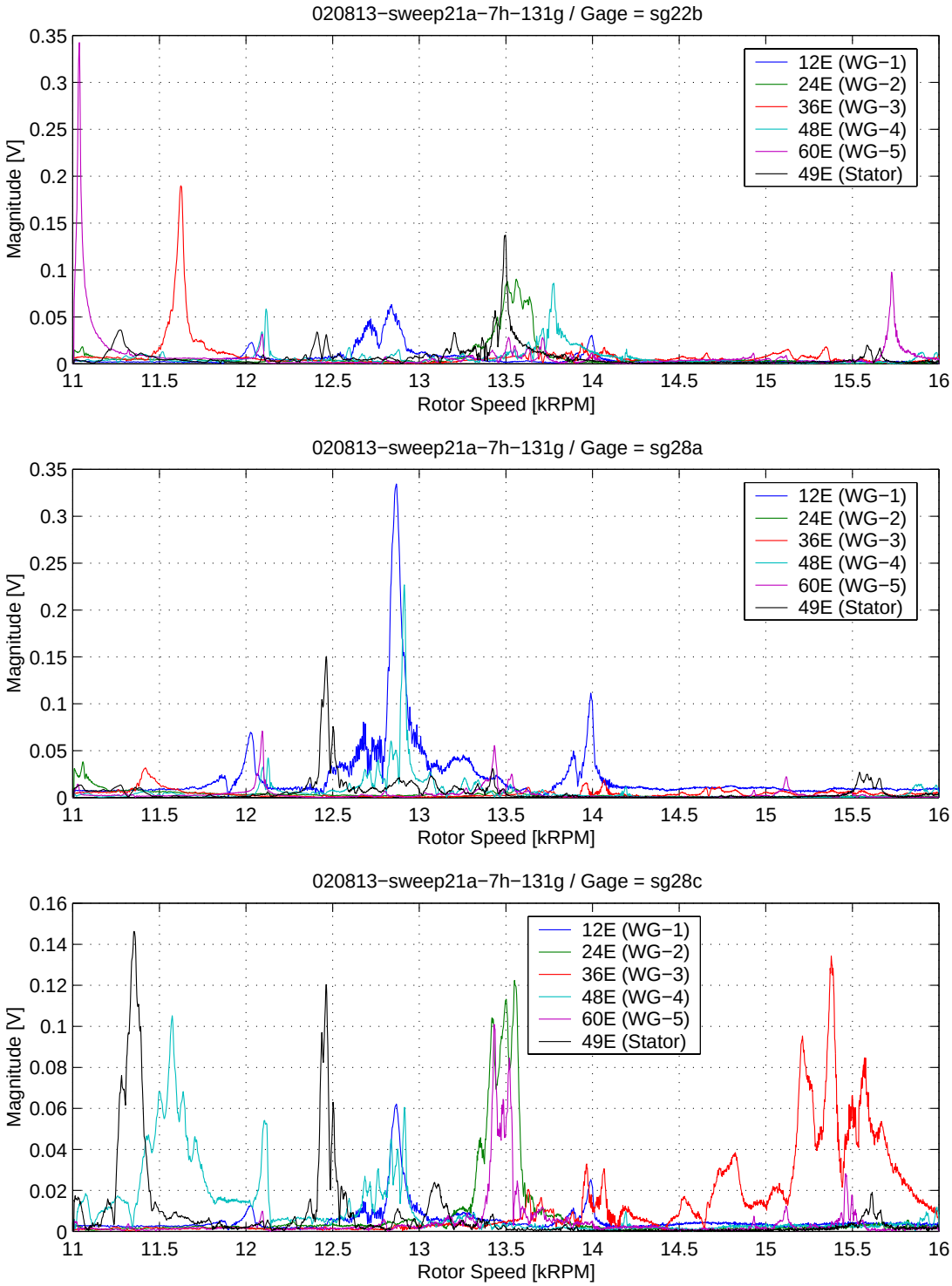

Figure B.15: Order tracks with 7-Hole TEB at 131 g/s (page 2 of 2).

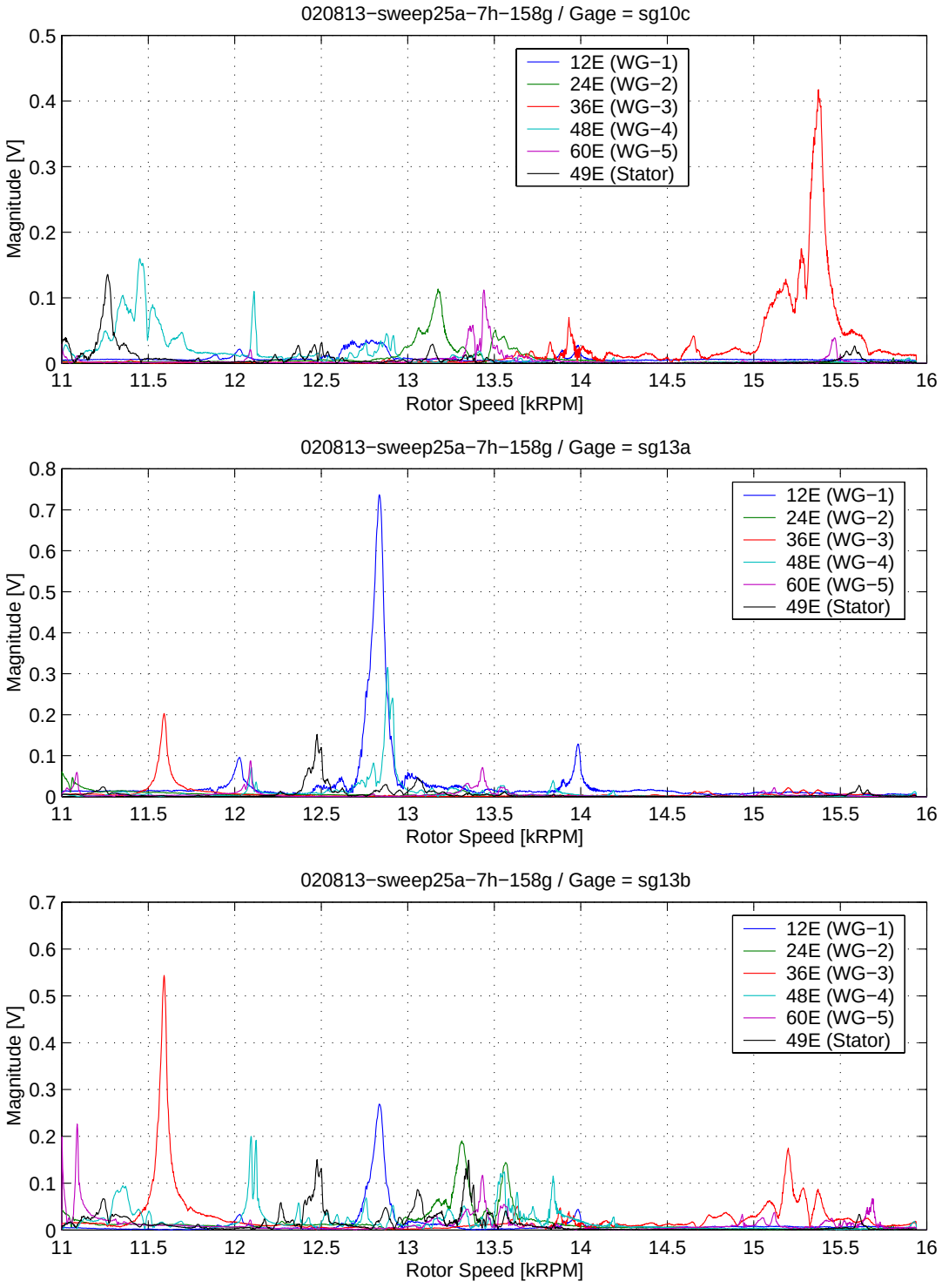

Figure B.16: Order tracks with 7-Hole TEB at 158 g/s (page 1 of 2).

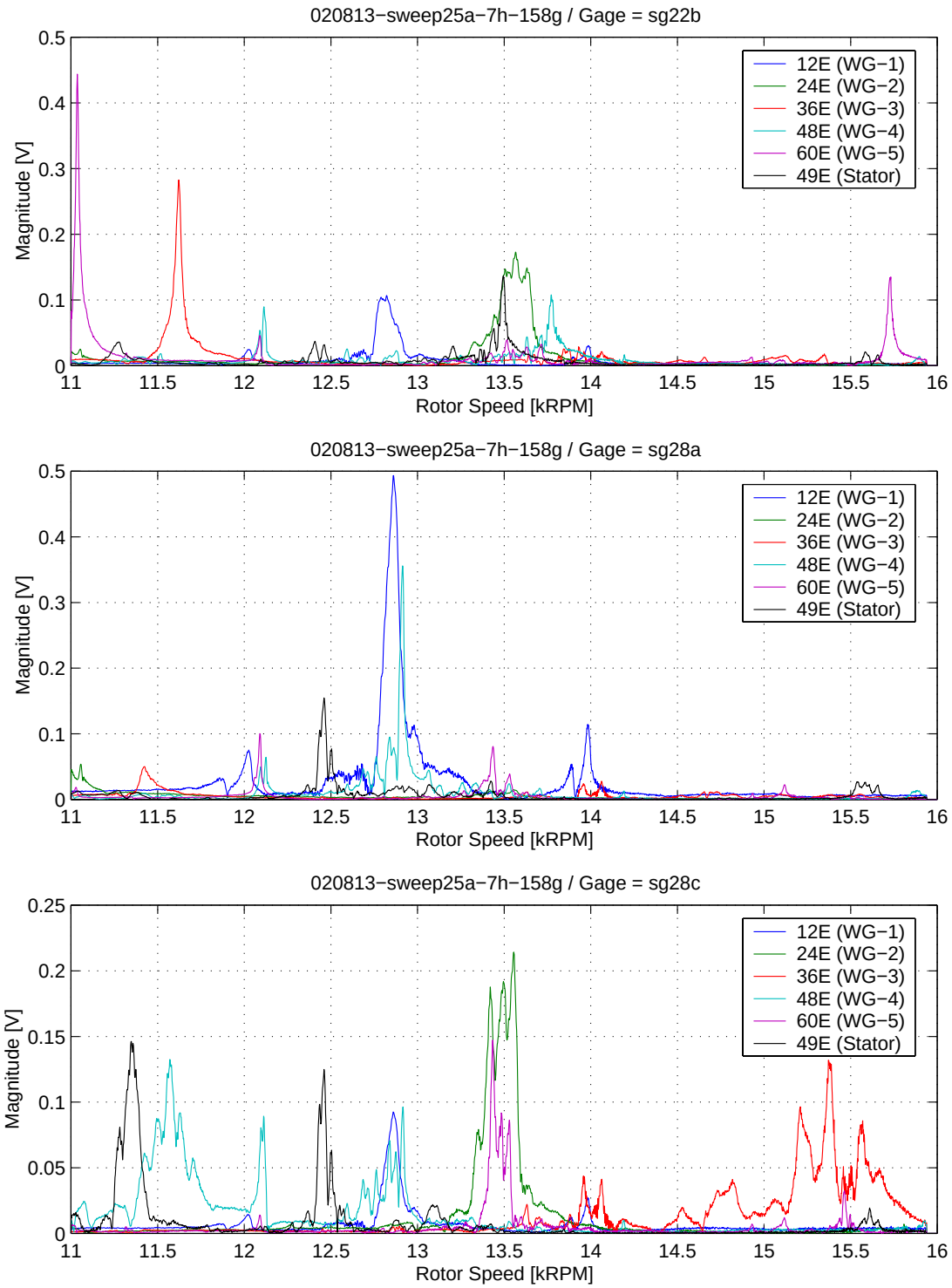

Figure B.17: Order tracks with 7-Hole TEB at 158 g/s (page 2 of 2).

B.3 5-Hole TEB Order Track Plots

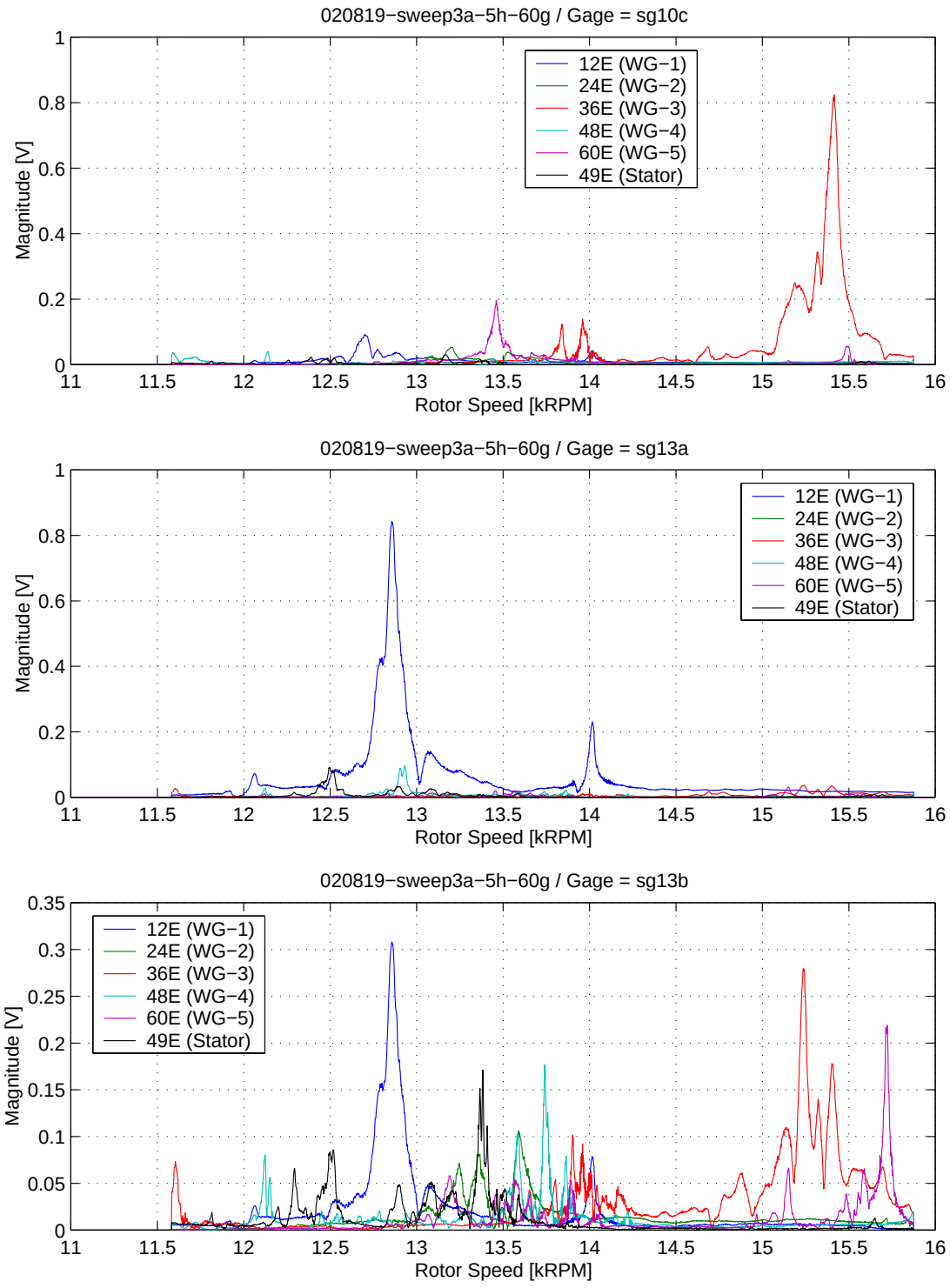

Figure B.18: Order tracks with 5-Hole TEB at 60 g/s (page 1 of 2).

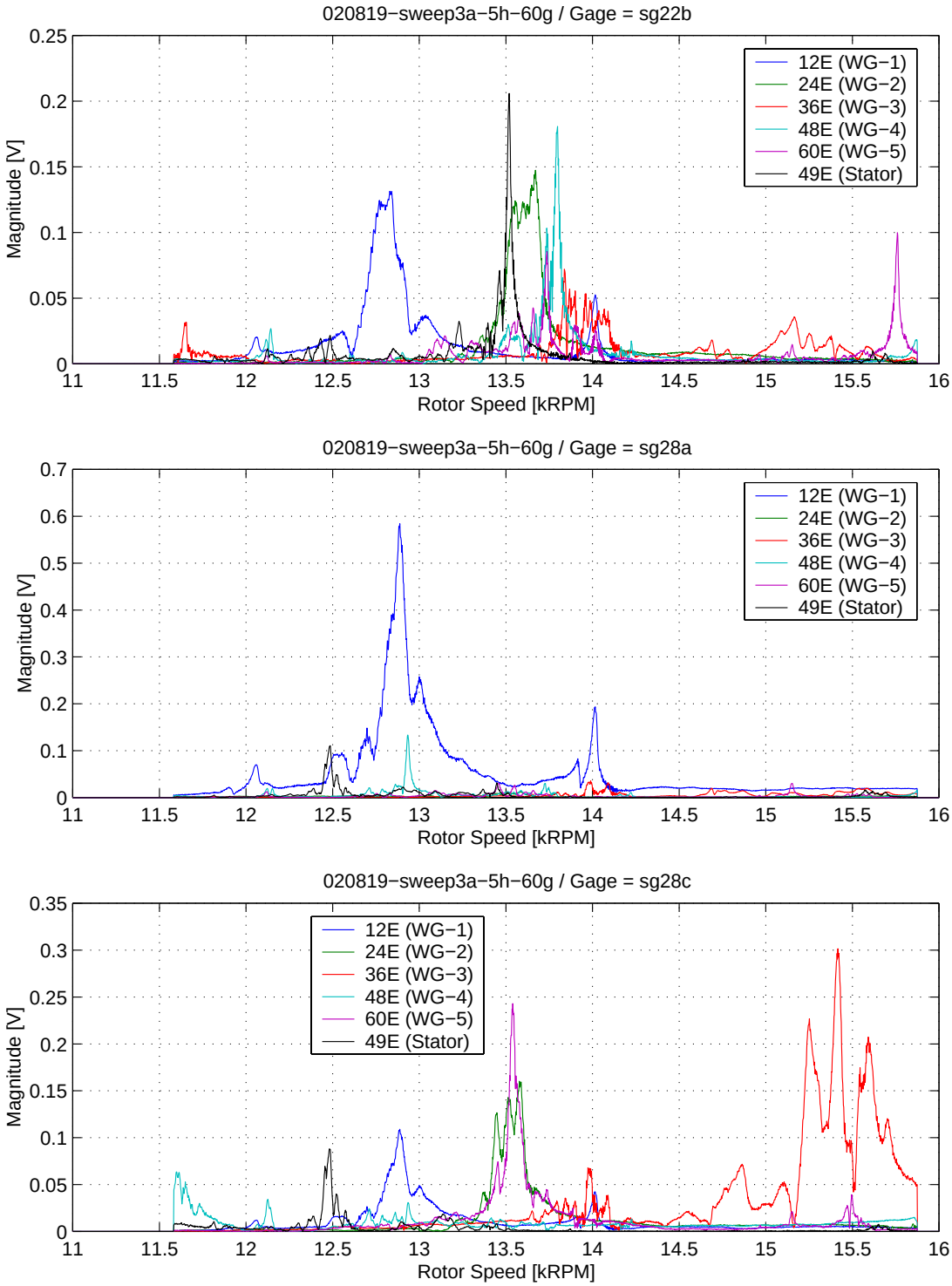

Figure B.19: Order tracks with 5-Hole TEB at 60 g/s (page 2 of 2).

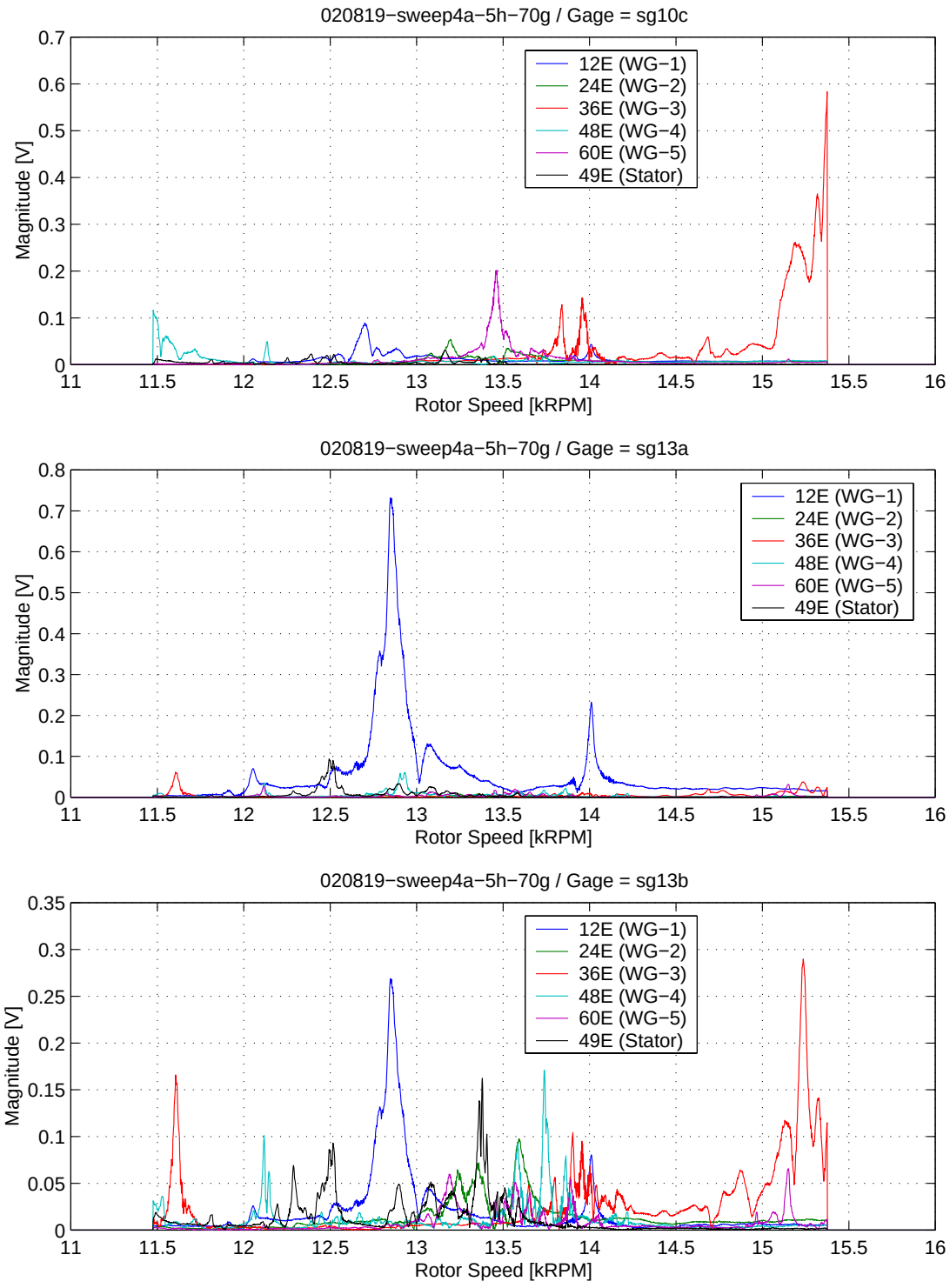

Figure B.20: Order tracks with 5-Hole TEB at 70 g/s (page 1 of 2).

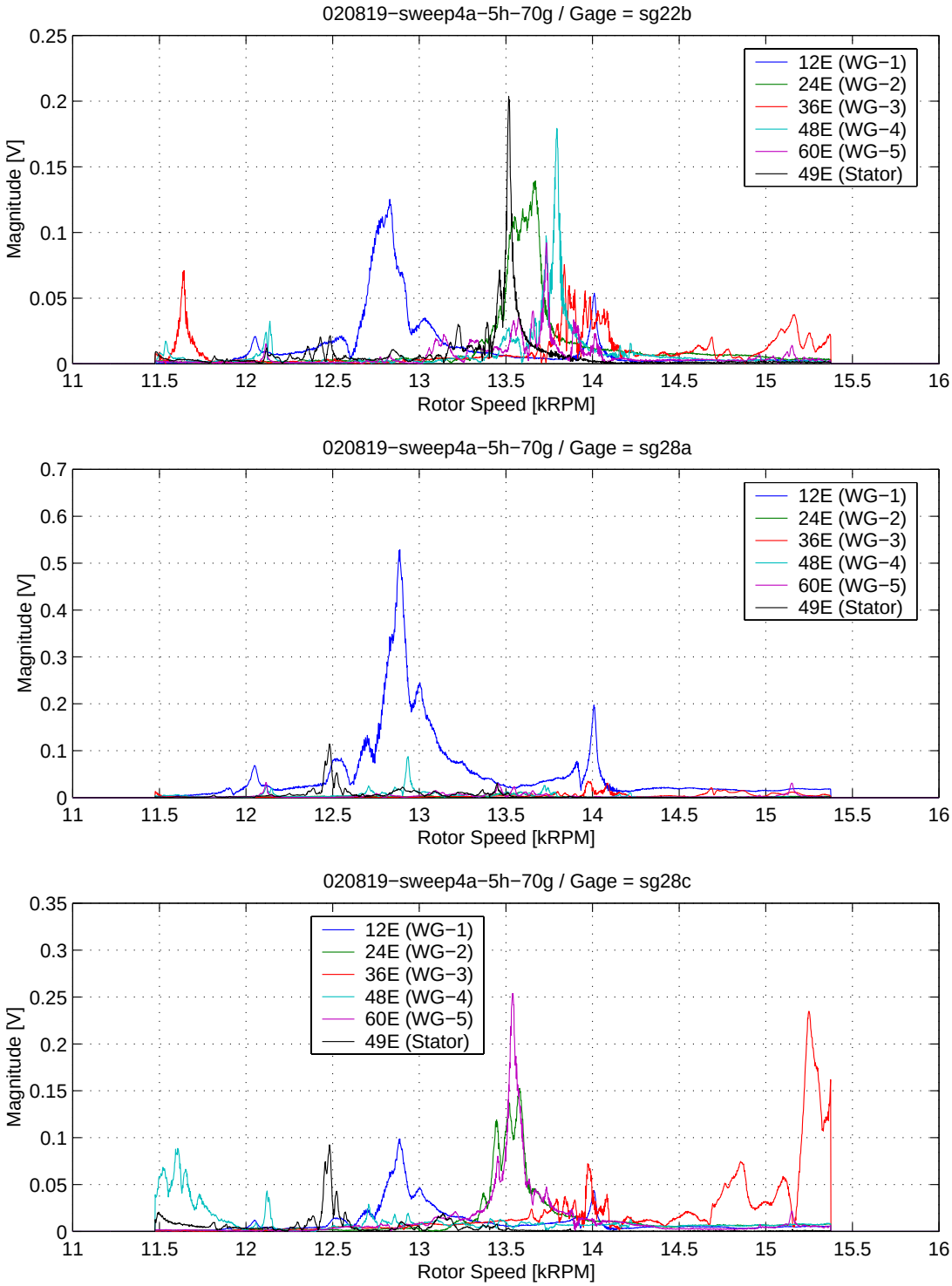

Figure B.21: Order tracks with 5-Hole TEB at 70 g/s (page 2 of 2).

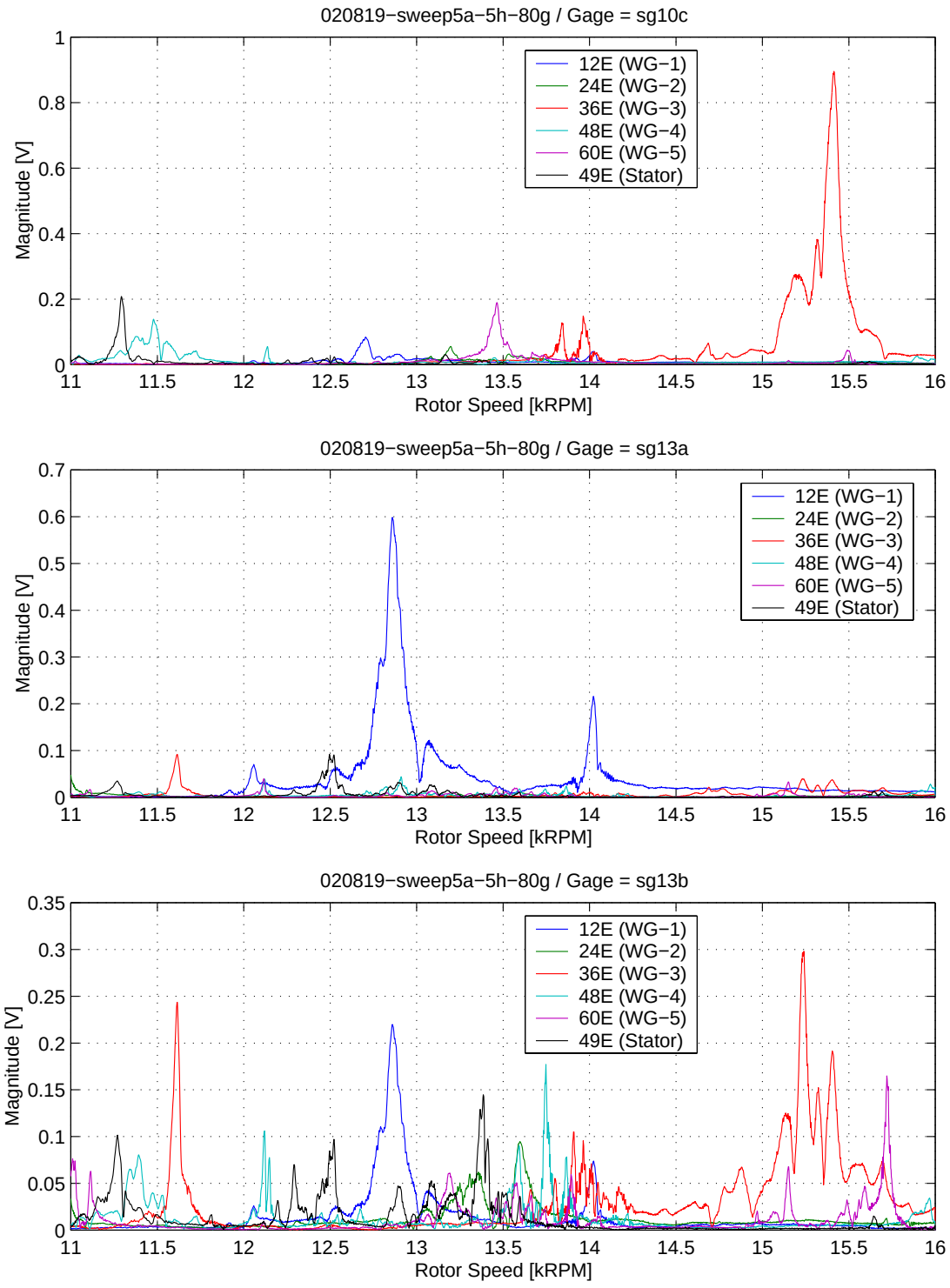

Figure B.22: Order tracks with 5-Hole TEB at 80 g/s (page 1 of 2).

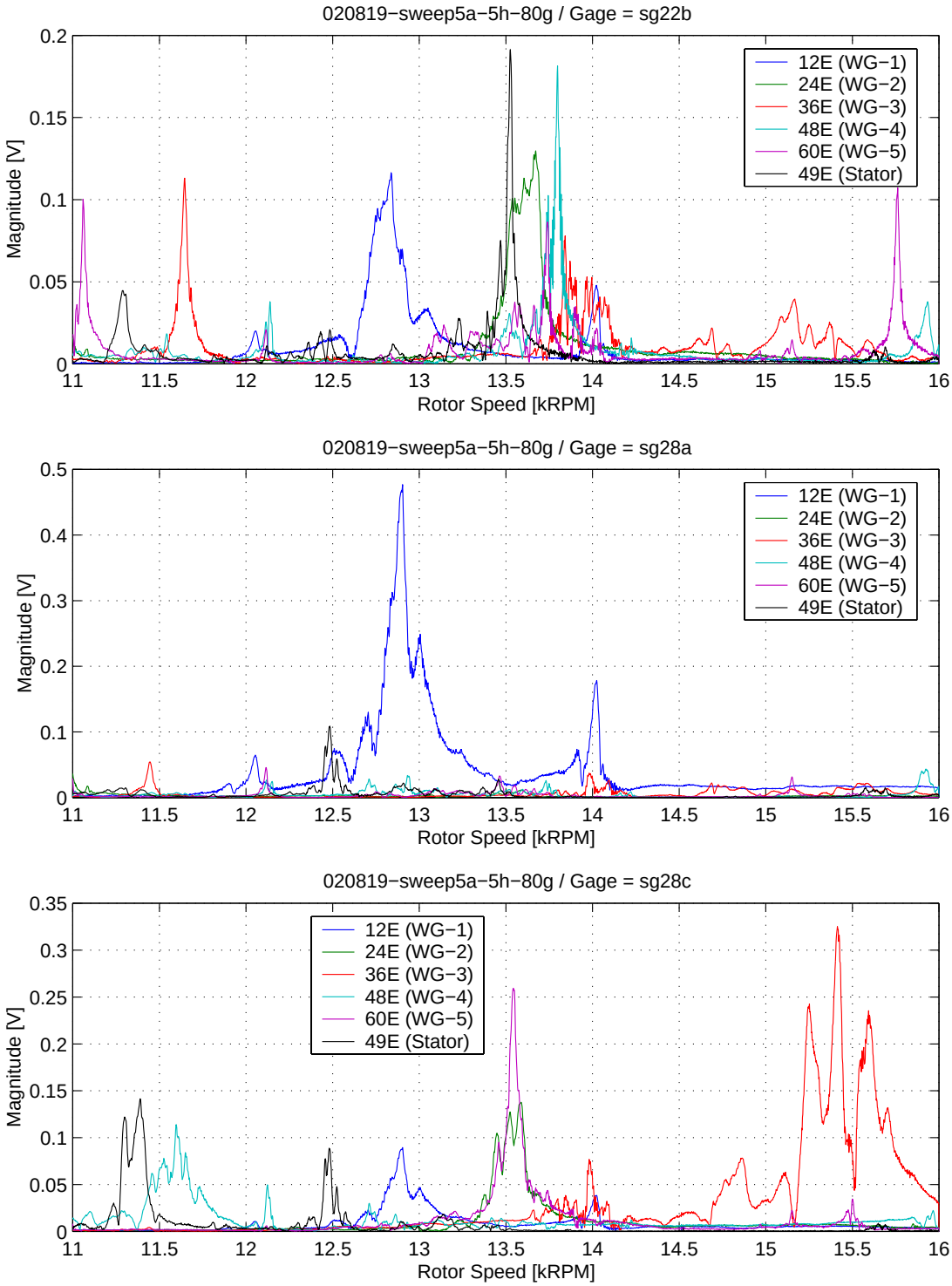

Figure B.23: Order tracks with 5-Hole TEB at 80 g/s (page 2 of 2).

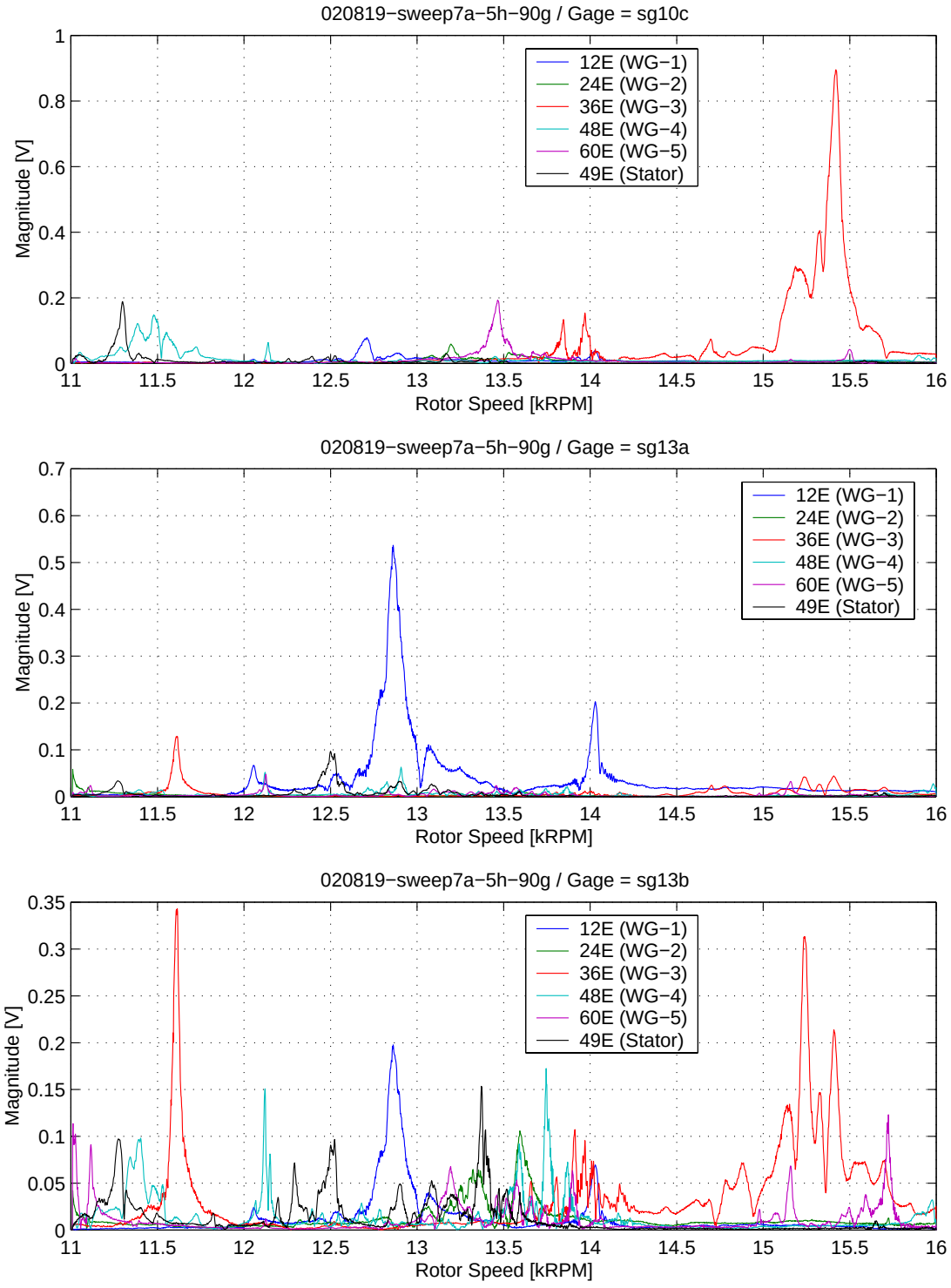

Figure B.24: Order tracks with 5-Hole TEB at 90 g/s (page 1 of 2).

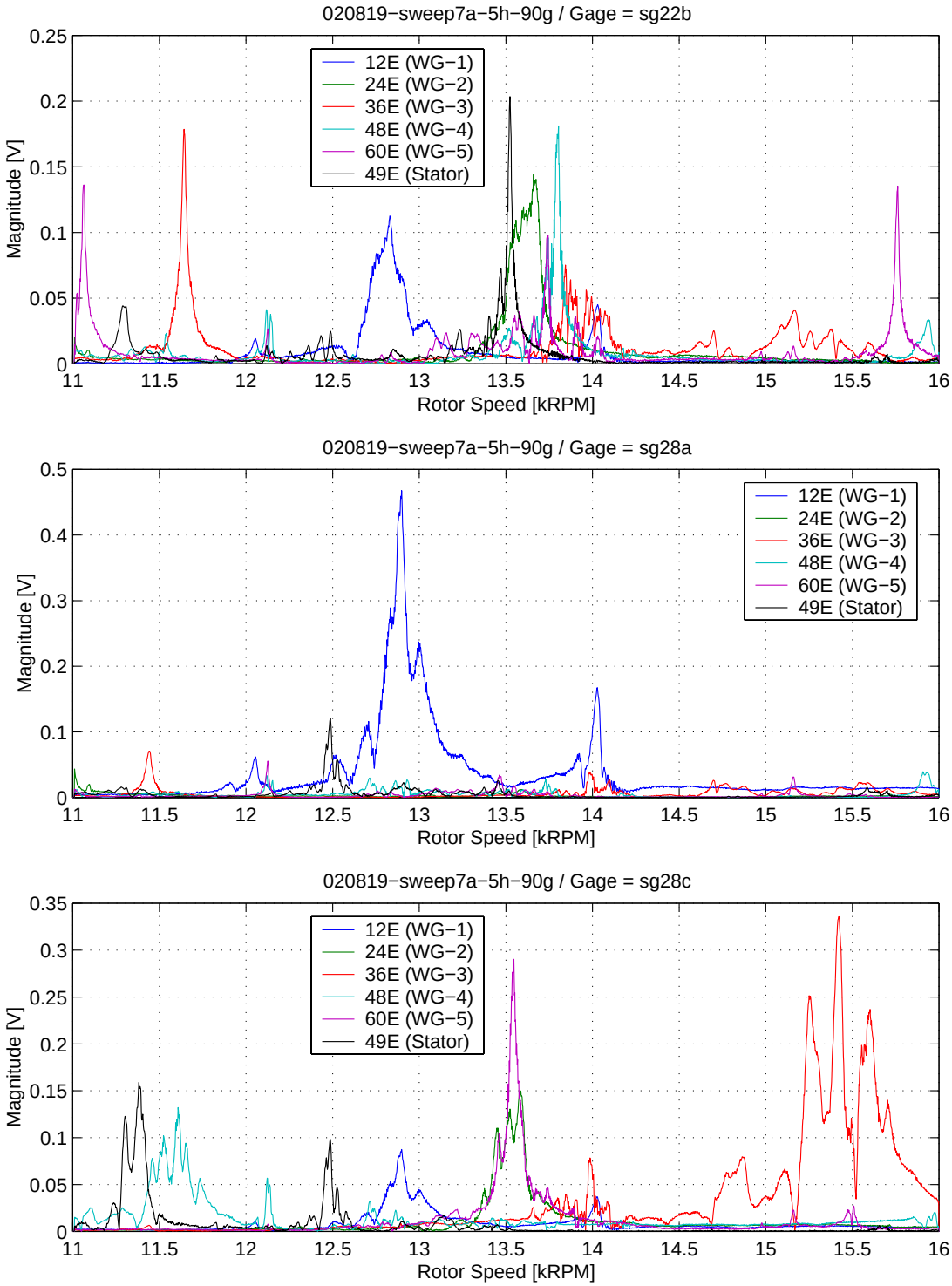

Figure B.25: Order tracks with 5-Hole TEB at 90 g/s (page 2 of 2).

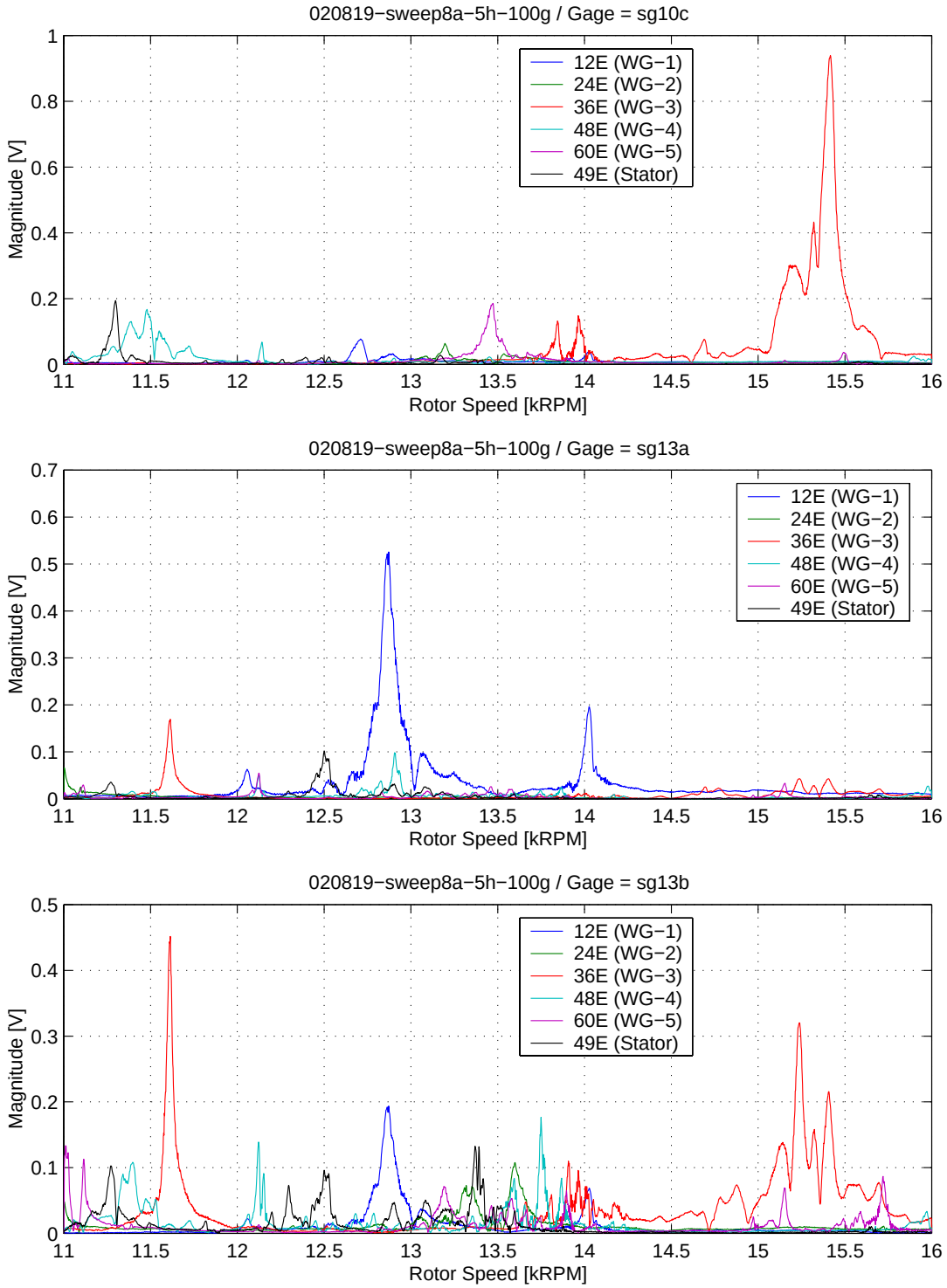

Figure B.26: Order tracks with 5-Hole TEB at 100 g/s (page 1 of 2).

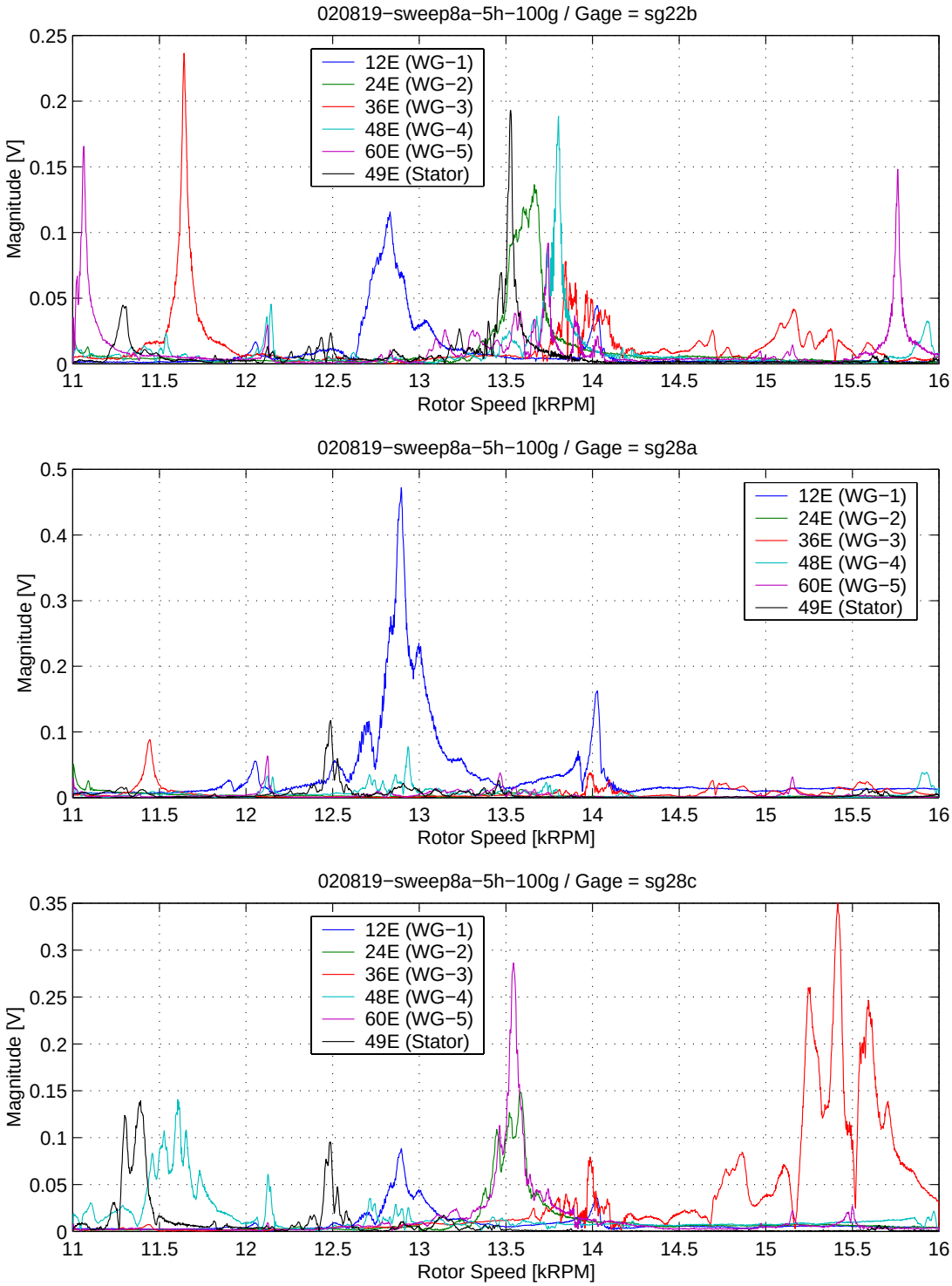

Figure B.27: Order tracks with 5-Hole TEB at 100 g/s (page 2 of 2).

B.4 3-Hole TEB Order Track Plots

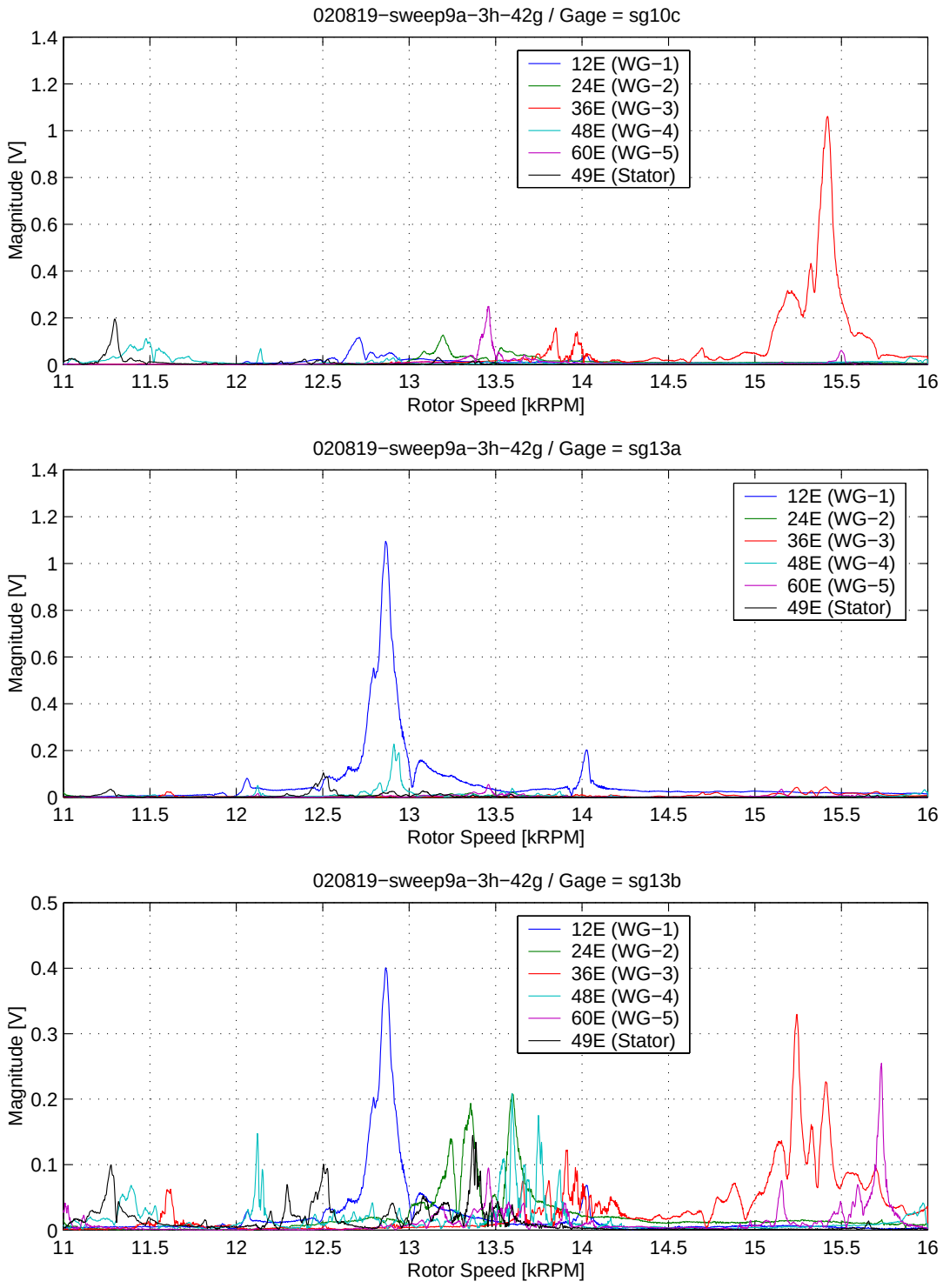

Figure B.28: Order tracks with 3-Hole TEB at 42 g/s (page 1 of 2).

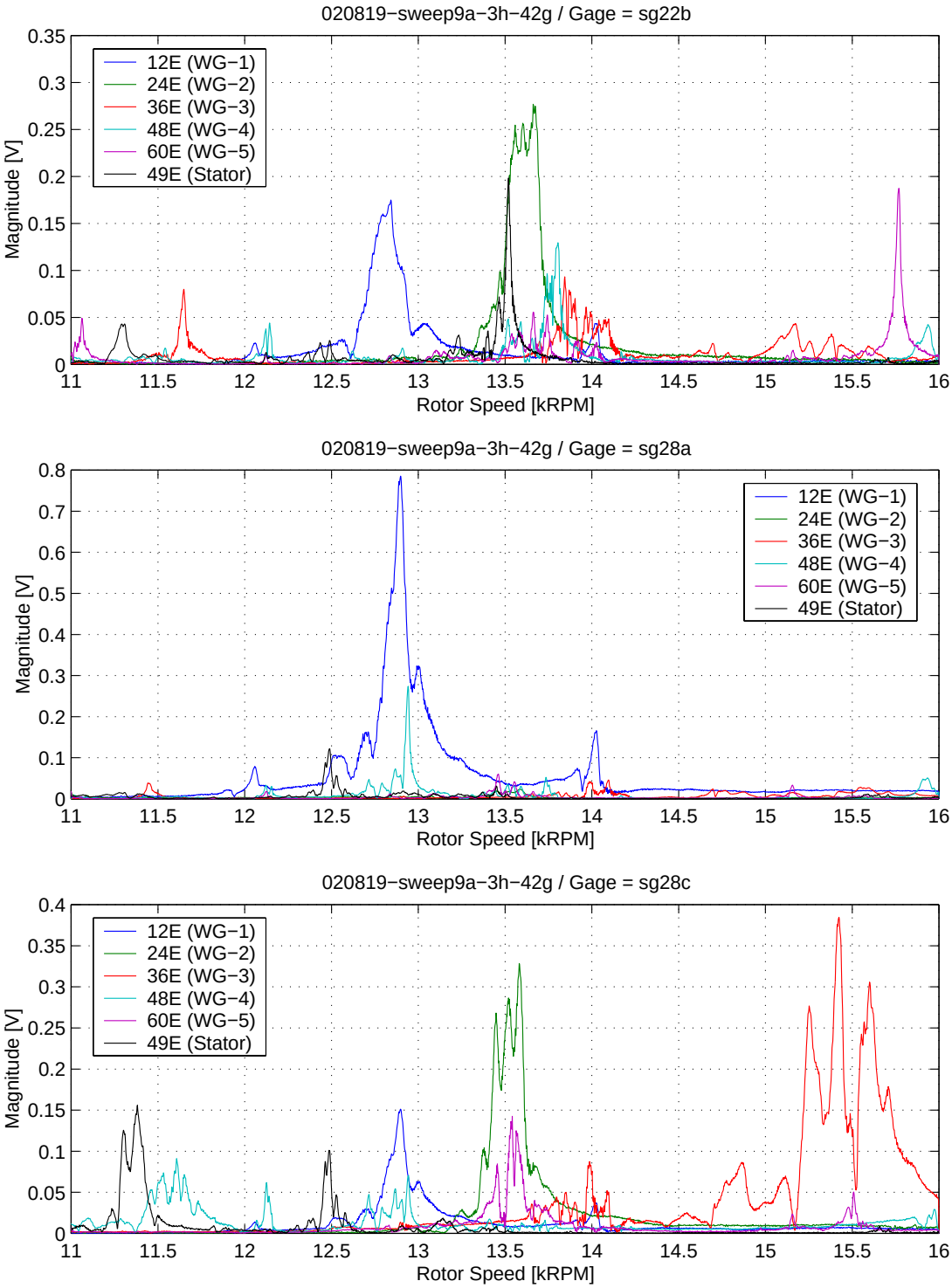

Figure B.29: Order tracks with 3-Hole TEB at 42 g/s (page 2 of 2).

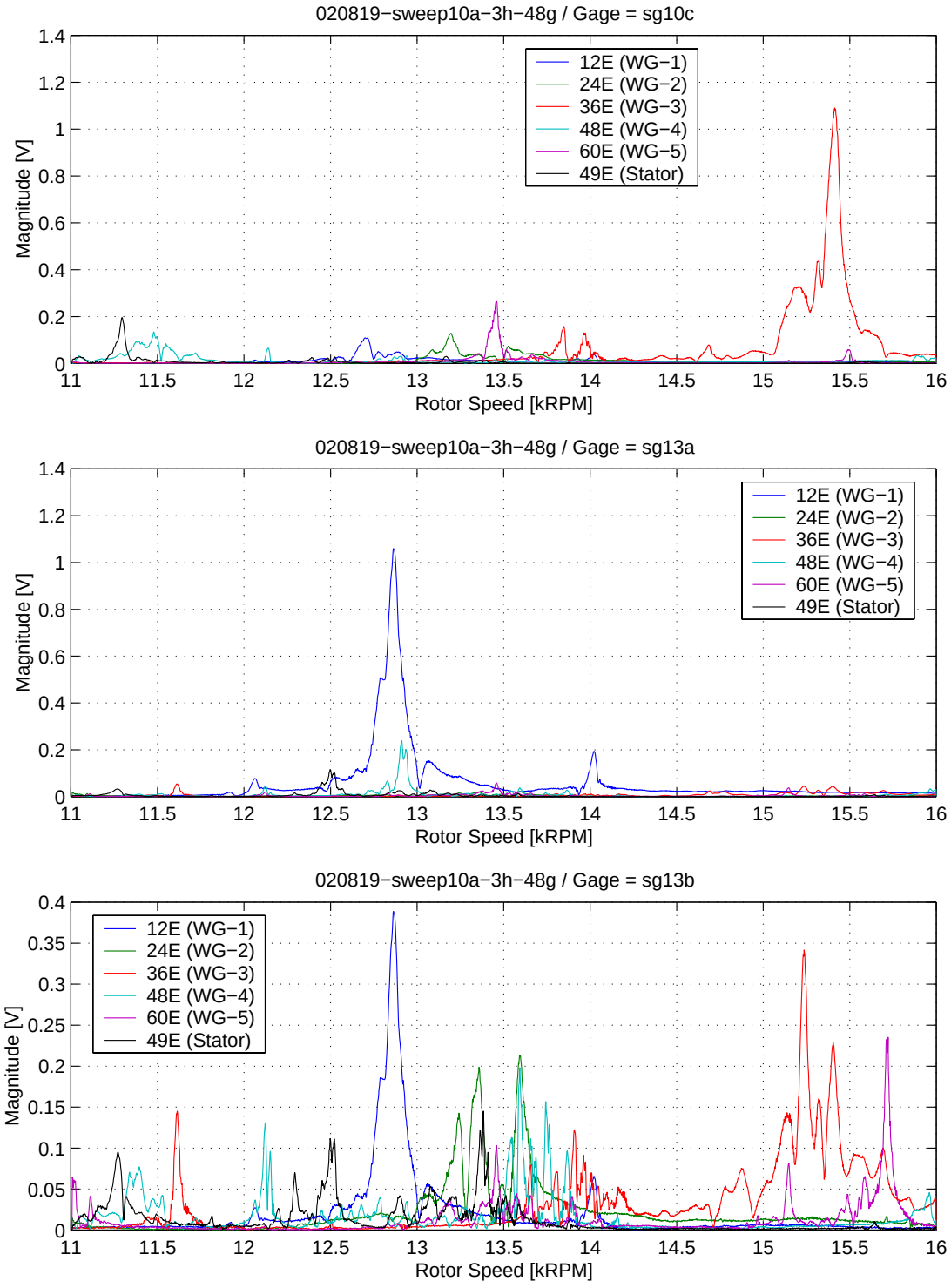

Figure B.30: Order tracks with 3-Hole TEB at 48 g/s (page 1 of 2).

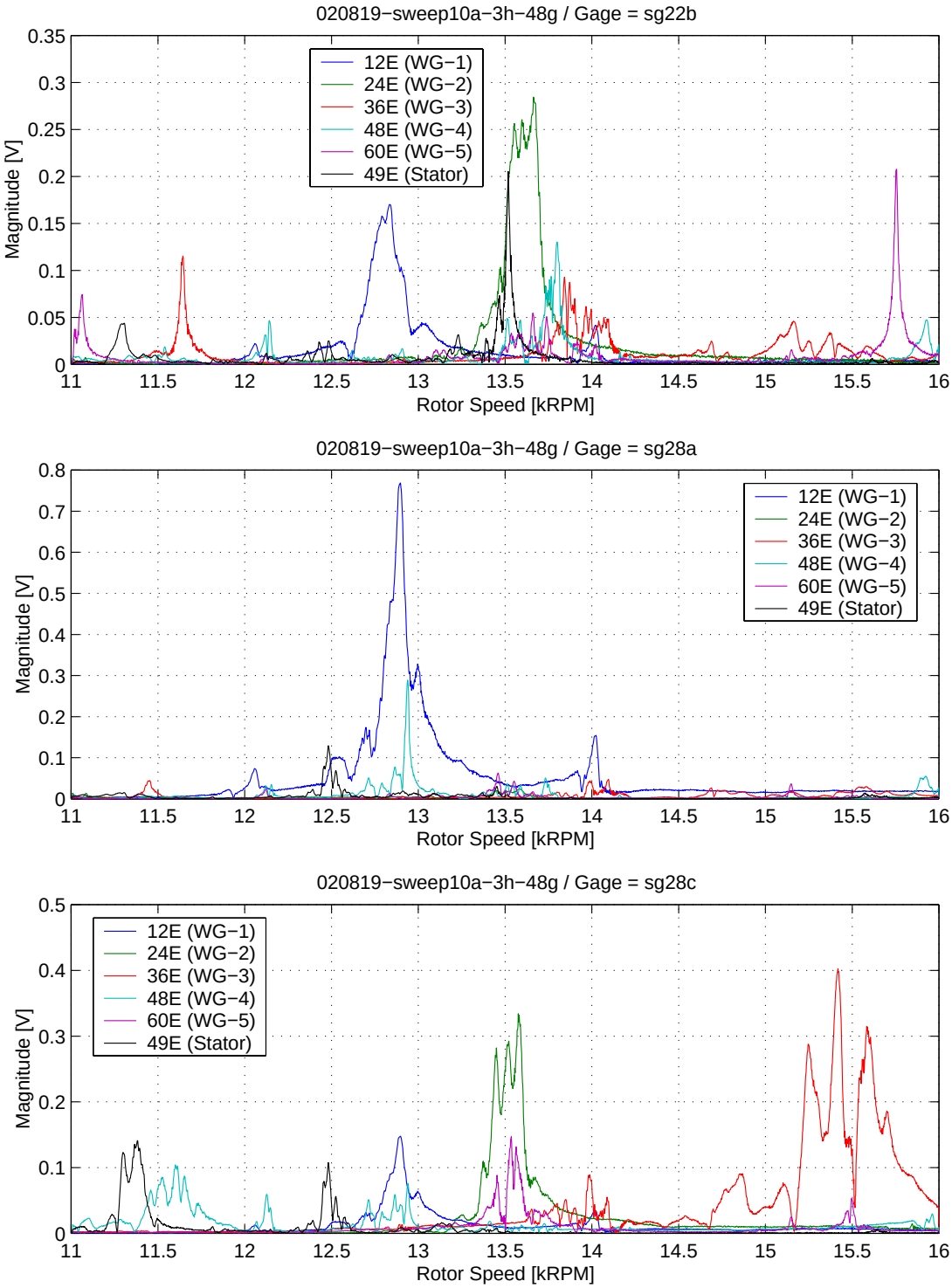

Figure B.31: Order tracks with 3-Hole TEB at 48 g/s (page 2 of 2).

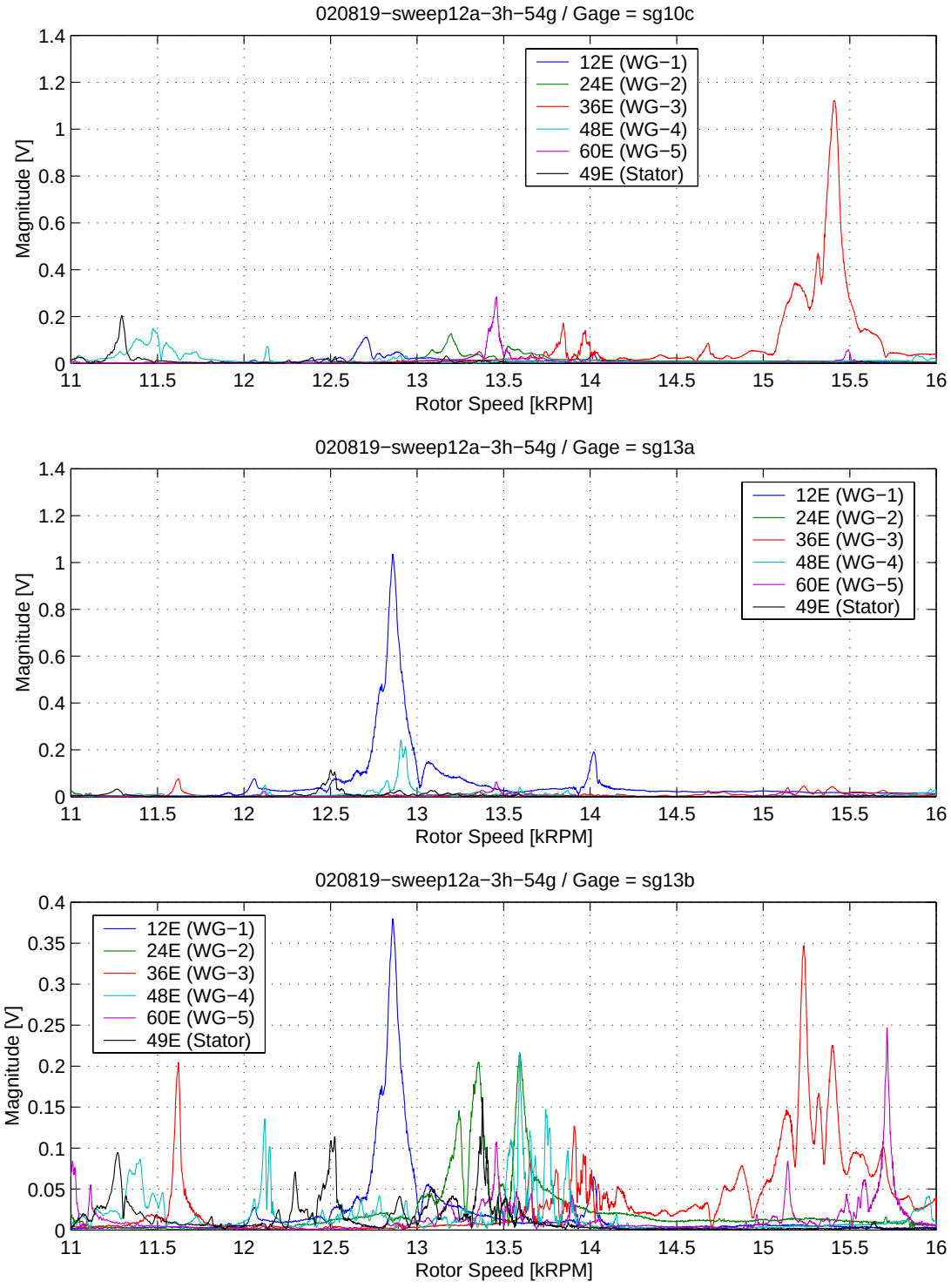

Figure B.32: Order tracks with 3-Hole TEB at 54 g/s (page 1 of 2).

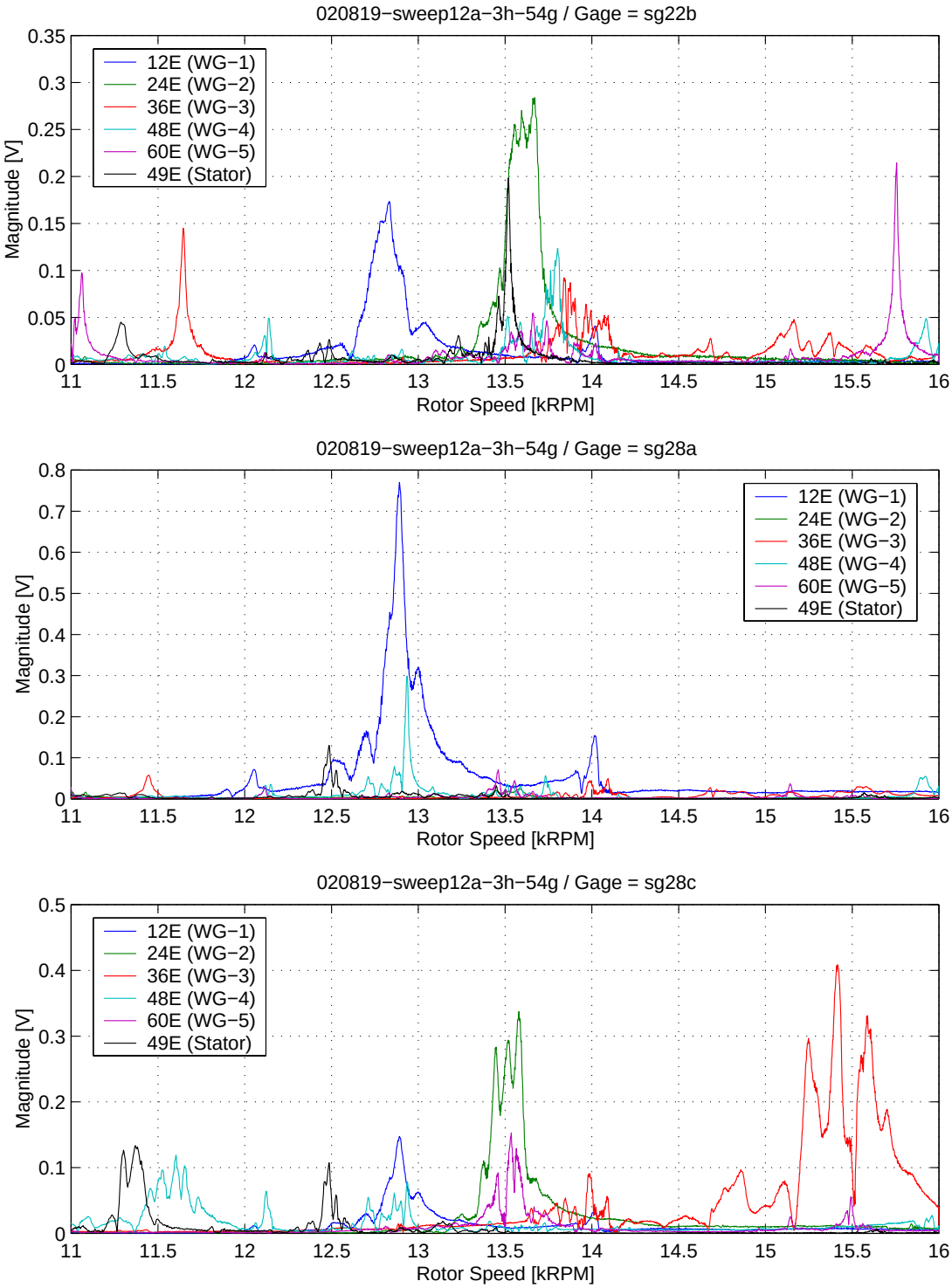

Figure B.33: Order tracks with 3-Hole TEB at 54 g/s (page 2 of 2).

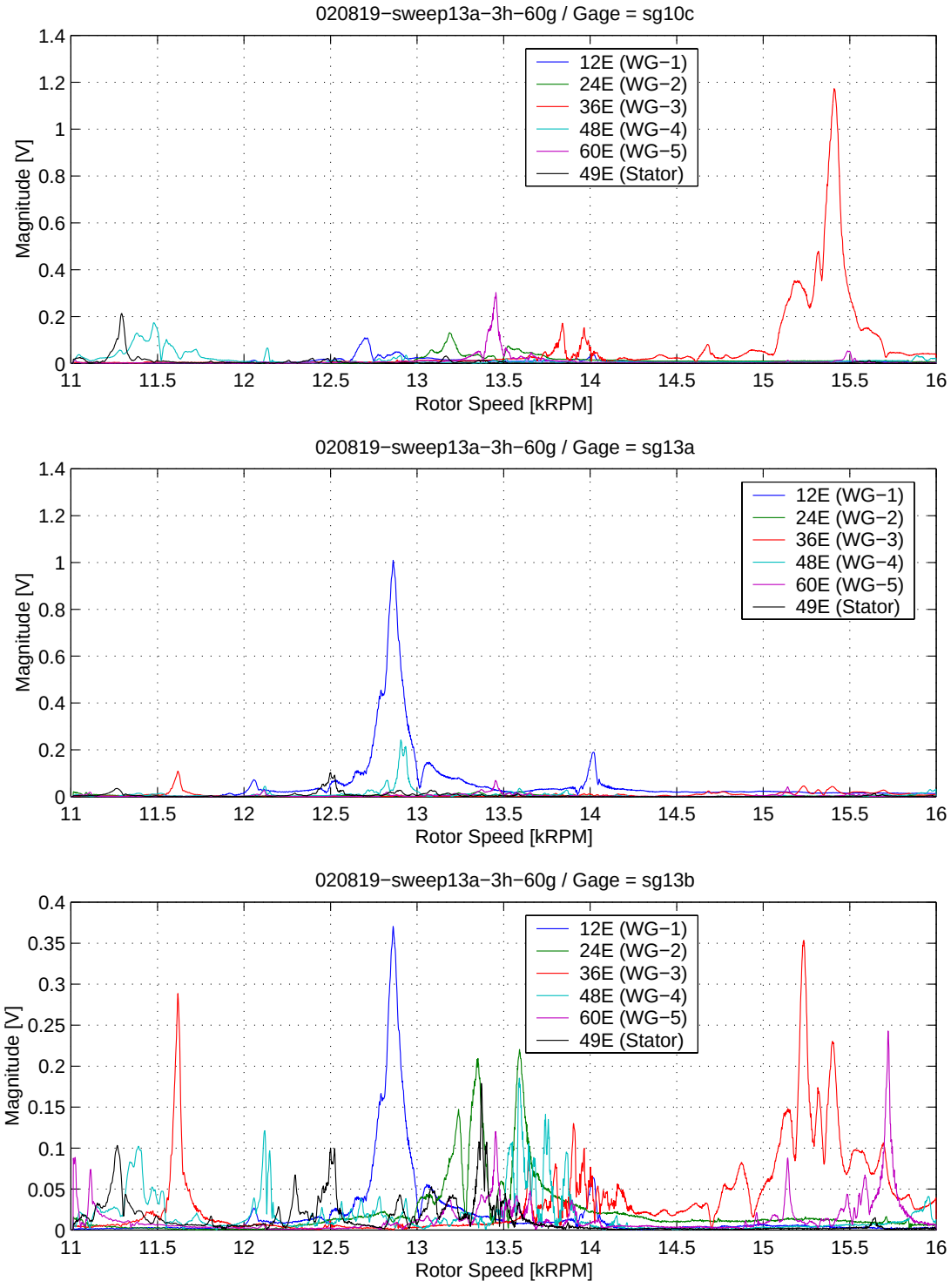

Figure B.34: Order tracks with 3-Hole TEB at 60 g/s (page 1 of 2).

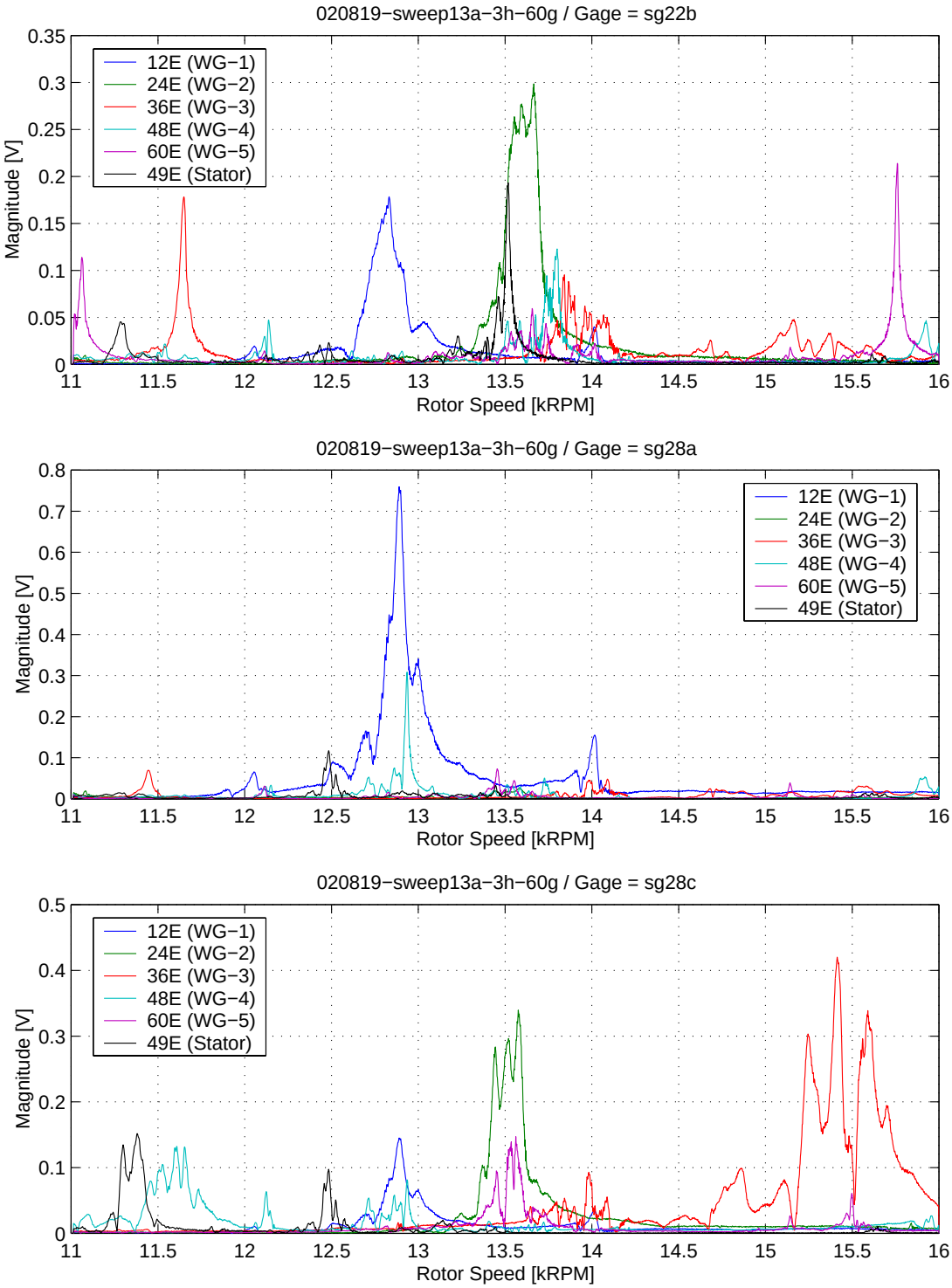

Figure B.35: Order tracks with 3-Hole TEB at 60 g/s (page 2 of 2).

B.5 1-Hole TEB Order Track Plots

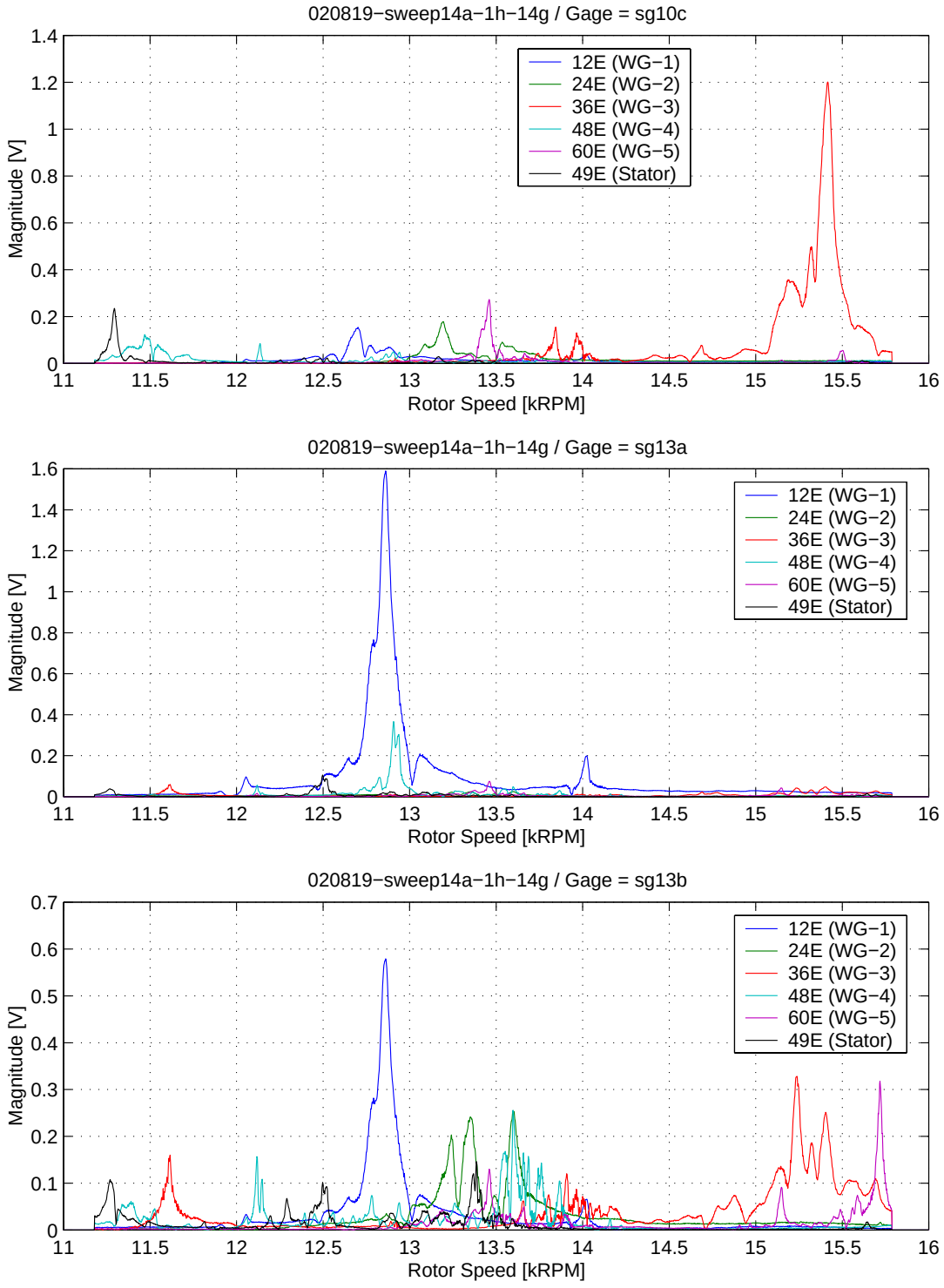

Figure B.36: Order tracks with 1-Hole TEB at 14 g/s (page 1 of 2).

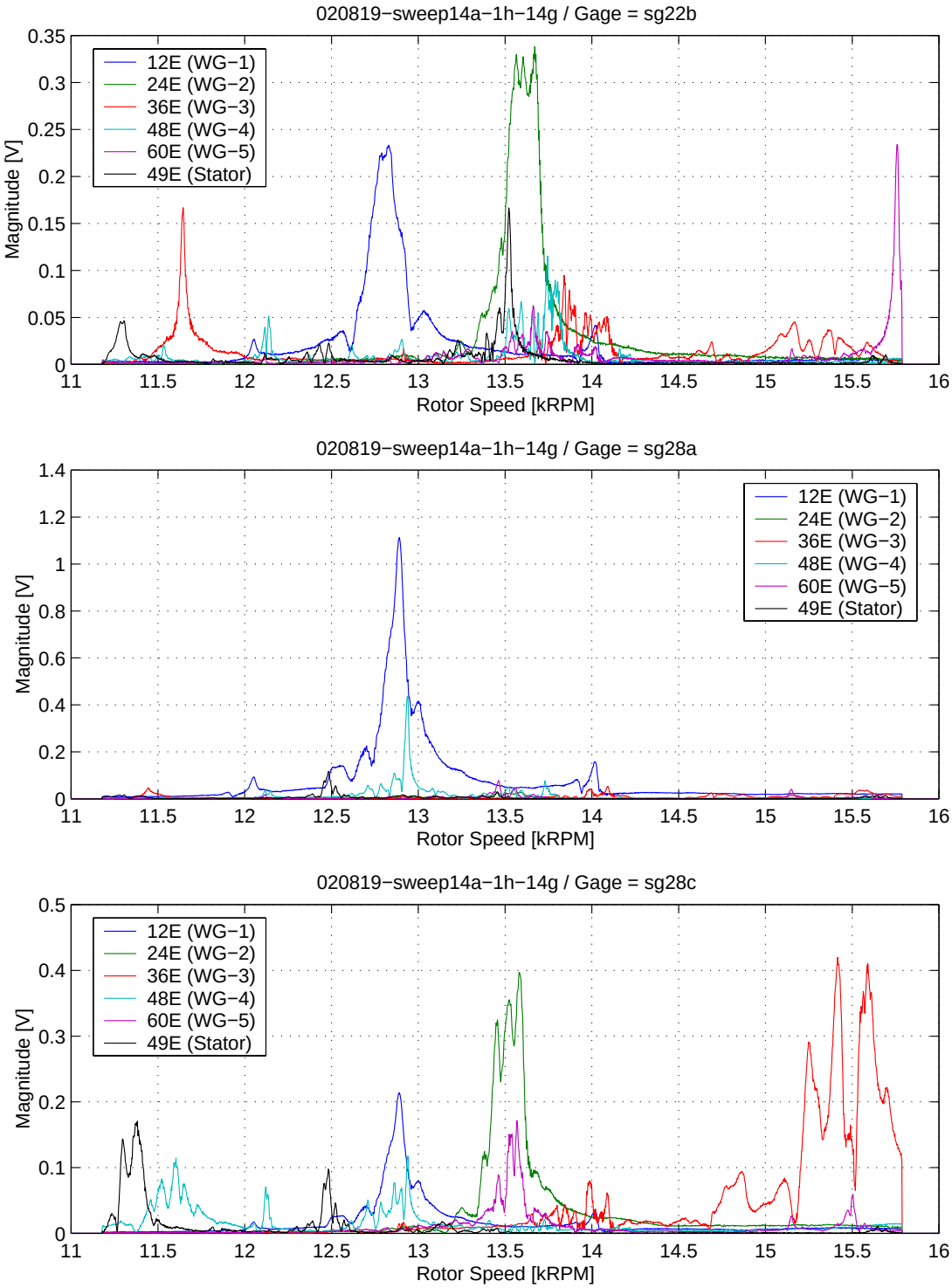

Figure B.37: Order tracks with 1-Hole TEB at 14 g/s (page 2 of 2).

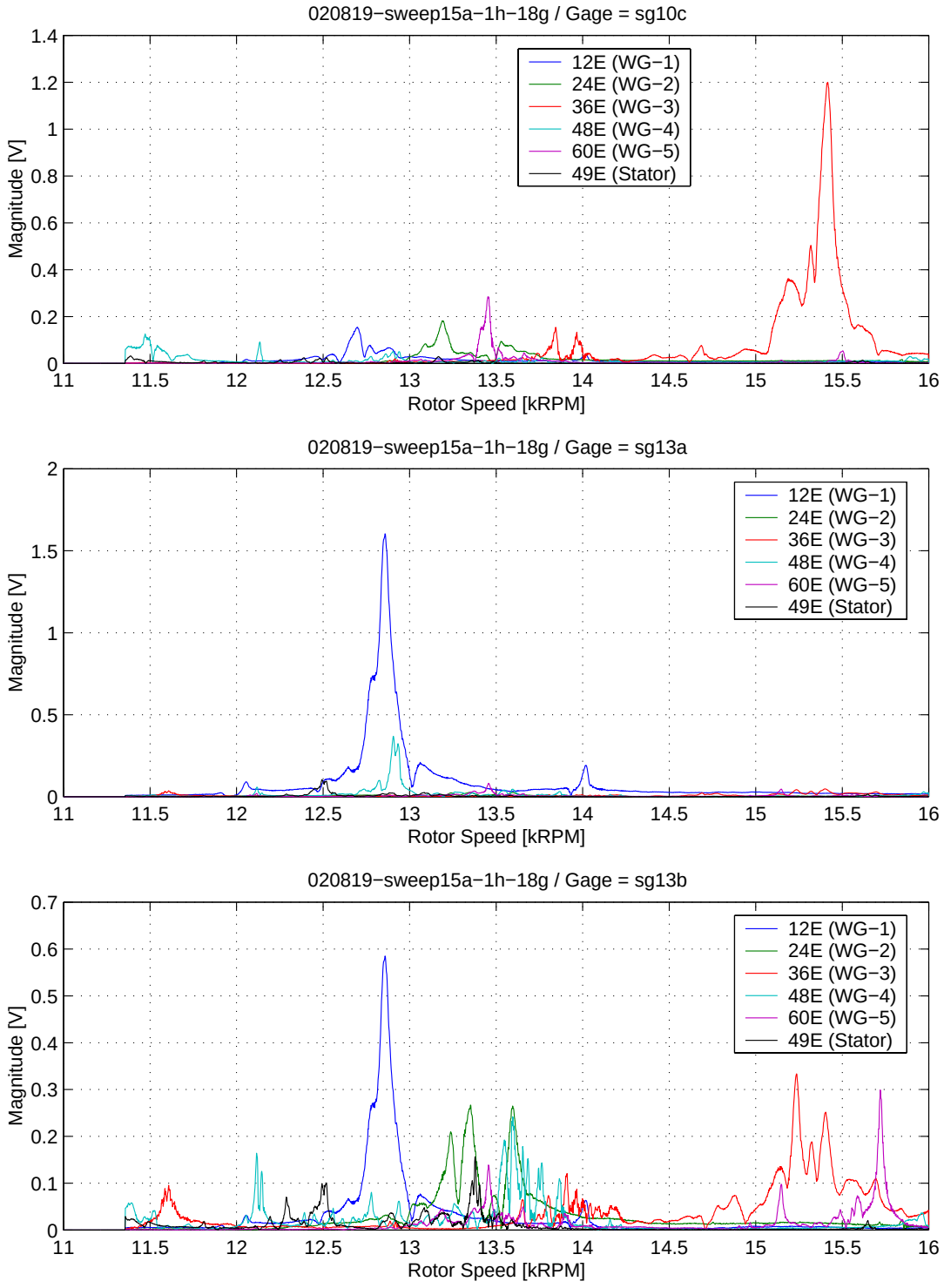

Figure B.38: Order tracks with 1-Hole TEB at 18 g/s (page 1 of 2).

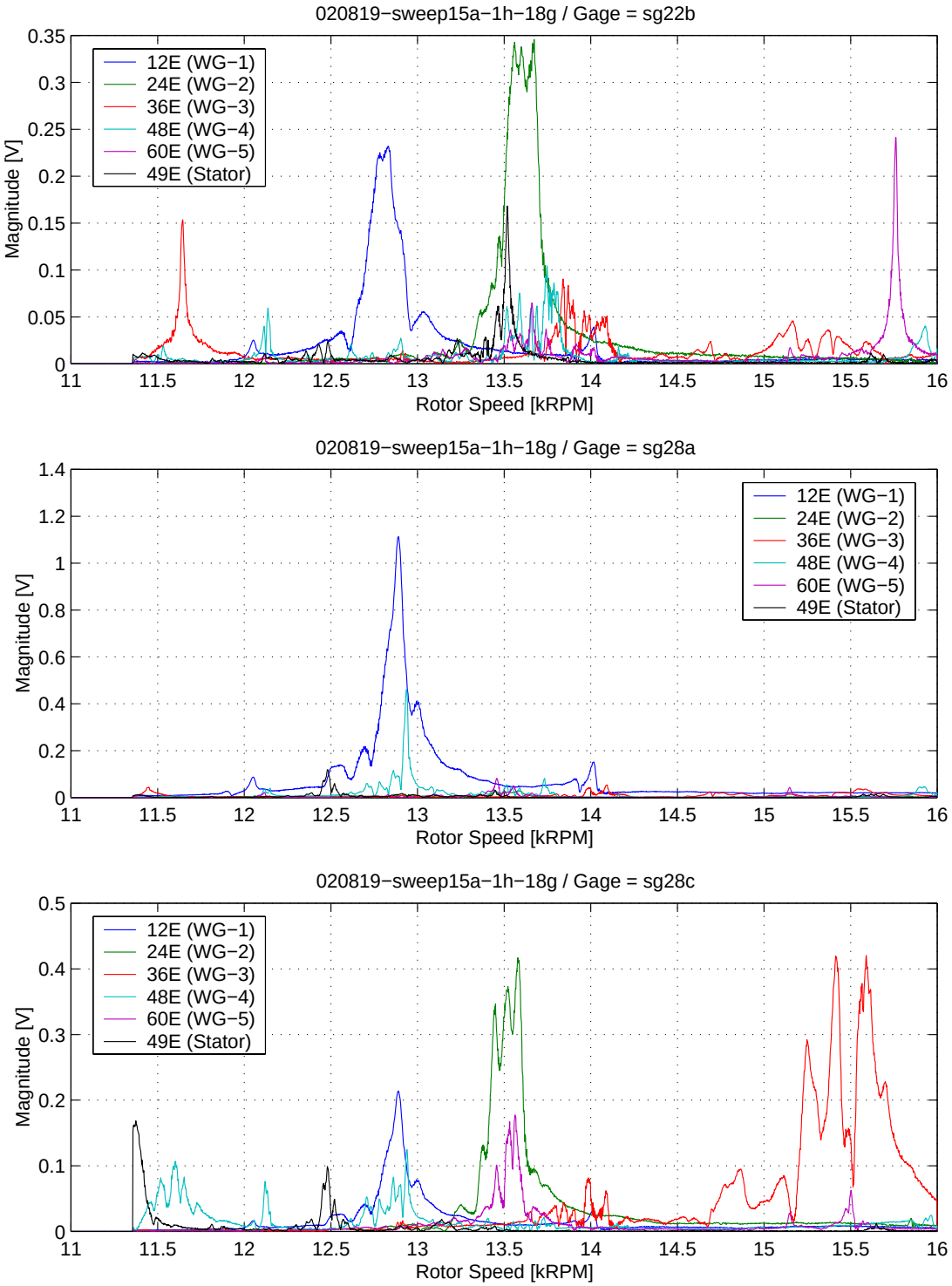

Figure B.39: Order tracks with 1-Hole TEB at 18 g/s (page 2 of 2).

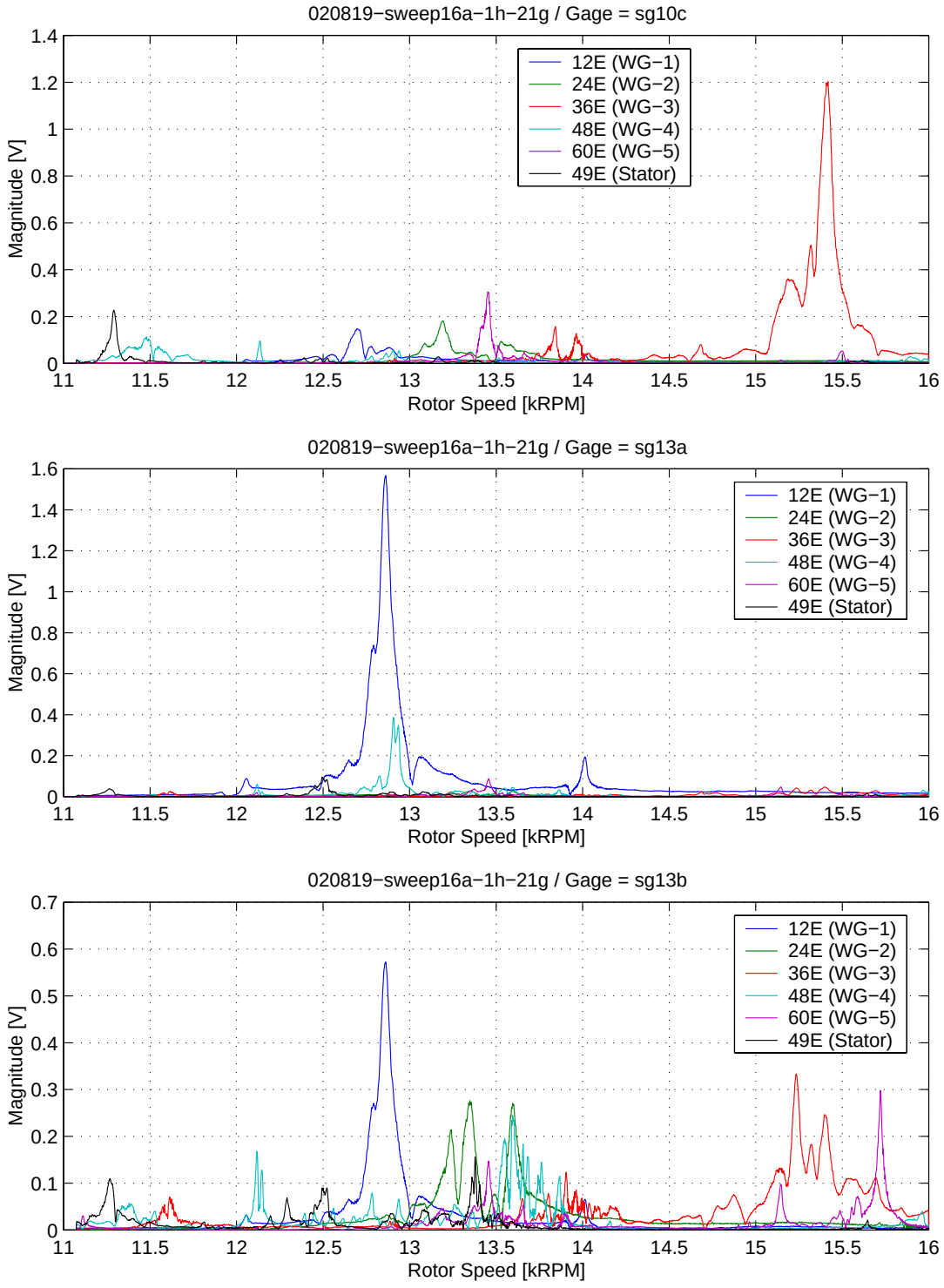

Figure B.40: Order tracks with 1-Hole TEB at 21 g/s (page 1 of 2).

Vita

Samuel Todd Bailie was born in Lexington, South Carolina, USA on April 25, 1975, to Arthur J. and Elizabeth G. Bailie. He attended Lexington High School. In 1993 he entered Clemson University in Clemson, SC. During his studies, he gained two years of industrial experience as an engineering co-op, including one year of research and development for aircraft engines. In 1998 he received his Bachelor of Science in Mechanical Engineering, graduating Summa Cum Laude and with Senior Departmental Honors. After spending the summer as a Research Assistant in Germany, in the Department of Gas Turbines and Flight Propulsion at the Darmstadt University of Technology, Todd began graduate studies at Virginia Tech. He has since served as Research Assistant, NSF Graduate Research Fellow and Instructor. He has also been an active member of the American Society of Mechanical Engineers and the Turbomachinery Committee of the International Gas Turbine Institute. Upon graduation he will begin work in the Propulsion Directorate of the Air Force Research Lab as a National Research Council Postdoctoral Associate.